Controls and Measurements of KU Engine Test Cells for Biodiesel, SynGas, and Assisted Biodiesel Combustion

By

Eric Daniel Cecrle

Submitted to the graduate degree program in School of Engineering's Mechanical Engineering Department and the Graduate Faculty of the University of Kansas in partial fulfillment of the requirements for the degree of Master of Science.

_____

Chairperson: Dr. Christopher Depcik

_____

Dr. Ronald Dougherty

_____

Dr. Bedru Yimer

Date Defended: 3/28/2011

The Thesis Committee for Eric Daniel Cecrle

certifies that this is the approved version of the following thesis:

Controls and Measurements of KU Engine Test Cells for Biodiesel, SynGas, and Assisted Biodiesel Combustion

_____

Chairperson: Dr. Christopher Depcik

Date approved: 3/28/2011

Abstract

This thesis is comprised of three unique data acquisition and controls (CDAQ) projects. Each of these projects differs from each other; however, they all include the concept of testing renewable or future fuel sources. The projects were the following: University of Kansas's Feedstock-to-Tailpipe Initiative's Synthesis Gas Reforming rig, Feedstock-to-Tailpipe Initiative's Biodiesel Single Cylinder Test Stand, and a unique Reformate Assisted Biodiesel Combustion architecture. The main responsibility of the author was to implement, develop and test CDAQ systems for the projects.

For the Synthesis Gas Reforming rig, this thesis includes a report that summarizes the analysis and solution of building a controls and data acquisition system for this setup. It describes the purpose of the sensors selected along with their placement throughout the system. Moreover, it includes an explanation of the planned data collection system, along with two models describing the reforming process useful for system control.

For the Biodiesel Single Cylinder Test Stand, the responsibility was to implement the CDAQ system for data collection. This project comprised a variety of different sensors that are being used collect the combustion characteristics of different biodiesel formulations. This project is currently being used by other graduates in order to complete their projects for subsequent publication.

For the Reformate Assisted Biodiesel Combustion architecture, the author developed a reformate injection system to test different hydrogen and carbon monoxide mixtures as combustion augmentation. Hydrogen combustion has certain limiting factors, such as pre-ignition in spark ignition engines and inability to work as a singular fuel in compression ignition engines. To offset these issues, a dual-fuel methodology is utilized by injecting a hydrogen/carbon monoxide mixture into the intake stream of a diesel engine operating on biodiesel. While carbon monoxide does degrade some of the desirable properties of hydrogen, it acts partially like a diluent in order to prevent pre-ignition from occurring. The result of this mixture addition allows the engine to maintain power while reducing biodiesel fuel consumption with a minimal NO_x emissions increase.

Table of Contents

Table of Figure

Paper 1: Control and Data Acquisition System for a Synthesis Gas Generator Rig

Table of Tables

Paper 1: Control and Data Acquisition System for a Synthesis Gas Generator Rig

Paper 2: Investigation of Biodiesel Feedstock Properties on Engine Performance and Emissions

Paper 3: Analysis of the Effects of Reformate (Hydrogen/Carbon Monoxide) as an Assistive Fuel on the Performance and Emissions of Used Canola-Oil Biodiesel

1. Introduction

Over the past two and one-half years, this researcher has had many different and unique opportunities. The ultimate goal was to obtain research experience in order to determine what career path to take upon graduation. During this time, the author has worked on three major projects that demonstrate three different types of engineering experiences. These projects are similar in nature but unique in themselves. Of importance, they all include the implementation of data collection equipment, data acquisition systems and controls. Moreover, there existed the opportunity to experience all of the different phases of a project. This is beneficial for the reason that in the real world, an engineer might not be included on a project until later stages. Alternatively, engineers might only perform the initial design work and never stay connected through its final product. Instead, this researcher has been provided the opportunity to experience all phases of a project while working at the University of Kansas.

The three experimental setups worked on include the Feedstock-to-Tailpipe Initiative's Synthesis Gas Reforming rig and Biodiesel Single Cylinder Test Stand, along with a unique Reformate Assisted Biodiesel Combustion architecture. For each of these endeavors, work was begun at a different point in the process or executed from start to end. This thesis will explain each of these projects in more detail along with what work was accomplished. Before explaining the projects, the context of a project must first be understood.

A project, as defined by the Project Management Institute (PMI) [1], is a task that has a start and end point that is unique to other products or projects. Therefore, it is always exclusive in nature. Depending on the objectives, it will always follow a different path even though the goal might be the same. An example of this would be a bridge construction project between Lincoln, Nebraska to Omaha, Nebraska on Interstate-80. Even though the bridges may be similar to other bridges of their kind, each construction path will be inherently different. The reason relates to the fact that each bridge built has different constraints such as dimensions, soil quality, and material qualities. Therefore, the task of an engineer for this project is to design safe bridges that can last for the next one-hundred years given the unique specifics of each area.

Every venture requires five phases to be classified as a project by PMI: Initiating, Planning, Executing, Monitoring/Controlling, and Closing. This method is known as the Project Management Body of Knowledge or PMBOK [2]. The Initiating phase is when the initial concept or scope for a project is obtained. This phase requires only minimal knowledge and design. For an engineer, this would involve the initial meeting with a client who needs an assessment or solution to their problem. An example of this would be a self-tinting car window. It is an idea new and unique to other products and methods on the market.

The second phase is known as the planning process. This is where the project is fully developed and organized for success. In the planning phase, many core processes are completed in order to develop a plan for execution. These are: Scope Planning, Scope Definition, Activity Definition, Activity Sequencing, Activity Duration Estimating, Schedule Development, Resource Planning, Cost Estimating, Cost Budgeting, and Project Plan Development. As defined by PMI in the PMBOK, the following are the definitions of those processes:

- Scope Planning involves the written scope statement that the project decision is based upon.
- Scope Definition is the subdivision of major project deliverables into smaller and manageable project components.
- Activity Definition is where specific activities are identified that must be performed to produce the desired deliverables.
- Activity Sequencing is where the small and manageable components are logically sequenced upon dependency in order to create a work timeline and tasks.
- Activity Duration Estimating is where tasks are given completion deadlines in order to finish the project by the requested deadline.
- Resource Planning is where staff, materials, equipment and their quantities are determined.
- Cost Estimating is where an initial project cost is determined based on the project length and resources required to complete the project by the given deadline.
- Project Plan Development takes the results from the previous processes and puts them into a written document in order to have a physical guideline for the employees working on the project.

Again, using the example from before, the planning for the self-tinting car window would define the wants of the project such as how fast and dark the window should tint along with how the window meets all government standards. Next follows the determination of the tasks needed for completion such as prototyping, testing, and marketing. Finally, the project manager would determine the cost, resources, and timeline needed to finish the project.

The third phase is the Executing Process or implementation of tasks in order to accomplish the project. In this phase, eight processes are completed. These processes are: Project Plan Execution, Scope Verification, Quality Assurance, Team Development, Information Distribution, Solicitation, Source Selection, and Contract Administration. These are defined as follows:

- Project Plan Execution carries out the task created in the planning phase.
- Scope Verification re-visits the original scope and updates or modifies the current scope to match the path of the project.
- Quality Assurance uses performance evaluations in order to determine the overall satisfaction of the customer requirements/needs for the project.

- Team Development is a tool that assists the individual in growth, teamwork, and skills in order to enhance the project performance and outcome.
- Information Distribution makes sure the needed information is available to all parties working on or invested in the project.
- Solicitation investigates external resources and acquires them if needed.
- Source Selection involves contacting external resources in order to bring them on-board as suppliers or vendors.
- Contract Administration includes managing the relationship with the supplier or vendor.

This phase requires the largest proportion of time and money to complete. An example of the Execution Phase following our self-tinting window case would be creating a prototype window, testing the window, contacting and making contracts with suppliers for required materials in order to mass-produce the window.

The fourth phase is the Monitoring or Control stage. This is when the checks and balances of a project are weighed against its completion schedule. There are seven processes during this period: Overall Change Control, Scope Change Control, Schedule Control, Cost Control, Quality Control, Performance Reporting, and Risk Control. There definitions are the following:

- Overall Change Control involves the project leader coordinating changes to the project.
- Scope Change Control organizes the changes made to the scope of the project.
- Schedule Control includes managing and updating the project timeline in order to insure that the project is completed on time.
- Cost Control evaluates the current expenditures and modifies the plan and potential requests for additional funding.
- Quality Control monitors the tasks and results in order to insure that the product complies with the project standards while eliminating unsatisfactory performance.
- Performance Reporting comprises the collection and analysis of performance information through project updates.
- Risk Response Control evaluates the risks and takes actions to prevent failure.

An example of this phase for our example product would involve a supplier of glass beads informing the project manager that the last shipment does not meet their company's quality control standards. The manager would then inform the research and manufacturing staffs in order to remove the material from the shelves. From there, the leader would contact the supplier for a new shipment or find a new supplier that can insure that the project is completed by its deadline.

The last phase is the Closing Process that encompasses disbanding the project team, obtaining final input about the project, along with completing the final reports, documents and contracts. This phase is normally negated for most projects; however, it is just as important as the others are in order to assist with future projects or endeavors.

2. Project Experience

With an understanding of what a project entails, this thesis provides a summary of the work accomplished over the past two and one-half years. Each project provided an experience involving all of the phases of the Project Management Body of Knowledge discussed in the previous section. For two of the projects, only partial completion of the project methodology was accomplished, with current students following up on these efforts to completion (Feedstock-to-Tailpipe Synthesis Gas Reforming Rig and Biodiesel Single Cylinder Test Stand). On one project, the researcher had the opportunity to start and end the work (Reformate Assisted Biodiesel Combustion). For each of these projects, this thesis contains an overview of the project along with a technical report or a future submitted publication to a peer-reviewed journal.

2.1. Synthesis Gas Reforming Rig Data Acquisition and Controls

The task undertaken for this project was to develop an implementation plan of the data acquisition and controls system on the Synthesis Gas Reforming Rig. With respect to PMBOK, the assignment was to complete the first two phases and begin the third phase. This is similar to many real-world situations where an engineer would generate a Request for Proposals (RFP) for a state project. The worker would complete the planning and initial design with the subsequent issue of an RFP. Bidders would then submit proposals and the state would award a contract with the winning firm acting to implement its design. This methodology was followed for this project because the Synthesis Gas Reforming Rig is complex and multi-faceted activity including three engineering disciplines. There have been several small and large objectives that have been completed on the system to date in order to get it into working condition (e.g., up to the point of RFP readiness). In this section, a background of the rig is given along with the past projects completed by the main author. This is followed by a project summary that allows other students to finish the rig in order to create journal quality data for publication.

2.1.1. Project Background

The Synthesis Gas (SynGas) reformer rig provided by Bill Ayres of R^3 Sciences has brought a unique opportunity to the University of Kansas (KU) for the Feedstock-to-Tailpipe (FTT) Initiative. The FTT Initiative is a multidisciplinary research project that is investigating future alternative fuels. The SynGas rig is an addition to this initiative allowing the university to reform the byproduct of biodiesel, glycerin, into a hydrogen rich mixture. The entities that are involved on this project are the Chemical and

Petroleum Engineering (CPE), Mechanical Engineering (ME), and Civil, Environmental and Architectural Engineering (CEAE) departments. CPE is responsible for designing, testing, and implementing the catalytic material to promote hydrogen production from the reformer system. ME is responsible for updating, implementing, and testing of the engine and generator. CEAE is responsible for monitoring and analyzing engine emissions. All of the systems managed by these departments will be explained in more detail in the next section.

Originally, KU was promised a completed rig, but due to the economic crisis of 2008, Biomass Energy Company (BEC) of Golden, Colorado (the original manufacturer of the rig), was allowed to remove equipment. The components that were removed are the following: the reformer catalytic material and, most importantly for purposes of this thesis, controls and data acquisition equipment. Figure 1 presents a picture of the SynGas Rig right after its initial arrival at KU.

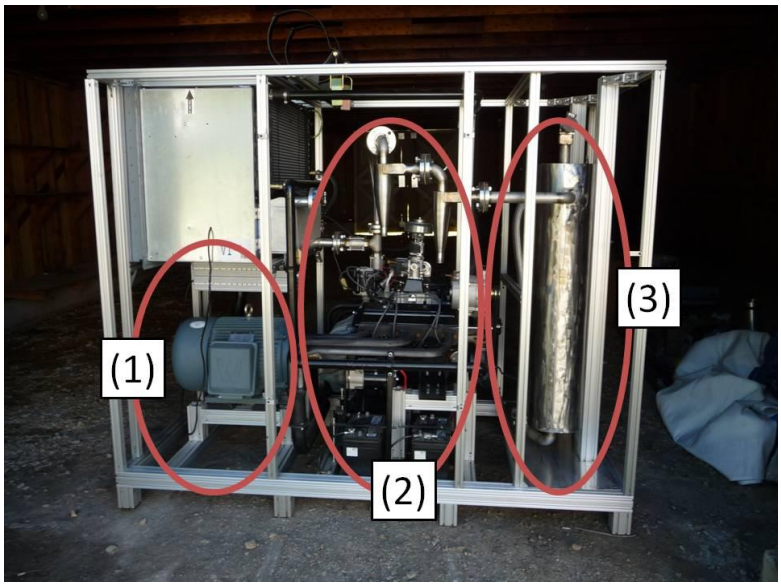

Figure 1. Feedstock-to-Tailpipe Initiative's Synthesis Gas Reforming Rig upon arrival at KU: (1) Generator section, (2) Engine section and (3) Reformer section.

The SynGas rig is comprised of three major sections as shown in Figure 1: the reformer, the engine, and the generator. The reformer system (Figure 1: Number 3) includes many different apparatuses. It uses propane pre-heating in order to warm the reformer to an adequate temperature, as glycerin does not vaporize and combust easily. It also uses a custom direct current (DC) pump to transport the glycerin to the reformer, where it goes through two heating elements in order to raise its temperature making it easier to vaporize. To reform the glycerin, the system needs to operate at a rich to an ultra rich fuel-to-air mixture to create single oxygen molecules (e.g., CO and OH) and non-oxygen molecules (e.g., H_2). Based on the stoichiometry of partially-oxidized glycerin ($C_3H_5(OH)_3$), this mixture can be up to

57% hydrogen (H_2) and 43% carbon monoxide (CO). Both of these components have an associated heating value (120 and 10 MJ/kg_{fuel}, respectively) that can be used as fuel for the engine in the system.

The engine (Figure 1: Number 2) is a General Motors (GM) V-8 that has a total displacement volume of 350 cubic inches and a compression ratio of 8.2:1. Currently, it is naturally aspirated with electronic spark timing. It uses a Woodward Air-Fuel Valve (AFV) that regulates the fuel-to-air mixture through monitoring a Bosch oxygen sensor. A Woodward Throttle Valve (TV) modulates the amount of air into the engine in order to control engine speed. The engine uses a custom propane carburetor that provides enough restriction with the TV in order to regulate the flow of air to maintain 1,800 revolutions per minute (rpm) needed for the generator. The current setup allows for all the components of the engine to be operated independent of each other; it is important to note that the original design by BEC did not allow for individual control demonstrating a substantial improvement in system operation by KU students. Placing the TV before the AFV allows for a constant flow of SynGas and a variable flow of air.

The generator (Figure 1: Number 1) was to be based on a 30 kilowatt (kW) alternating current (AC) three-phase motor, which is monitored by a Woodward voltage and current sensor. By talking to experts in this field, it was found that this motor could be used as a generator by first requiring an input of 30 kW of power. Then, the engine would run slightly faster in order to change the flow of electrons effectively converting the motor to a generator. However, this was not feasible in the current setup, because the current location on university property does not have 30 kW of 208 VAC 3-phase capabilities. As a result, a standalone power take-off (PTO) generator will be used to replace the motor. The PTO purchased for this system is a Mecc Alte ECO32-2L/4 alternator with installation and testing to be completed in the near future by a separate researcher.

2.1.2. Previously Completed Projects

Since KU obtained the syngas rig from BEC in 2008, many sub-projects have been completed in order to get the system into a functional state. Each of these endeavors was necessary to be able to determine if this system was capable of producing the advertised output that BEC and R^3 Sciences promised. In specific, this work laid the foundation so that the time spent developing the data acquisition and controls plan was worth the effort:

- Moved syngas rig from BEC to West Campus at the University of Kansas.
- Decoupled the reformer and engine for independent testing and control.
- Designed and constructed a temporary site of operation on West Campus for housing the unit.
- Fabricated an independent glycerin transport system for easier transport of material.
- Upgraded the mechanical spark timing system to an electronic version in order to enhance performance capability of syngas combustion.

- Modified propane combustion and ignition setup for uniform pre-heating of the reformer.
- Minor engine and rig upgrades for repeatable operating and working conditions.
- Preliminary research by CPE student in order to increase hydrogen selectivity from the glycerin reformation process.
- Initial attempts to run the engine on reformed propane.

The remainder of this section will explain the sub-projects that were completed in part or fully by the author in order to make developing a data acquisition and controls plan feasible.

The first major objective was a relocation plan for the SynGas rig from its location at BEC in Golden, Colorado to West Campus here at KU. This project was developed with the assistance of Lou McKown from the 2008-2009 EcoHawk class of Dr. Depcik. Many options were considered in order to move the rig; renting a truck and trailer and driving out to BEC, using a professional trucking company, and even employing Portable-On-Demand storage units (PODS). The best solution determined was to hire a professional trucking company to perform the bulk of the efforts. Once the logistics were finalized, this researcher flew out to BEC to supervise the packing of the equipment as seen in Figure 2. Moreover, this allowed the opportunity to talk with one of the original designers in order to obtain as much information as possible about the rig. This part of the project was completed once the rig was placed on the gravel floor of a newly requisitioned boat barn (by Dr. Depcik) on West Campus as seen in Figure 3.

Figure 2. Picture of the SynGas rig loaded on a flat-bed semi-trailer in Golden, Colorado.

Figure 3. Temporary placement of the SynGas Rig in the boat barn.

As stated before, R^3 Sciences originally proposed giving KU a complete SynGas rig unit, but upon arrival and inspection, it was found to be in poor condition. However, this was actually more beneficial to the researchers because the initial investigation determined that the reformer unit and engine unit were coupled together making it impossible to test one without running the other. This created a huge non-linearity in its operation making it extremely difficult to control either or both at the same time. Therefore, by not having a functional system, the students working on this project were allowed to decouple and modernize each separate system making it more useful for research purposes.

As a result, the second project involved decoupling and tuning the engine so it could operate purely on propane. Propane is used to pre-heat the engine in order to find operational baselines for performance and emissions. This is done through the creation of an initial propane fuel map (as a function of air-to-fuel ratios) that will be revised using the syngas created from glycerin. A trial-by-error procedure was used to troubleshoot and learn about the Woodward TV control, as seen in Figure 4. This project was completed after obtaining an understanding of the recalibration process of the electronic values and achieving continuous engine operation on propane combustion at 1800 RPM.

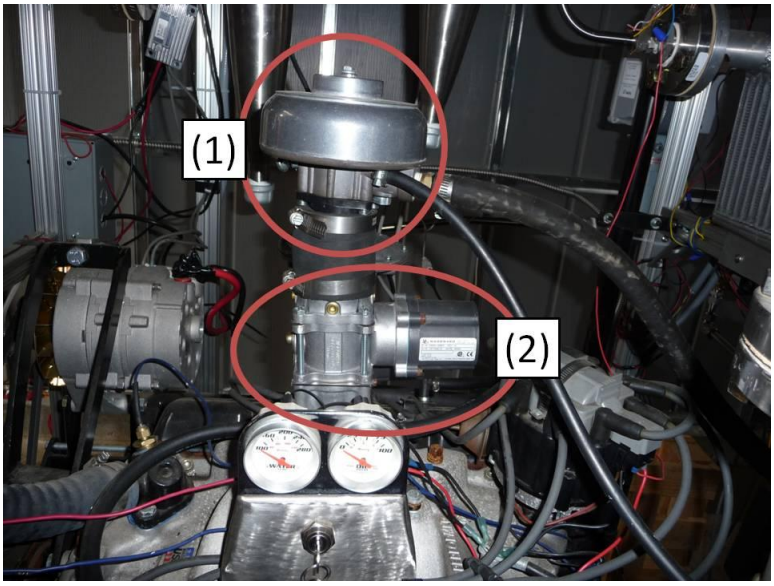

Figure 4. SynGas Rig intake setup: (1) Propane carburetor and (2) Woodward throttle valve.

The third project was to design and construct a temporary building on university property as shown in Figure 5. There were four major parts to this project: the foundation, structure, construction, and amenities. The foundation part involved working with the university Department of Construction Management (DCM) along with the Department of Environmental Hazard and Safety in order to design the necessary proper housing. At the same time, multiple build options were being considered for the structure; from construction by hand to a pre-fabricated building. It was determined that a pre-fabricated building was the most economical and with assistance from the class of 2009-2010 EcoHawks, the building was completed next to the barn temporarily housing the SynGas rig. While waiting for the foundation to be poured, consideration was given as to what the building was going to include. This resulted in electronic outlets and lights currently functional within the building. Other items were postulated such as incorporating insulation in order to protect the equipment from harsh winter conditions, along with a heating and cooling system to provide comfort for the graduate students while working. Unfortunately, these amenities were not implemented due to the costs and electrical requirements needed for a sufficient system.

Figure 5. Temporary building on university property (West Campus).

The fourth project included the installation of a 12-volt direct current (DC) glycerin pump and controller. This involved replacing the power-steering pump formerly used for feeding the glycerin into the reformer. On an older engine like this one, the power-steering pump was belt driven; therefore, requiring the engine to be running in order to operate the reformer. This required a complex control structure using propane and syngas at the same time, which is difficult to control and optimize. The new system uses a 12-volt DC motor, gear pump, and 12-volt DC motor controller that allows for a variable flow rate to the reformer independent of the engine running, as seen in Figure 6. This incorporates greater flexibility when running the reformer and will be extremely important when comparing reformer effectiveness through the different catalytic materials being researched by CPE students. In other words, reformer operation and testing can be performed without needing to run the engine at all. Moreover, this system is designed to handle pure glycerin which is a challenge given its highly viscous properties as described in a later section.

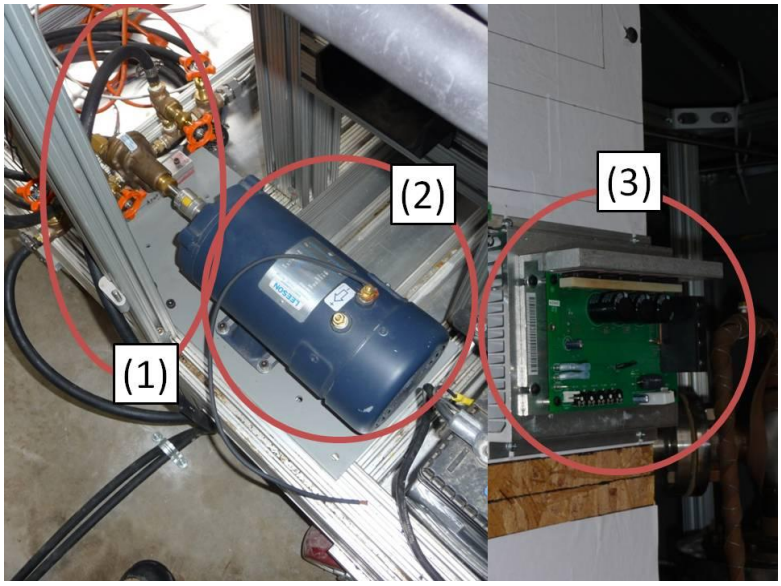

Figure 6. SynGas Rig 12-volt DC glycerin pump: (1) Oval-gear pump, (2) 12-Volt DC motor, and (3) 12-Volt DC motor controller.

Another project performed in conjunction with a Mechanical Engineering graduate student, Nick Wanklyn, included outfitting the engine with an aftermarket Engine Control Unit (ECU) in order to control the cylinder spark timing. Originally, spark timing was fixed through an old mechanical vacuum advance distributor system. Since different fuels have unique properties and heating values, this leads to dissimilar spark timing settings. As a result, the spark timing that works best for propane may not lead to optimal combustion of the syngas mixture. Variable spark timing allows for optimization of syngas engine performance based on the ratio of H_2/CO leaving the reformer that is function of the catalytic material and temperature. The ECU is installed as indicated in Figure 7 and has proven its effectiveness to date by preventing engine knock when running on propane or syngas.

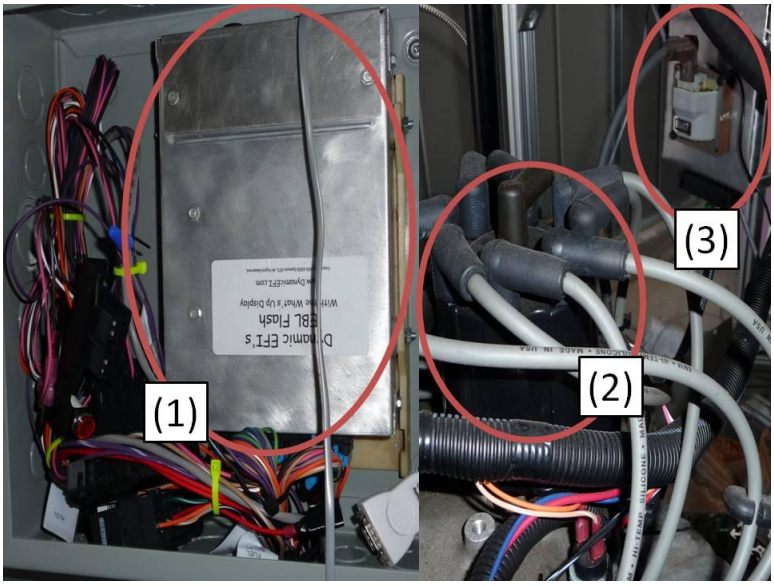

Figure 7. Electronic spark timing system: (1) Aftermarket ECU, (2) Modern distributor, and (3) Ignition coil

Another necessity associated with the SynGas rig was to develop a system that can provide uniform propane pre-heating of the reforming unit. There were two major components to this endeavor with the first involving a new ignition system. The original system was comprised of a neon sign transformer and glide-arc materials. A transformer is an electrical device that converts a given input voltage into either a higher or lower voltage amount through a modification in the electrical current. An example of this would be the transformation of 120 volts alternating-current (AC) into 9,000 volts AC. A glide-arc system normally consists of two metal rods placed close enough together to allow electricity to transfer between the two bars or jump the gap (similar to a Jacob's ladder) [3]. It was found that the glide-arc system was unreliable because of carbon build up and it was difficult to re-align the wires after being removed for cleaning. The system was upgraded to a more traditional spark plug system using the neon transformer as shown in Figure 8. A spark plug is similar to a glide arc, but it is a self-contained device with a pre-calibrated distance for electrons to jump the gap. It is more reliable, but still prone to carbon build up given the rich fuel-air nature of the mixture entering the reformer.

The second component included creating a uniform flow of gaseous propane into the reformer from its liquid form in a storage tank. Originally, the system utilized a large heat exchanger to provide the needed vaporization of propane; however, the size of the system was too large to be beneficial. Different attempts were made to remove the heat exchanger and use propane regulators to step down the pressure and provide a smooth transition to a gas. However, this method did not allow for complete vaporization. As a result, the final system reuses the heat exchanger as an expansion chamber in Figure 9, along with propane regulators and smaller plumbing lines in order to obtain a controlled uniform propane

stream for combustion. It was found that one of the reasons the heat exchanger did not work originally was because it was subject to leaking (subsequently fixed).

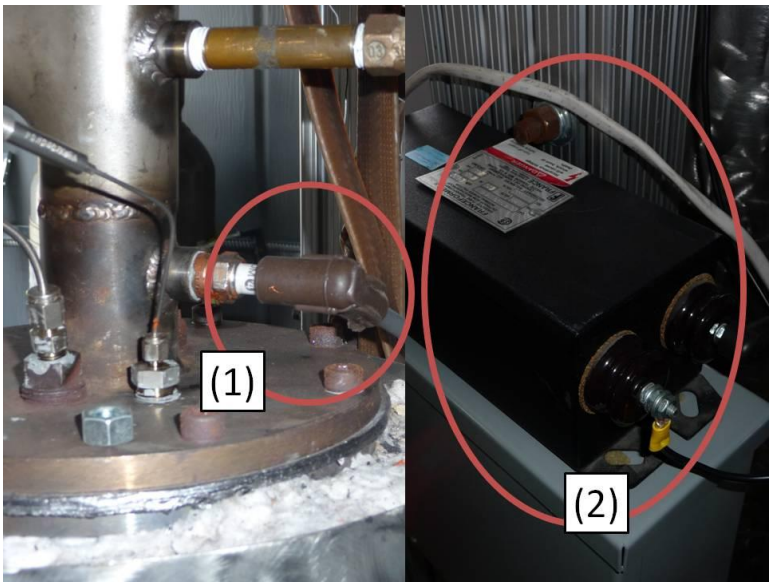

Figure 8. Spark-Plug System for reformer: (1) Automotive spark-plug and (2) 9,000 Volt AC transformer.

The author and co-workers have completed other smaller projects along the way. These include the installation of an aluminum floor for chemical spills, casters, fusing, and the replacement of a 120-volt AC fan with two DC car fans of equivalent capacity. This was necessary because a DC-to-AC voltage inverter running off a lead-acid battery could not handle the current draw needed to power the AC fan. For clarity, a DC-to-AC inverter transforms DC voltage into a higher or lower voltage while regulating the flow of electrons in order to produce the alternating positive and negative voltage of AC variety. Since engines generally output one-third of their energy through mechanical means (connected to the PTO generator), one-third through their metal surroundings into an engine coolant, and one-third leaves through the exhaust gases, it is important to maintain proper engine coolant temperature in order to prevent engine overheating and destruction. The fan is used to reduce the temperature of the engine coolant by forcing flow across a radiator (heat exchanger) and out of the building. The result of this effort was the installation of two new, low current DC car fans that provide proper engine cooling.

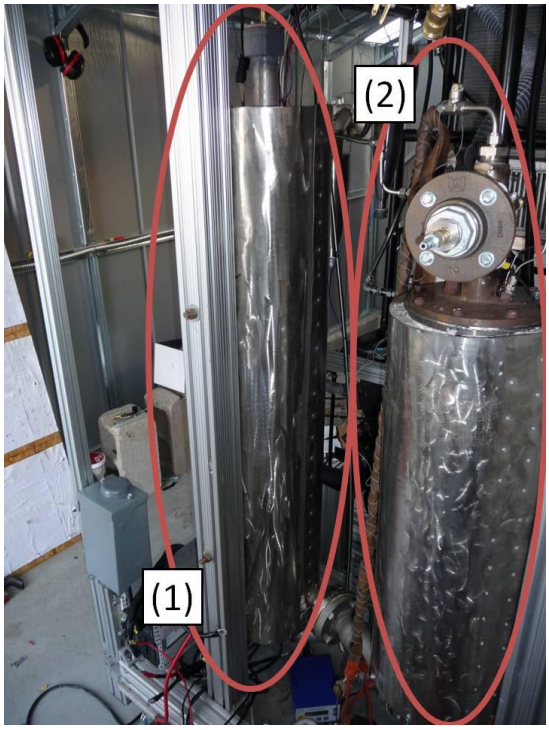

Figure 9. Propane heating system and reformer: (1) Large heat exchanger and (2) Reformer.

Other projects that are currently in progress include the re-plumbing of the reformer system and testing of catalytic material by a CPE student. As mentioned before, the original majority of the plumbing on the system was removed; therefore, piping and Swagelok fittings are being implemented in order to complete the system. This task will not be finished until it is determined that no more test equipment needs to be installed during the system upgrade. The focus of the CPE student involves laboratory scale reactor tests in order to determine what catalytic material and glycerin/water mixture will promote the best hydrogen selectivity.

The last major sub-project that was completed involved starting the engine on reformed propane in order to demonstrate the feasibility of the revised setup. This was performed by heating the reformer to 800K and reducing the amount of air into the reformer. This promotes the formation of a H_2/CO rich mixture as including too much air will convert these species fully into CO_2 and H_2O (described more in a later section). This effort has been successful and the engine can be started repeatedly on syngas demonstrating viability and readiness for glycerin usage.

Again, the syngas rig was in non-working order when initially received; however, this has provided the opportunity for graduate students to learn real-world skills while supplementing the research equipment of the university. Along the way, a number of items have been completed: obtaining the syngas rig, decoupling the systems for independent operation, construction of a dedicated building, running the engine on propane, and fabrication of a repeatable system. The major milestone of this project

was the successful running of the engine on a reformed propane mixture consisting of CO and H_2. The CPE student verified this by connecting a Gas Chromatograph (GC) analyzer to the reformer outlet with proof of concept results from the rig provided in Figure 10 by Luke Silvey in CPE. It is important to note that a GC cannot measure H_2, but it can be inferred to be on the same order of magnitude through the combustion reactions described later in this thesis.

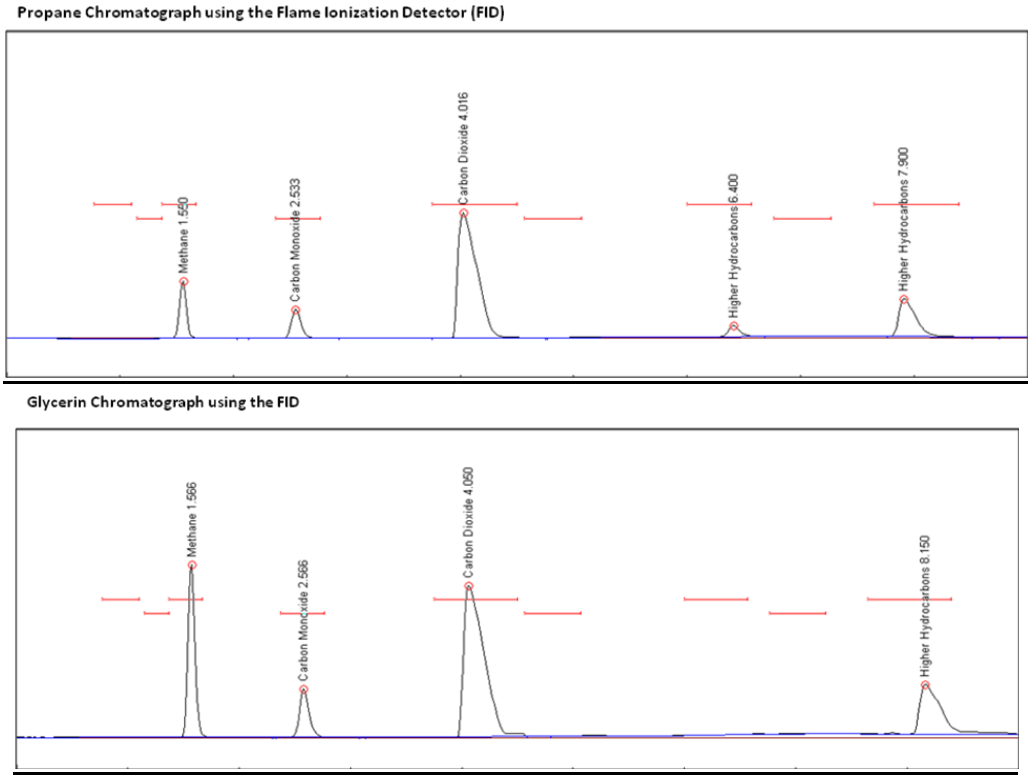

Figure 10. Gas Chromatograph results from reformer in SynGas Rig provided by Luke Silvey in CPE.

2.1.3. Future Improvements

While the previous efforts were on going at getting the system to a functional state, this researcher was asked to develop a subsequent plan for re-implementing the data acquisition and control system originally scavenged by BEC. A later section of this thesis outlines this plan, what equipment is necessary, the respective cost along with models that will help control glycerin and airflow rates in order to produce the needed H_2/CO mixtures and take literature quality data. This section further explains the background information regarding available sensors in collecting the needed information.

A quick summary of the plan recommends the use of National Instruments hardware for monitoring and controlling, Omega K-type thermocouples to measure temperatures, Omega PX-319 pressure sensors, and multiple mass/volumetric flow meter/controllers for the different systems. The total cost estimate for equipment is $7,900 but does not include flow meters or controllers at this time, because the system currently operates with a few already employed. In the future, the implementation of another

flow meter and controller will allow for better controllability and data collection. An example of this would be a flow meter on the propane stream in order to collect all the mass flow rates into the reformer. Finally, the last task of the plan was to develop a model that could be used in the control program in order to predict the needed flow rates of glycerin and both air constituents; one for the reformer, one for the engine. This will provide the initial estimates as to the parameters until research data has been collected and these models are updated.

In particular, two models determine the potential reforming options. The first model is a generic non-catalyst predictor model that uses the stoichiometric balance for combustion along with the governing equation of mass, gas properties, and an energy balance in order to control the glycerin pump through the software. The second model follows similarly but uses a glycerin/water mixture to promote H_2 generation along with a continuous propane addition. The main reason that this model was developed is to combat the endothermic process of steam reforming that occurs during the reformation of glycerin with the added water. The results show that the addition of propane combustion actually degrades the process; hence, the control system will attempt to keep the temperatures high enough to prevent significant steam reforming. This will hurt H_2 production slightly, but maintain continual glycerin reformation. Currently, implementation is underway with the students following the plan set forth in Paper 1.

2.2. Biodiesel Test Stand Data Acquisition and Controls Project

The task undertaken for this project was to implement the data acquisition and controls system for a single-cylinder engine test stand as part of the larger Feedstock-to-Tailpipe Initiative investigating biofuels involving multiple faculty in different disciplines. The implementation of this system began in January 2008, and it had been pre-determined that a National Instruments cRIO system would be the hardware framework. Moreover, a number of pressure and temperature sensors had been purchased, along with flow meters in order to capture the needed experimental data. Hence, the initial phases of planning and design were accomplished before the author's arrival on campus. Therefore, this researcher's task was to complete the execution, monitoring/controlling, and closure phases. For the execution phase, the equipment was installed and a data collection program was developed using National Instruments LabView software. For the monitoring/controlling, preliminary tests were run in order to validate or modify the code ensuring accurate readings. During this phase, additional equipment was purchased in order to replace the sensors that were found to output inaccurate readings. The closure phase occurred when the students and Dr. Chris Depcik reviewed test data and accepted the individual measured values along with the subsequent experimental error calculation.

The work accomplished as part of this project is one of many key objectives needed to ensure success of the FTT Initiative. A team of faculty and associated graduate students (including the author)

will be submitting a research paper within this year using the results measured from this system. It is important to note that author's efforts are a major factor in capturing repeatable and accurate data from the engine. The objective of the test stand is measurements that determine the feasibility of different biodiesel fuels for diesel engines involving a wide variety of dissimilar feedstock sources (soybean oil, canola oil, coconut oil, etc…). This work investigates the performance of these fuels and their subsequent hazardous and greenhouse gas emissions. The paper at the time of this thesis can be seen in Paper 2. (Advisor note: Eric Cecrle has completed all requirements for the data collection put forth; the fact that the paper is incomplete at the time of this thesis is due to a malfunctioning emissions analyzer that is out of the control of Eric's responsibilities.) In the next section, a summary of the effort needed to get the system ready for journal quality data is presented.

2.2.1. Biodiesel Test Stand Setup

The system is comprised of a single-cylinder diesel engine, five pressure sensors, five K-type thermocouples, a laminar flow element, a Coriolis mass flow meter, and a power meter. A basic layout of the test stand can be seen in Figure 11. All sensors are currently being measured by the data acquisition system developed by the author. In particular, there are six sections of the engine that are being monitored: environmental conditions, intake air stream, fuel stream, engine, exhaust stream, and a load cell. Each of these sections is used in order to obtain the normalized values preferred by the literature; examples include the specific brake fuel consumption, fuel conversion efficiency, and specific brake emissions.

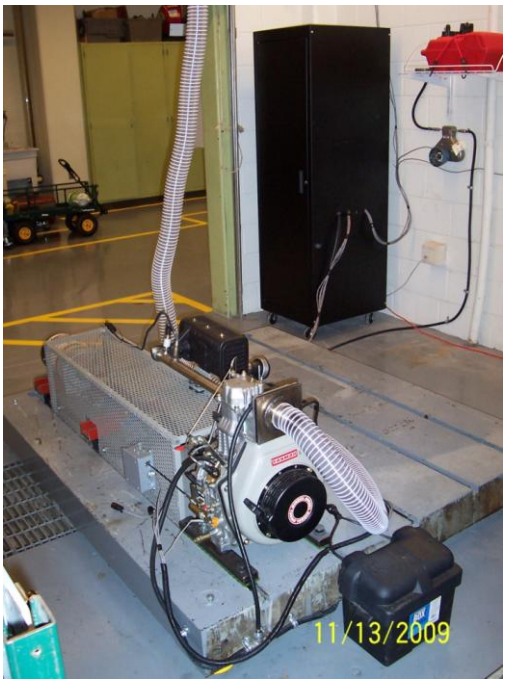

Figure 11. Feedstock -to-Tailpipe Initiative's single-cylinder biodiesel test stand.

The first section involves measurement of the environmental conditions. To have consistent and repeatable data, the barometric pressure, temperature, and relative humidity are being monitored in order to determine their influence on different biodiesel fuels via performance and emissions. This area of data acquisition uses two Omega EWS sensors, as seen in Figure 12, in order to obtain these three values. In particular, an Omega EWS-BP-A measures the barometric pressure from 20.8 to 32 inches of Mercury (in_{Hg}) (10.2 to 15.7 psia) with an accuracy of ± 1.0% of the range. It outputs either a voltage or current signal that is captured by the cRIO system and costs $145; currently the CRIO system is monitoring the voltage via a NI-9201 module. The EWS-BP-A is pre-calibrated by the manufacturer in order to ensure repeatability and easy installation

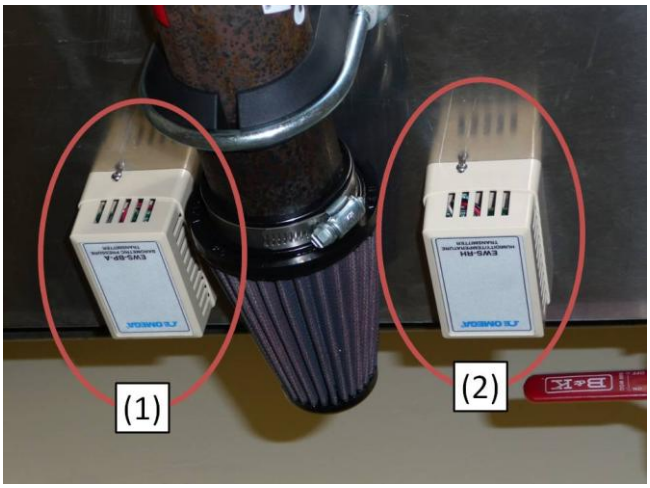

Figure 12. Environment sensors: (1) EWS-BP-A for barometric pressure and (2) EWS-RH for temperature and relative humidity.

The test condition barometric pressure requires an adjustment of the signal from the EWS-BP-A via the following calibration equations in either the voltage mode [4],

$$P_{barometric}\left(psia\right)=\frac{\left(15.72\ psia-10.20\ psia\right)}{\left(5V-1V\right)}\left(V_{in}-1V\right)+10.2\ psia=\frac{5.52\ psia}{4V}\left(V_{in}-1V\right)+10.2\ psia \quad (1)$$

or the current mode [4]:

$$P_{barometric}\left(psia\right)=\frac{\left(15.72\ psia-10.20\ psia\right)}{\left(0.020\ A-0.004\ A\right)}\left(I_{in}-0.004\ A\right)+10.2\ psia=\frac{5.52\ psia}{0.016\ A}\left(I_{in}-0.004\ A\right)+10.2\ psia \quad (2)$$

The Omega EWS-RH measures both temperature and relative humidity with ranges of -15 to 60°C (5 to 140°F) and 5 to 95% relative humidity respectively, with an accuracy of ±1.4°C for temperature and ± 4% for relative humidity while costing $145. Current monitoring of the EWS-RH happens via a NI-9201 module with the calibration curves given in the following equations through either voltage [5],

$T_{env}(F)=\frac{(140F-5F)}{(5V-1V)}(V_{in}-1V)+5F=\frac{135F}{4V}(V_{in}-1V)+5F$	(3)
$RH(\%)=\frac{(100\ \%-0\ \%)}{(5V-1V)}(V_{in}-1V)+0\ \%=\frac{100\ \%}{4V}(V_{in}-1V)$	(4)

or current [5]:

$T_{env}(F)=\frac{(140F-5F)}{(0.020A-0.004A)}(I_{in}-0.004A)+5F=\frac{135F}{0.016A}(I_{in}-0.004A)+5F$	(5)
$RH(\%)=\frac{(100\ \%-0\ \%)}{(0.020A-0.004A)}(I_{in}-0.004A)+0\ \%=\frac{100\ \%}{0.016A}(I_{in}-0.004A)$	(6)

The second section involves the intake air stream comprised of one flow meter and one pressure sensor. A Meriam volumetric Laminar Flow Element (LFE) (Z50MW20-2) measures the airflow rate from zero to 42.033867 scfm (standard ft^3/min at 8 inches of H_2O pressure differential) with an accuracy of 0.75% and costs $1,194. In order to calculate the volumetric flow rate from the LFE, a differential pressure sensor is required.

The pressure sensor selected was an Omega PX277-30D5V sensor, as seen in Figure 13. The PX277 can measure up to a 15 inches of water (in_{H2O}) pressure differential with an accuracy of 1% of the span and costs $195. This sensor can be configured to output either a 0-5 volt or 0-10 volt signal and a variety of unique differential pressure ranges. For this effort, it was configured to provide a 0-10 volt signal over the 0-7.5 inches range of H_2O pressure differential. The voltage is being monitored through a NI-9201 module, which utilizes the following calibration curve [6]:

$P_{diff}\left(in_{H_2O}\right)=\frac{\left(7.5in_{H_2O}-0in_{H_2O}\right)}{(10V-0V)}(V_{in}-0V)+0in_{H_2O}=\frac{7.5in_{H_2O}}{10V}V_{in}$	(7)

In conjunction with the PX277, two environmental sensors (EWS-BP-A and EWS-RH, previously shown in Figure 12) are used to convert the standardized volumetric flow rate to a standardized mass flow rate that is needed for air-to-fuel ratio calculations.

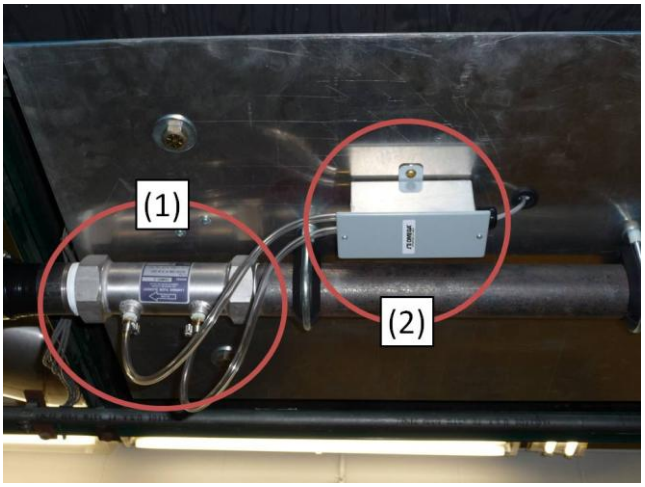

Figure 13. Intake air system: (1) Meriam Laminar Flow Element and (2) Omega PX277 differential pressure sensor for air mass flow rate.

Of importance, every manufacturer of differential pressure transducers uses unique water density standards. Therefore, the first step is to adjust the measured differential pressure to a water density at 4°C needed for the LFE volumetric flow calculation presented later. Since the PX277 is calibrated at a water density of 4°C, the following equation is not necessary. But if a different differential pressure was used with the standard of water density being 20°C, then adjustment involves the following [7]:

$$P_{diff\,@4^\circ C}\left(in_{\mathrm{H_2O}}\right)=\frac{\rho_{device}\left(\frac{lb}{ft^3}\right)}{\rho_{\mathrm{H_2O}@4^\circ C}\left(\frac{lb}{ft^3}\right)}P_{diff}\left(in_{\mathrm{H_2O}}\right)$$
$$=\frac{\rho_{\mathrm{H_2O}@20^\circ C}\left(\frac{lb}{ft^3}\right)}{\rho_{\mathrm{H_2O}@4^\circ C}\left(\frac{lb}{ft^3}\right)}P_{diff}\left(in_{\mathrm{H_2O}}\right)=\frac{62.316\,\frac{lb}{ft^3}}{62.426\,\frac{lb}{ft^3}}P_{diff}\left(in_{\mathrm{H_2O}}\right) \quad (8)$$

Using this adjusted differential pressure, the LFE volumetric flow rate can now be determined from the following manufacturer's curve [7]:

$$\dot{Q}_{air}\left(cfm\right)=5.57399P_{diff\,@4^\circ C}-3.99692\times10^{-2}P^2_{diff\,@4^\circ C} \quad (9)$$

This flow rate can then be normalized to actual runtime conditions utilizing the viscosity of the air [7]:

$$\dot{Q}_{air}\left(acfm\right)=\frac{\mu_{std}\left(micropoise\right)}{\mu_f\left(micropoise\right)}\dot{Q}_{air}\left(cfm\right)=\frac{182.903\,micropoise}{\mu_f\left(micropoise\right)}\dot{Q}_{air}\left(cfm\right) \quad (10)$$

where the viscosity is a function of the temperature of the air as follows [7]:

$$\mu_f\left(micropoise\right)=\left(\frac{\mu_{wet}}{\mu_{dry}}\right)\left[\frac{14.58\cdot T\left(K\right)^{\frac{3}{2}}}{110.4+T\left(K\right)}\right] \quad (11)$$

In the above equation, the viscosity of the flow is solved using the temperature measured by the EWS-RH (units: Rankine) and ratio of viscosity of wet/dry air that is a function of relative humidity and

temperature measured by EWS-RH (units: % and Fahrenheit). This ratio of viscosity is given in a table in the manual [7] and implemented in LabView using a 2D interpolation Virtual Instrument (VI) code structure that provides a real-time solution for any given temperature and relative humidity.

With the actual volumetric flow rate solved, the standard volumetric flow rate can be found using the following equation [7]:

$$\dot{Q}_{air}\left(scfm\right)=\left[\frac{T_{std}\left(R\right)}{T_{f}\left(R\right)}\right]\left[\frac{P_{f}\left(in_{\mathrm{Hg}}\right)}{P_{std}\left(in_{\mathrm{Hg}}\right)}\right]\left(\frac{\rho_{wet}}{\rho_{dry}}\right)\dot{Q}_{air}\left(acfm\right)=\left[\frac{529.67\,\mathrm{R}}{T_{f}\left(R\right)}\right]\left[\frac{P_{f}\left(in_{\mathrm{Hg}}\right)}{29.92in_{\mathrm{Hg}}}\right]\left(\frac{\rho_{wet}}{\rho_{dry}}\right)\dot{Q}_{air}\left(acfm\right) \quad (12)$$

Similar to equation (11), equation (12) uses three ratios to standardize the flow: temperature, pressure, and density. The temperature ratio comes from the measured value provided by the EWS-RH unit (units: Rankine). The pressure ratio uses the measured value from the EWS-BP-A (units: psia); whereas, the density ratio is a function of temperature and relative humidity (units: Fahrenheit and %) which are measured by the EWS-RH. The density ratio information is given in the manual as a table with a LabView 2D interpolation VI utilized by the author for solution [7].

Conversion from a standard volumetric flow ratio to a mass flow rate happens via the following equation [8]:

$$\dot{m}_{air}\left(\frac{lbm}{min}\right)=\rho_{std}\left(\frac{lbm}{ft^{3}}\right)\dot{Q}_{air}\left(scfm\right)=\left(0.074887\frac{lbm}{ft^{3}}\right)\dot{Q}_{air}\left(scfm\right) \quad (13)$$

In particular, Meriam uses the National Institute of Standards and Technology (NIST) dry air standard of 70°F (21.1°C) and 29.92 inches of mercury (Hg) (101.3 kPa) [7]. Therefore, the standardized density present in equation (13) is given as 0.074887 lbm/ft^3.

The third section includes monitoring the fuel stream using an Emerson coriolis mass flow meter; Elite CMF-010 with a 2500 Model transmitter. The CMF-010 can be seen in Figure 14 and the 2500 Model transmitter can be seen later in Figure 20. This flow meter is the best option for testing different fuels as it can determine the mass flow rate of the fuel, the temperature, and density simultaneously. This is because it incorporates the Coriolis effect present in fluid mechanics in order to determine the flow rate, density, and temperature of any given fuel. Other types of flow meters are limited to a single calibratable fuel and can only provide flow rates. An example of another option would be an oval-gear flow meter, which is a positive displacement pump. Using this pump, while the flow rates between fluids may stay relatively the same, in order to obtain a mass flow rate requires another sensor for calculation of the average density of the fluid. This reduces the accuracy of the system and adds to its complexity. The CMF-010 can measure up to 22.67 g/s of fuel, has an accuracy of ± 0.25% of the value, and costs $5,648 [9]. It is important to note that while it can measure up to 22.67 g/s of fuel, the Yanmar engine used only outputs a maximum mass flow rate of 0.60 g/s. However, the flow meter utilized is the smallest coriolis meter possible and that is why it was chosen.

Figure 14. Fuel flow meter: MicroMotion CMF-010 coriolis flow meter.

The 2500 Model transmitter, costing $2,206, calculates the flow, density, and temperature of the fluid. It can send either an analog signal captured by the cRIO hardware or a digital signal. This researcher found during the development of this system that directly reading the digital signal output reduced the response time of the cRIO system. This can be explained by how Field-programmable Gate Array (FPGA) programming is accomplished using LabView. For any non-communication modules, all of the channels and modules can be read at one instance or simultaneously, as shown in Figure 15 (number 3). When using communication modules, data streams to it independently of the rest of the signals. Moreover, these signals are read through each port in series, as shown in Figure 15 (numbers 1 and 2). Therefore, in order to communicate with a device in this manner, it must receive and send data before the code will move forward. In addition, the complete FPGA protocol has to be developed in a series manner as seen in Figure 15 where below the orange line represents the FPGA read/write protocol. An analogy would be if people had to enter a subway train through one set of doors instead of multiple causing everyone to wait.

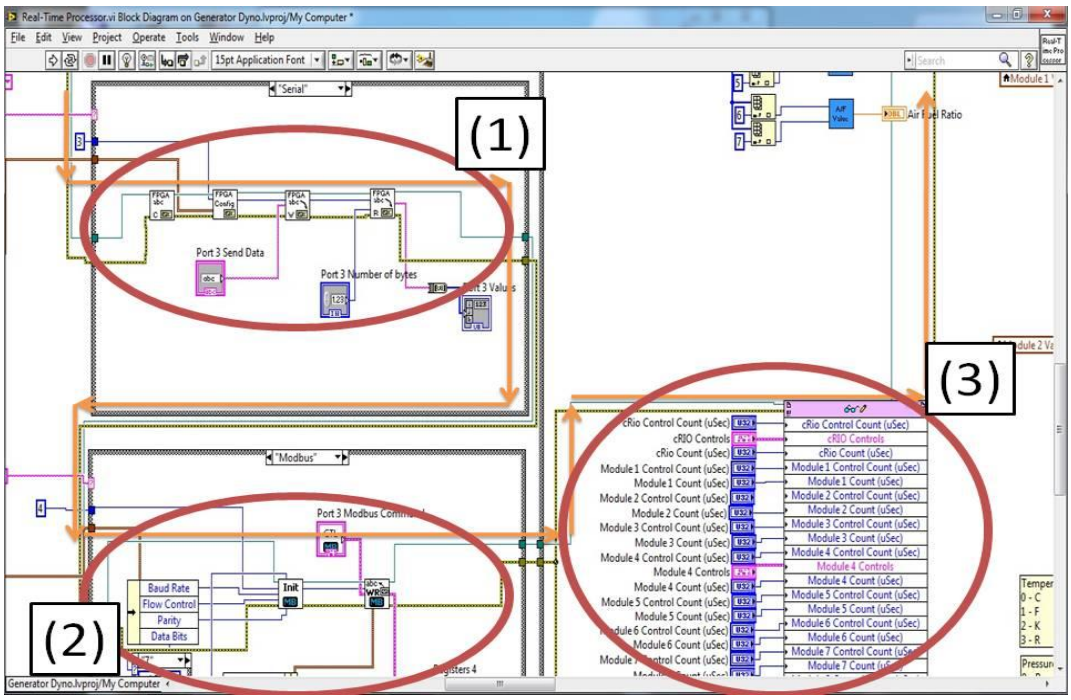

Figure 15. LabView internal code for FPGA programming: (1) Serial protocol, (2) Modbus protocol, and (3) non-communication modules.

For example, one serial communication and one analog voltage module would be developed to first read port 1 of the serial module then ports 2, 3, and 4 of the voltage module. This requires reading the serial module first before the analog voltage module can be read. Therefore, if each port takes a half a second to process and respond, the complete system response is now over two seconds per one sample taken. For the digital signal of the MicroMotion transmitter, the company uses a Modbus serial protocol that reads and process thousands of values resulting in an half a second to a second of response time. Hence, in order to increase the system response, the analog output method (current signal) was chosen. This is being monitored via a NI-9203 module in order to obtain the density and mass flow rate of the fuel through the following calibration curves [9]:

$\rho_{fuel}\left(\frac{kg}{m^3}\right)=\frac{\left(1000\frac{kg}{m^3}-0\frac{kg}{m^3}\right)}{\left(0.020\,A-0.004\,A\right)}\left(I_{in}-0.004\,A\right)+0\frac{kg}{m^3}=\frac{1000\frac{kg}{m^3}}{.016\,A}\left(I_{in}-0.004\,A\right)$	(14)
$\dot{m}_{fuel}\left(\frac{g}{s}\right)=\frac{\left(1\frac{g}{s}-0\frac{g}{s}\right)}{\left(0.020\,A-0.004\,A\right)}\left(I_{in}-0.004\,A\right)+0\frac{g}{s}=\frac{1\frac{g}{s}}{.016\,A}\left(I_{in}-0.004\,A\right)$	(15)

From this information and equation (13), the critical property of air-to-fuel ratio can be calculated in order to help normalize the performance and emissions of different fuels [10]:

$AF=\frac{\dot{m}_{air}\left(\frac{g}{s}\right)}{\dot{m}_{fuel}\left(\frac{g}{s}\right)}$	(16)

The fourth section covers the naturally aspirated, air-cooled Yanmar L100V single-cylinder engine. This engine uses a mechanical high-pressure direct-injection fuel system that injects fuel 15.5° before top dead center along with a self-adjusting fuel pump. This pump uses momentum from the camshaft and springs in order to dynamically adjust the flow rate of the fuel. This engine has a compression ratio of 21.2 with a bore of 86mm, a stroke of 75mm and can produce up to 6,200 watts of power.

With respect to data collection, this engine contains four sensors. The first two sensors are found in the intake manifold in order to measure the temperature and pressure as seen in Figure 16. These sensors are an Omega PX329-030AI pressure transducer and an Omega K-Type (TC-K-NPT) thermocouple. The PX329, costing $175, measures from 0 to 30 psia, accurate within ±0.25% of the span, while outputting a current signal captured by the cRIO hardware (NI-9203 module) and calibrated using the following curve [11]:

$$P(psia) = \frac{(30\,psia - 0\,psia)}{(0.020\,A - 0.004\,A)}(I_{in} - 0.004\,A) + 0\,psia = \frac{30\,\text{psia}}{0.016\,A}(I_{in} - 0.004\,A) \quad (17)$$

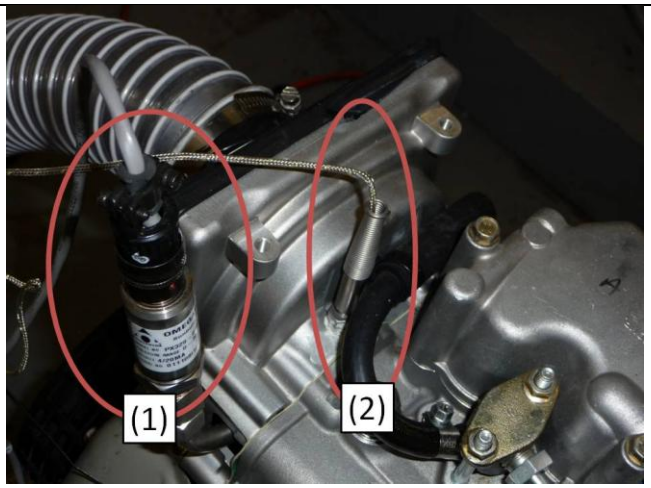

Figure 16. Intake sensors: (1) Omega PX329 for intake pressure and (2) Omega K-type thermocouple for intake pressure.

The Omega K-type thermocouple measures temperatures up to 650°C (1200°F) and costs $34 [12]. The information from this sensor is transmitted via an extension thermocouple wire into a NI-9211 module that monitors the millivolt voltage differential output. Thermocouples have multiple curves for different temperature ranges and require special referencing in order to convert the voltage signal to a temperature value. National Instruments has developed special VI's that convert the voltage signal to an actual temperature value based on the hardware utilized in the specific NI-9211 module.

The last two sensors for the engine are found in the oil pan and reservoir, as seen in Figure 17. Since oil is a critical component for engine operation, its pressure and temperature are monitored in order

to ensure that the engine does not fail. The sensors utilized for this task are an Omega PX329-1KGI pressure transducer and an Omega KQXL K-type thermocouple probe. This PX329 maintains the same percent accuracy and current signal capabilities as before, but this specific version measures between 0 to 1000 psig because of the higher pressures seen in the oil system. The information from the sensor is calibrated to an actual pressure via the following [11]:

$$P(psia) = \frac{(1000\ psia - 0\ psia)}{(0.020\,A - 0.004\,A)}(I_{in} - 0.004\,A) + 0\ psia = \frac{1000\,\text{psia}}{0.016\,A}(I_{in} - 0.004\,A) \quad (18)$$

The KQXL thermocouple for the oil system has the same properties and calibration curve as explained before but costs $30.

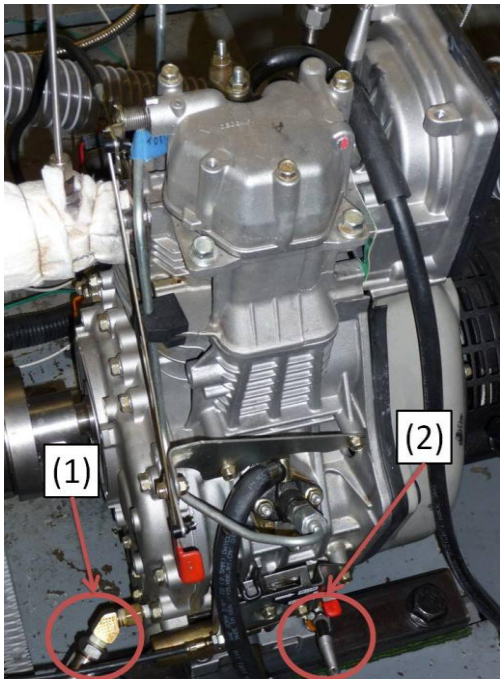

Figure 17. Engine sensors: (1) Omega PX329 for oil pressure and (2) Omega K-type thermocouple for oil temperature

The fifth section entails the exhaust stream that includes an insulated stainless steel pipe with two temperature sensors and a pressure sensor, as seen in Figure 18. The temperature sensors are both KQXL K-type thermocouples that are placed at the beginning (Figure 18: Number 1) and end of the pipe (Figure 18: Number 3) in order to monitor the exhaust temperature. The first temperature sensor measures the fluctuations in the exhaust gas leaving the cylinder right after the exhaust valve. This provides a decent indication of combustion timing of the different fuels depending on relative temperature levels; hotter indicates later combustion due to a reduced amount of time for heat transfer losses. The second sensor downstream designates an average exhaust temperature (pressure fluctuations are largely normalized) helpful in determining when steady-state conditions are reached. The pressure sensor is a PX329-030AI,

which is the same version as found in the intake and can measure up to 30 psia, costs $175, and has a calibration curve given via equation (17).

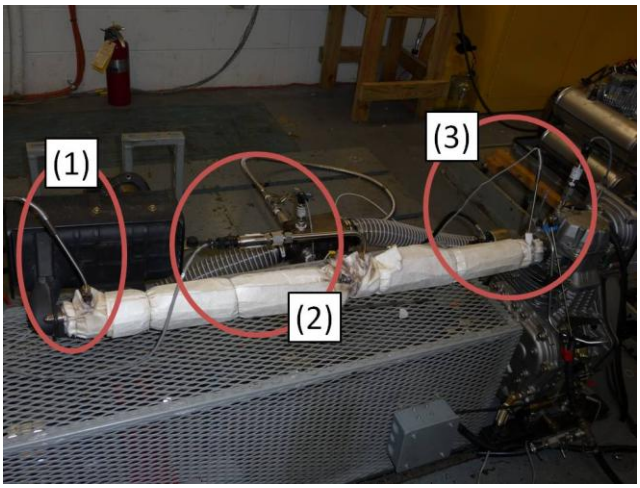

Figure 18. Exhaust pipe: (1) Downstream K-type thermocouple, (2) Pressure sensor, and (3) Upstream K-type thermocouple.

The final section involves the load cell of the engine, which can be used to investigate the different performance and emission characteristics across its operating range. The engine is currently connected to aftermarket 5000-watt AC generator head that was purchased from Northern Tools with resistance heaters acting as the power sink. To ensure redundancy in this system, two sensors are being used. The first sensor is a Futek TRS705 torque sensor, shown in Figure 19, which can measure up to ±20 N-m of rotational torque and costs $3,175 [13]. It is placed between the engine and the generator head in order to ensure the complete power output from the engine is being obtained. It outputs a voltage signal to the cRIO (NI-9201 module) that indicates relative power versus voltage with the calibration curve as [13]:

$$\tau\left(N\cdot m\right)=\frac{\left(20\,N\cdot m-0\,N\cdot m\right)}{\left(5V-0\,\mathrm{V}\right)}\left(V_{in}-0V\right)+0\,N\cdot m=\frac{20\,N\cdot m}{5\,V}V_{in} \quad (19)$$

The second sensor is a Woodward power meter that measures the voltage and current draw from the heaters in order to determine the energy draw. The power meter outputs two current signals to a NI-9203 module in order to monitor the power and frequency of the system. These signals are set to indicate power between 0 to 6,000 watts and frequencies between 55 to 65 Hertz as follows [14]:

$$P\left(watts\right)=\frac{\left(6000\,watts-0\,watts\right)}{\left(0.020\,A-0.004\,A\right)}\left(I_{in}-0.004\,A\right)+0\,psia=\frac{6000\,watts}{0.016\,A}\left(I_{in}-0.004\,A\right) \quad (20)$$

$$f\left(Hz\right)=\frac{\left(65\,Hz-55\,Hz\right)}{\left(0.020\,A-0.004\,A\right)}\left(I_{in}-0.004\,A\right)+55\,Hz=\frac{10\,Hz}{0.016\,A}\left(I_{in}-0.004\,A\right)+55\,Hz \quad (21)$$

From this information, a percent loading of the engine can be calculated. Having the percent load allows researchers to explain trends in fuel economy, brake specific fuel consumption, and brake specific emissions for differential fuels.

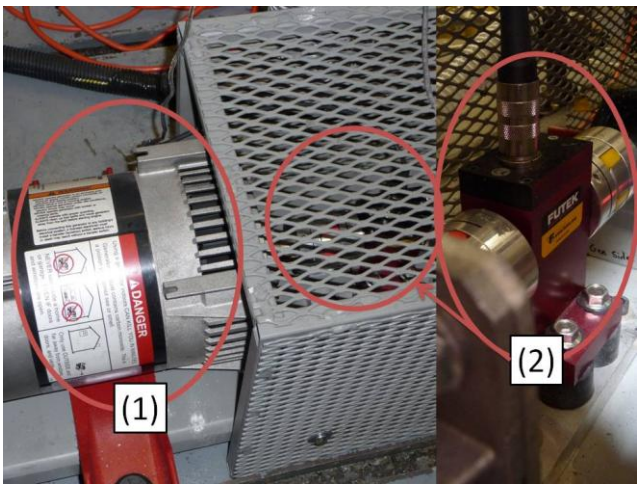

Figure 19. Engine load cell: (1) Northern Tool 5000-watt AC generator head and (2) Futek TRS torque sensor.

All of these sensors are brought into a data acquisition cabinet in order to monitor and record the values, as seen in Figure 20. This cabinet contains the cRIO hardware and modules, along with the power supplies for the equipment. The cRIO system (Figure 20: Number 1) uses a Real-time controller (cRIO-9014), an 8-slot chassis (cRIO-9114), along with data collection and control modules. For the reader's reference, a module is an interchangeable device added or removed from the cRIO chassis. This allows a modular approach to be taken ensuring flexibility both now and in the future. Currently seven modules are in use: 2x 4-channel Thermocouple modules (NI-9211), 1x 4-port Serial (RS-232) Module (NI-9870), 1x 8-channel High-Speed digital input/output module (NI-9401), 2x 8-channel current module (NI-9203), and 1x 8-channel voltage module (NI-9201). Of importance, this setup took a year to complete along with multiple iterations of the code in order to reach the current accurate and highly repeatable setup. Visual description of the data collected is presented via a LabView graphical user-interface provided in Figure 21.

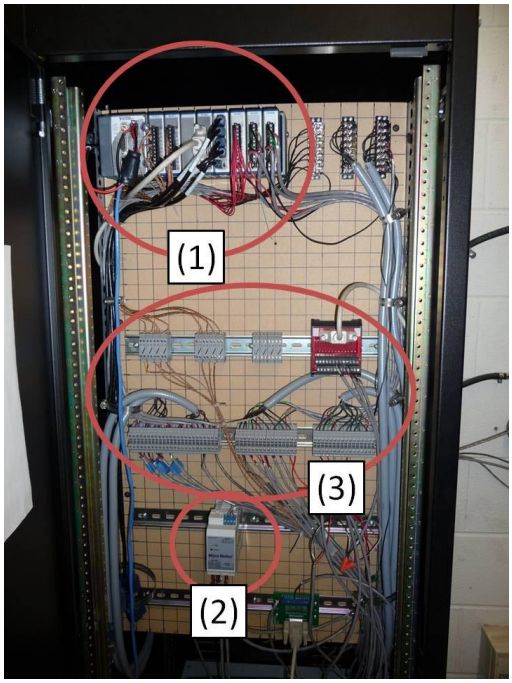

Figure 20. Data acquisition cabinet: (1) National Instruments CompactRIO system, (2) MicroMotion 2500 model transmitter, and (3) Quick disconnect terminals.

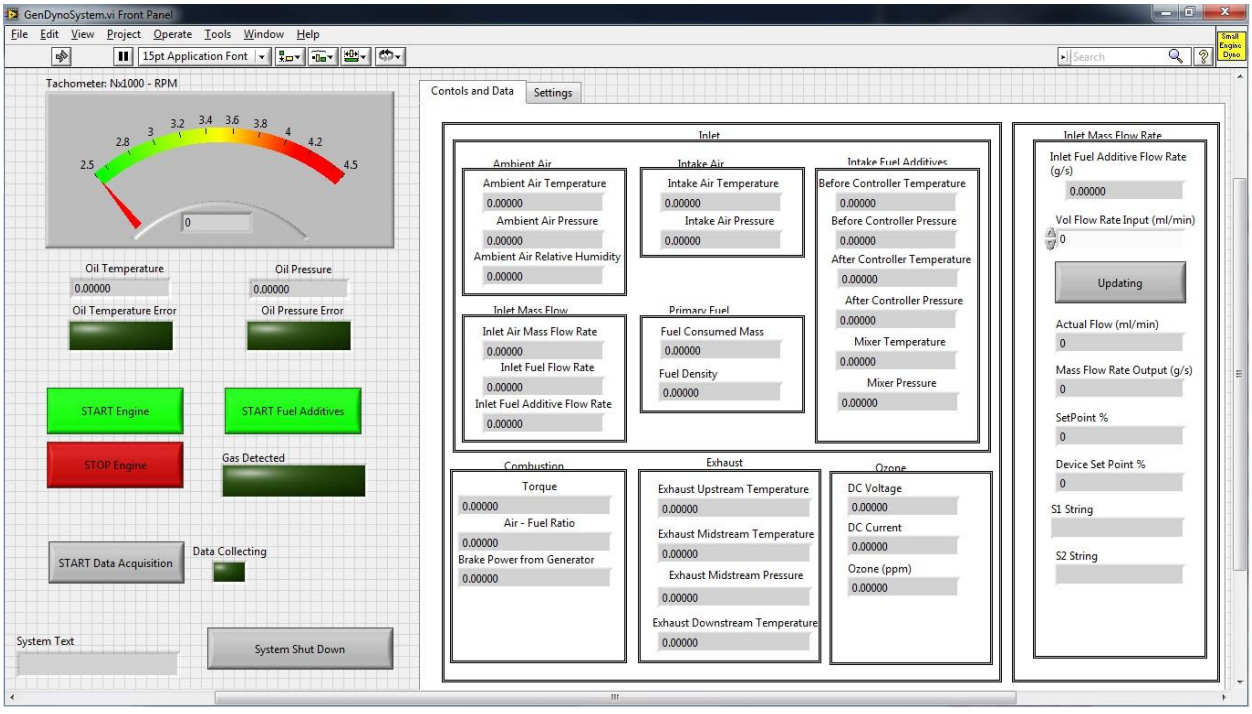

Figure 21. Test stand data acquisition program developed using National Instruments LabView software.

With the data collected and recorded in the LabView program, values such as fuel conversion efficiency and brake specific fuel consumption can be calculated. Fuel conversion efficiency is the ratio,

or percent of combusted fuel that leaves the engine as useful work output. The following equation describes the calculation of the fuel conversion efficiency [10]:

$$\eta_f = \frac{W_{out}}{Q_{in}} = \eta_{th}\eta_c \quad (22)$$

which is a function of the thermal efficiency (η_{th}), which relates the actual work per cycle to the amount of fuel chemical energy released in the combustion process, and the combustion efficiency (η_c) which is the fraction of fuel energy supplied to the engine that is liberated in the combustion process. In this equation, the indicated work (W_{out}) can be found as a function of torque (N·m) and engine speed (rpm) that are measured.

$$W_{out}(W) = \tau(N \cdot m)\left(\frac{2\pi}{rev}\right)\frac{N(rpm)}{60\left(\frac{\text{sec}}{\text{min}}\right)} \quad (23)$$

The second term (Q_{in}) in equation (22) is the total amount of energy input by the fuel or fuels. This can be solved using the following equation by inputting the lower heating value of the fuel (Q_{lhv}), and taking the measured fuel flow rate $(\dot{m}_f)$:

$$Q_{in}(W) = \dot{m}_f\left(\frac{kg}{s}\right)Q_{lhv}\left(\frac{kJ}{kg}\right)\left(\frac{1000\,W}{1\,kW}\right) \quad (24)$$

An example from this test stand is as follows: Found parameters include a measured fuel flow rate of 0.461 g/s of Ultra-Low Sulfur Diesel (aka. No. 2 Diesel), engine speed was 3528.8 rpm, and a torque output of 15.71 N-m. The indicated work can then be computed as 5805.4 W with an energy input of 19,721.6 W using the lower heating value of diesel as 42,780 kJ/kg. This resulted in a fuel conversion efficiency of 29.437%

Combustion efficiency describes the liberation of fuel chemical energy during the combustion process. Hence, it denotes how much initial added energy is actually available to move the piston and perform work. Its computation uses the exhaust species' constituents that have energy, like CO and HC, and compares this amount of energy to the input fuel energy [10]:

$$\eta_c = 1 - \frac{\sum_{j=1}^{n} X_j \cdot Q_{lhv,j}}{\sum_{i=1}^{n}\dot{m}_{f,i}Q_{lhv,i} \Big/ \left(\sum_{i=1}^{n}\dot{m}_{f,i} + \dot{m}_a\right)} \quad (25)$$

where *i* represents the different input fuels, *j* represents the emissions species, X_j is the measured emissions fraction, and Q_{lhv} is the lower heating value of emissions and fuels. Note, for this calculation, the lower heating value used for HC emissions was estimated at 44,700 kJ/kg-K. Dividing the fuel conversion efficiency by the combustion efficiency results in the thermal efficiency [10]:

$$\eta_t = \frac{\eta_f}{\eta_c} \quad (26)$$

This parameter relates the actual work produced to the amount of fuel chemical energy released in the combustion process.

The brake specific fuel consumption (BSFC) is a normalized value that can be used to relate the fuel consumed by an engine to its indicated work output (W_{out}) [10]:

$$BSFC\left(\frac{g}{kW \cdot hr}\right) = \frac{\dot{m}_f\left(\frac{g}{s}\right) \cdot 3600\left(\frac{sec}{hr}\right)}{W_{out}(W) \cdot \left(\frac{1\,kW}{1000\,W}\right)} \quad (27)$$

It is preferred to have a lower value of BSFC as less fuel is utilized to create a given amount of power, and from the example of before, the BSFC during the test would equal 285.9 g/kW-hr. This might appear high for a diesel engine; however, since the engine does not include boosting via a turbocharger, this value is reasonable for naturally aspirated diesels [10].

Another variable that provides indicative values for an engine is the volumetric efficiency that characterizes how efficiently the engine brings in air. Calculation of this value includes the measured air mass flow rate $(\dot{m}_a)$ divided by the theoretical air mass flow rate the engine could bring in given a standard pressure and temperature [10]:

$$\eta_{th} = \frac{\dot{m}_a\left(\frac{g}{s}\right)}{2 \cdot \rho_a\left(\frac{kg}{m^3}\right) \cdot \left[\frac{N(rpm)}{60\left(\frac{s}{min}\right)}\right] \cdot V_d\left(m^3\right) \cdot 1000\left(\frac{g}{kg}\right)} \quad (28)$$

The density (ρ_a) is solved using the pressure and temperature of the environment (aka ambient) and the gas constant for air (R = 286.9865 J/kg-K), as shown in equation below [15]:

$$\rho_a = \frac{P_{env}\left(\frac{N}{m^2}\right)}{286.9865\left(\frac{J}{kg \cdot K}\right) \cdot T_{env}(K)} \quad (29)$$

The engine speed (N) is measured and the volumetric displacement (V_d) is determined for the engine based on the bore (b) and stroke (s) previously mentioned [10]:

$$V_d = \frac{\pi b^2}{4} s \quad (30)$$

For this test stand, the engine displacement volume is 435 cm^3 or 4.35E-04 m^3. Using the same example as before, the air mass flow rate was found to be 10.996 g/s, the environmental pressure and temperature were 98080.4 Pa and 302.5 K, respectively, resulting in a density of 1.1298 kg/m^3 and theoretical air flow rate of 14.553 g/s. With the same engine speed as before, the volumetric efficiency was found to be 76.09%. Traditionally for diesel engines, the volumetric efficiency ranges from 80% to 90% and higher. For this engine, the lower volumetric efficiency can be attributed to an internal exhaust

gas recirculation (EGR) passage present within the cylinder head. Depending on the pressure difference between the exhaust pipe and the intake passage, the flow of EGR will vary between tests. This is because the engine manufacturer used the principles of an orifice flow meter in order to regulate the EGR level (seen later in equation (31)). Future endeavors involve blocking off the EGR passage and fabricating an external system in order to test for the influence of different levels and temperatures of EGR on diesel and biodiesel combustion.

The majority of the sensors are used to monitor the engine and determine variation between tests. The values that are monitored are the environmental conditions, engine oil pressure and temperature, and exhaust pressure and temperatures. As explained before, some of the sensors are meant for safety features and other are for repeatability. The main measurement values used for analysis are the intake air mass flow rate, fuel mass flow rate, engine speed, torque, and load. From these variables, normalized values provide a methodology of comparing and contrasting different fuels.

2.2.2. Future Improvements

Currently, this system is undergoing two major upgrade projects to be performed by succeeding students. The first upgrade project involves replacing the generator head with a DyneSystems 12HP Alternating Current regenerative dynamometer. This system will allow for a pre-set or more accurate loading in order to test the differential fuels replacing the current resistance heater approach. This project is targeted for completion by the end of the summer. The second upgrade project includes changing the mechanical injection system to a common-rail fuel injection system with hardware from Bosch Motorsport. The advisor of the author is working on obtaining the needed materials and plans are underway for implementation by the end of 2011. In both cases, the data acquisition system developed by the author will be the foundation for these efforts by linking the respective upgrades through the cRIO hardware and LabView software.

2.3. Reformate Assisted Biodiesel Combustion Project

For this project, the researcher had the opportunity to execute and complete all phases of the PMBOK. The objective was to design a fuel additive system for the single-cylinder engine test stand described in the previous section. This additive system utilizes the reformate (hydrogen rich syngas) mixture created in the SynGas rig reformer to positively affect the combustion of biodiesel by minimizing the fuel consumption difference between diesel and biodiesel. Note that because biodiesel has a lower energy content (37 vs. 44 MJ/kg_{fuel}), its brake specific fuel consumption increases causing a larger cost to the consumer; e.g., more fuel is needed to provide the same power. By adding a hydrogen rich mixture into the intake of the single-cylinder engine, effectively replacing air with a second fuel, this should reduce the fuel consumption of biodiesel making it more advantageous as a renewable fuel.

This project would not have been possible without the previous efforts on both the SynGas rig and single-cylinder setup. This allowed for a complete understanding of reformate creation and single-cylinder experimentation that allowed this project to be seen through to completion. Currently, the author is submitting this research for publication with the journal submission given in Paper 3.

2.3.1. System

This author implemented a continuous manifold injection method shown in Figure 22 versus other fuel induction methods, such as timed manifold injection or direct-injection. As the paper in the later section explains in detail, hydrogen has been researched for a few decades as a replacement fuel for petroleum based derivatives. In brief, hydrogen can provide for the lowest amount of hazardous emissions and does not release any greenhouse gases. Moreover, it is potentially an energy dense source if storage issues can be alleviated. However, hydrogen combustion has its limitations as the majority of the research found that combustion is limited by either pre-ignition or knocking. Moreover, due to the near constant volume combustion characteristics of hydrogen, it is more apt to have an increased amount NO_x emissions.

Figure 22. Fuel additive system for the single-cylinder engine test stand.

The complete fuel additive system is comprised of a Matheson Gas Series 3210 Two-Stage Stainless Steel High-Purity regulator (Figure 23) that is connected to a Brooks Instrument SLA5850 thermal mass flow controller (Figure 24). The Brooks thermal mass flow controller is calibrated for a 50% H_2/50% CO_2 mixture and a flow range from 0 to 20 splm (standard liters/minute) with a inlet pressure of 75 psig and pressure drop of 50 psig while costing $2,100. This controller uses an orifice plate in order to measure the flow rate as described in following equation [16]:

$$\dot{Q}_{actual}\left(\frac{mL}{min}\right)=C(-)\cdot Y(-)\cdot A_2\left(m^2\right)\cdot\sqrt{2\cdot\rho_1\left(\frac{kg}{m^3}\right)\cdot\left(P_1-P_2\right)(Pa)} \quad (31)$$

where C is the orifice flow coefficient, Y is an expansion factor, A_2 is the cross-section area of the orifice, P_1-P_2 is the pressure differential for the orifice, and ρ_1 is density of the flow upstream. The expansion factor is a function of unchoked flow [16]:

$$Y = \sqrt{r^{2/k}\left(\frac{k}{k-1}\right)\left(\frac{1-r^{\frac{k-1}{k}}}{1-r}\right)\left(\frac{1-\beta^4}{1-\beta^4 r^{\frac{2}{k}}}\right)} \quad \beta > 0.25 \tag{32}$$

and choked flow [16]:

$$Y = \sqrt{r^{2/k}\left(\frac{k}{k-1}\right)\left(\frac{1-r^{\frac{k-1}{k}}}{1-r}\right)} \quad \beta \leq 0.25 \tag{33}$$

where β is the ratio of the orifice hole diameter to pipe diameter, r is the pressure ratio of the orifice, and the k is the ratio specific heats.

In cases when β is greater than 0.25, equation (32) is valid, otherwise equation (33) is valid. Brooks uses a modified version of this equation via the law of conservation of energy and the orifice equation, equation (31), in order to solve for the flow rate based on the energy added to the sampling stream of their device. For this, this researcher chose to use the large pressure drop of 50 psig for two reasons. This allows for a wider flow range than a lower pressure drop as equation (31) demonstrates. In addition, equation (31) describes that the mass flow rate is a function of the density into the controller; hence, a lower inlet pressure would result in a lower maximum mass flow rate adding to its accuracy given the low flow conditions of the experimental setup. Note that a slight positive pressure on the outlet flow is added as a safety feature in order to prevent any air from flowing back towards the controller.

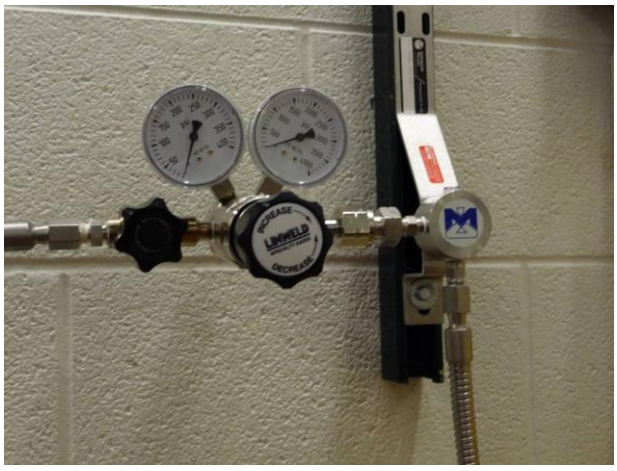

Figure 23. Fuel additive system: Matheson Gas series 3210 Two-Stage stainless steel high-purity regulator.

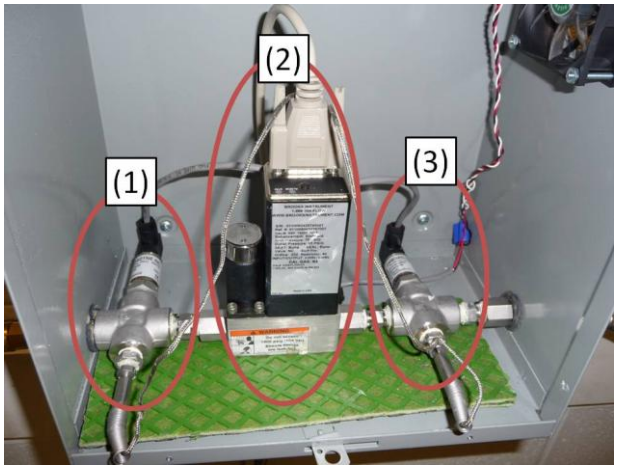

Figure 24. Fuel additive system: (1) Downstream pressure and temperature sensor, (2) Brooks thermal mass flow controller, and (3) Upstream pressure and temperature sensors.

The flow controller has two options for control through either an analog voltage signal or a digital RS-485 connection. Because Brooks Instruments developed a LabView library for this controller (aiding in its initial choice), this system was configured to be controlled digitally. In order to accomplish this, a RS-485 to RS-232 converter (Omega OM-CONV-SER, $25) with a RS-232 to Serial Adapter (IOGear GUC232A, $30) was used to communicate with a network-based USB hub (IOGear GUIP204, $100). The IOGear equipment was on loan and has been removed from the setup. To facilitate a re-connection to this system, a dedicated rack mounted computer is required to read and process the data from the flow controller or to redevelop the original testing system. This effort will require a Serial-to-USB adapter, and the code will need to be modified to include LabView Network Stream functions in order to communicate between multiple computers and LabView programs. These stream functions allow the user to send and receive data over the network using dedicated call names, which would result in faster and uninterrupted display and data collection.

The reason a network-based approach was used is from experience with the RS-232 module. As explained in section 2.2.1, the use of a serial connection can restrict the data collection frequency of the cRIO. Most flow meters do not use a simple serial protocol and instead utilize higher-level protocols, such as Modbus or Profibus [9, 17, 18], which can have thousands of registries that require reading. In addition, until the flow controller responds to the serial command, the remainder of the FPGA code sits idle. Therefore, this researcher chose to off-load the processing time required to read the flow controller to an independent program through a different communication pathway since Brooks had already developed a LabView library to read and control this device.

As a result, there are three possible methods in order to communicate with and manage the mass flow controller. The first method is through a networked-based USB hub that creates a virtual USB port over the network. In this manner, the LabView library developed by the company can be used as an

independent program. The second method would involve using a dedicated rack mount computer in order to increase the communication speed to the flow controller as the network hub method can be somewhat restricting. The third method would be to work with Brooks and develop a high-speed FPGA library to communicate with the controller. This would overcome the standard half-second delay that most equipment has when using higher-level serial protocols.

The benefit of using the thermal mass flow controller is that this setup can test any fuel additive mixture by simply adjusting constants in our LabView code. The final values are seen on the main tab of the Test Stand Program, shown in Figure 21, and the setup of the flow controller is presented in Figure 25. In order to adjust the mixture type and concentration, the manufacturer provides the following equations and a table of specific heat constants [18]:

$$\dot{Q}_{actual}\left(\frac{mL}{\min}\right)=\left(\frac{GF_{new}}{GF_{old}}\right)\dot{Q}_{device}\left(\frac{mL}{\min}\right) \quad (34)$$

$$GF=\frac{100}{\sum_{i=1}^{n}\left(Y_i/GF_i\right)} \quad (35)$$

where *GF* is the gas factor for any gas listed in the Brooks 5800s Flow Controller Manual (seen in Table 1), *Y* represent the volume fraction of the gas in the mixture, and *i* represents the species. Therefore, Equation (35) is a specific heat ratio function that uses the volumetric fractions to adjust the energy content of the mixture.

Table 1. Brooks Instruments gas factor for thermal mass flow controllers [17].

Gas Species (*i*):	Gas Factor (GF):	Gas Species (*i*):	Gas Factor (GF):
Air	0.998	Methane (CH_4)	0.763
Argon (Ar)	1.395	Nitric Oxide (NO)	0.995
Carbon Dioxide (CO_2)	0.740	Nitrogen (N_2)	1.000
Carbon Monoxide (CO)	0.995	Nitrogen Dioxide (NO_2)	0.785
Helium (He)	1.386	Oxygen (O_2)	0.988
Hydrogen (H_2)	1.008	Water Vapor (H_2O)	0.861

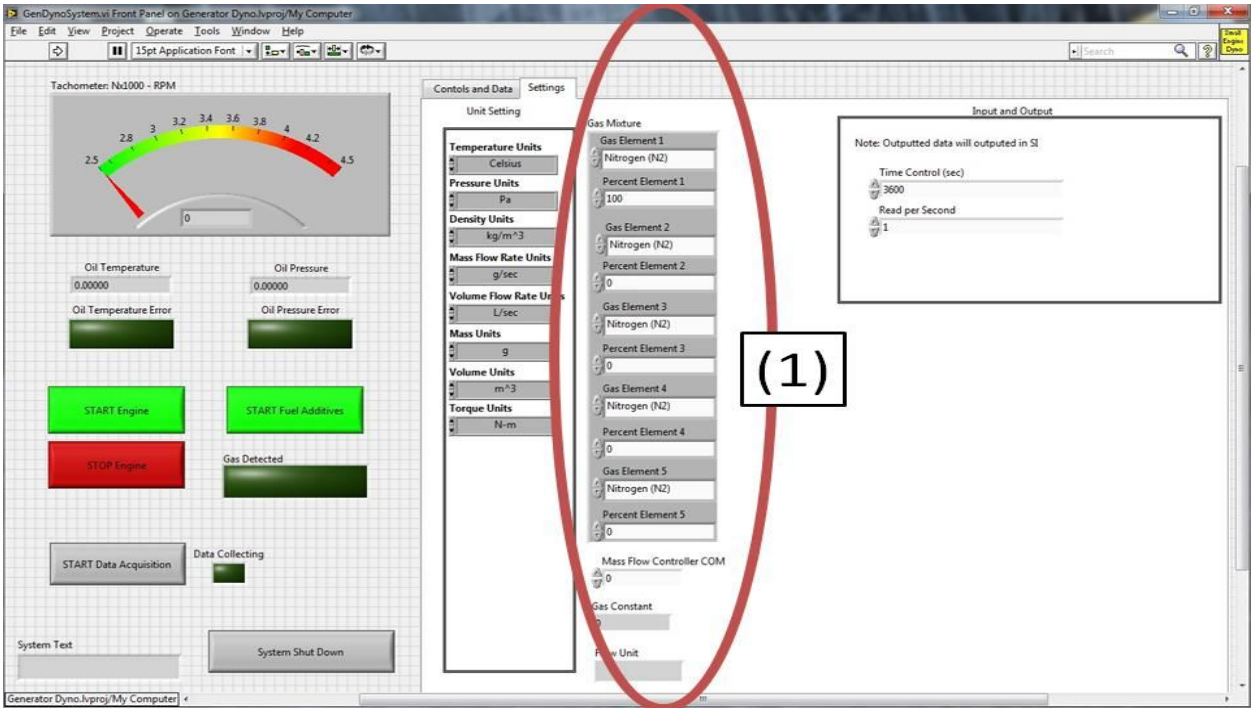

Figure 25. Fuel additive system: Setting tab in test stand program represents the input variables.

Device calibration was completed by the manufacturer using the following mixture combination: 57% H_2 and 43% CO_2. The advantage of pre-calibrating the device reduces the need to calculate equation (34), since most customers do not vary their gas mixture in standard operation. For this test stand, the calibration request resulted in following for the gas factor from equation (34):

$$GF_{old} = \frac{100}{(57/1.008)+(43/0.740)} = 0.872176 \quad (36)$$

Using equations (34) through (36), any gas mixture can be tested. Since the mixture used in the author's efforts involved 57% H_2 and 43% CO, a new gas factor (GF_{new}) was calculated to be 1.002369. From this, the gas factor ratio would be 1.149273; hence, if the device is indicating a flow of 1,000 ml/min, the actual flow of the gas would be 1,1492.73 ml/min. In the future, the author suggests sending the flow controller back to the manufacturer and for re-calibration with just nitrogen. This is because Brooks uses nitrogen as the standard calibration gas, as indicated in Table 1, and calculates all other specific heat in comparison to this value. This would simplify the subsequent calculation by setting GF_{old} equal to one in equation (34).

The complete system complies with the necessary safety standards for hydrogen testing [19]. All of the plumbing is double reinforced stainless steel hoses and all fitting and sensors are made from stainless steel. In addition to the thermal mass flow controller, three Omega PX-319 pressure transducers (unit cost $225) and three Omega K-type thermocouples (unit cost $25) were implemented in order to obtain fluid properties. They are paired up before (upstream, shown in Figure 24: Number 3) and after the

thermal mass flow controller (downstream, shown in Figure 24: Number 1) with a third set added to the mixing chamber in the air intake stream (shown in Figure 26: Number 1). The LabView program controls the flow with the pressure sensors monitored by a NI-9203 module and the thermocouples through a NI-9211 module. The upstream pair uses a PX319-300GI pressure sensor that measures up to 300 psi of gauge pressure with the signal converted using the following calibration curve [11]:

$$P_{mix}\left(psig\right)=\frac{\left(300\ psig-0\ psig\right)}{\left(0.020\,A-0.004\,A\right)}\left(I_{in}-0.004\,A\right)+0\ psig=\frac{300\ psig}{0.016\,A}\left(I_{in}-0.004\,A\right) \quad (37)$$

In order to solve for the density, the pressure needs to be in an absolute units. Therefore, the barometric pressure measured through the EWS-BP-A, explained in section: 2.2.1, is added [16]:

$$P_{mix}\left(psia\right)=P_{mix}\left(psig\right)+P_{barometric}\left(psia\right) \quad (38)$$

Thermocouple usage follows as previously described through the LabView VI methodology.

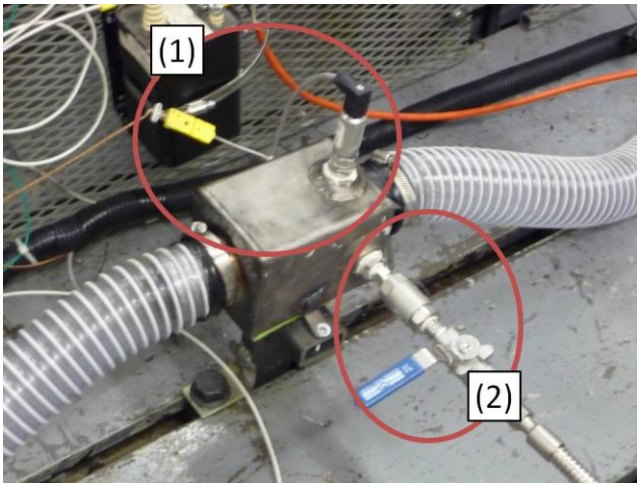

Figure 26. Fuel additive system: Mixing chamber with (1) temperature and pressure sensors and (2) check-valve.

In addition to measuring the pressure and temperature at the upstream location, the density is calculated in order to obtain the mass flow rate of the mixture. To do so, the molar weight of the mixture needs to be found using the same volume fractions used to find the gas factor [15]:

$$MW_{mix}\left(\frac{kg}{kmol}\right)=\sum_{i=1}^{n}\left[MW_i\left(\frac{kg}{kmol}\right)\cdot Y_i\left(\%\right)\right] \quad (39)$$

where MW_i is the species molar weight and the volume fractions are now given in fractional form (e.g., 0.57 instead of 57 for H_2). From this, the gas constant can be determined [15]:

$$R_{mix}\left(\frac{J}{kg\cdot K}\right)=\frac{8314\left(\frac{J}{kmol\cdot K}\right)}{MW_{mix}\left(\frac{kg}{kmol}\right)} \quad (40)$$

and the density calculated [15]:

$$\rho_{mix}\left(\frac{kg}{m^3}\right)=\frac{P_{mix}\left(\frac{N}{m^2}\right)}{R_{mix}\left(\frac{J}{kg\cdot K}\right)\cdot T\left(K\right)} \quad (41)$$

Using the density and the volumetric flow rate, the mass flow rate of the mixture can be computed [15]:

$$\dot{m}_{mix}\left(\frac{kg}{s}\right)=\rho_{mix}\left(\frac{kg}{m^3}\right)\cdot\dot{Q}_{actual}\left(\frac{m^3}{s}\right) \quad (42)$$

At the downstream location, a PX319-150GI pressure sensor was used which can measure up to 150 psi of gauge pressure. The same adjustment to absolute pressure via equation (38) is applied to the output of the following calibration curve [11]:

$$P\left(psig\right)=\frac{\left(150\ psig-0\ psig\right)}{\left(0.020\ A-0.004\ A\right)}\left(I_{in}-0.004\ A\right)+0\ psig=\frac{150\ psig}{0.016\ A}\left(I_{in}-0.004\ A\right) \quad (43)$$

At the mixing chamber, a PX319-030AI pressure sensor was used in monitoring the influence that the syngas had on the intake air stream. The PX319-030AI is the same as the previous PX329-030AI sensor, but with a different connection style; therefore, the same calibration curve can be used. In order to test with this system, a hydrogen compliant tank with a 350CGA (Compressed Gas Association, they develop and promote safety standards and practice for compressed gas) fitting is required.

2.3.2. Test Concept

Tests were performed using a 57% H_2 and 43% CO mixture, which would be similar to a theoretical or best-case scenario output of the SynGas rig based on glycerin reformation. In a real world application, the reforming of glycerin would result in a mixture consisting of H_2 and CO along with CO_2, H_2O, N_2 and potentially some lighter hydrocarbons (ignored in these efforts for simplicity). The addition of CO_2, H_2O, and N_2 to an engine commonly occurs through exhaust gas recirculation (EGR) which acts as a diluent or knock limiting agent. EGR changes the physical properties of the mixture in order to reduce in-cylinder temperatures specifically targeted for the reduction of nitrogen oxides (NO_x). One issue with EGR in the reformate stream is that it will reduce the overall energy content of the mixture, as indicated by the lower heating value:

$$Q_{LHV,mixture}\left(\frac{kJ}{kg}\right)=\sum_{i=1}^{n}\left[Q_{LHV,i}\left(\frac{kJ}{kg}\right)\cdot X\left(\%\right)\right] \quad (44)$$

where *X* represents the mass fraction of the mixture. Since each of the species in EGR have a lower heating value equal to zero, any presence in the mixture will result in a lower mixture-averaged heating value.

For this research effort, the decision to use only H_2 and CO in the mixture involved three reasons. The first involved an investigation into the maximum potential that syngas derived from glycerin reformation could obtain as a combustion additive. The second reason was that, at the time of testing,

only conceptual values of EGR were known; therefore, this made it impossible to devise a mixture that would relate to real world results from the SynGas rig. The third reason involved the efforts of the CPE student at enhancing H_2 selectivity in the reformation process. Hence, once the SynGas rig is operational and a catalytic material is added to the reformer, analysis of the exhaust constituents leaving the reformer will be utilized for combustion augmentation on the single-cylinder engine.

2.3.3. Results

For different loadings (0,000 W/no load, 1,250 W, 2,500 W, 3,450 W, and 4,200 W/full load) of the generator, a zero to 15 slpm injection of the mixture was implemented. The paper presented later (Paper 3) provides the results in more depth; however, in brief, the results from this research found the following:

- Improved fuel economy for the biodiesel fuel
- No pre-ignition or no noticeable knocking during testing
- More complete combustion as indicated by exhaust temperatures
- Significant CO combustion of the reformate
- Minimal NO_X emission increases.

As higher flow rates of the mixture were injected into the intake stream, the biodiesel flow rate decreased significantly. In fact, the results demonstrate that using reformate in this manner could match the fuel consumption rate of diesel, therefore making the effective energy content of biodiesel similar. Moreover, at some of the test points, the biodiesel fuel economy surpassed that of the diesel fuel.

Using the continuous manifold injection method was a risk in that it provided a higher likelihood of pre-ignition or knock of the hydrogen mixture. This researcher found that this did not occur which could be explained by the CO component of reformate. Past researchers have tried using diluents, such as helium, nitrogen, and water vapor to prevent hydrogen from igniting too early. This research shows that these diluents did reduce and even removed knock using any type of fuel induction method. While CO is technically considered a fuel source with a lower heating value of 10 MJ/kg, it does combust in this mixture. This is evident by the slight increase of CO emissions during testing as a portion of the CO injected is unburned.

It was also found that combustion is more complete as indicated by monitoring the exhaust temperature. As more reformate was injected, the exhaust temperature rose respectively; therefore, indicating that the in-cylinder temperature and pressure were increasing. This can only be explained by a change in combustion characteristics as research illustrates that hydrogen more closely follows a constant volume combustion process where the energy release is over a more narrow volume change (fewer crank angles). However, the higher temperatures created can lead to the formation of greater NO_x emission. Of

interest, while the exhaust temperature increased significantly, the overall change in NO_x emission was minimal. This can partly be explained by the method of injection. As more reformate is added to the air intake stream, it is displacing/removing air from the engine, thereby reducing the amount of available nitrogen to convert to NO_x. Moreover, adding H_2 and CO into the engine has the potential to modify the Super Extended Zeldovich Mechanism that explains the reaction kinetics of NO_x formation [20]. More research is needed on this effort, and is planned through a subsequent student, with the implementation of an in-cylinder pressure transducer to get a better reading of in-cylinder temperatures; however, the results are very promising.

3. Energy Cost for the SynGas System and Reformate System

It is important to understand the energy cost for the SynGas Rig and the Reformate systems in order to promote their usage as potential future fuels. These analyses were completed based on the cost per gallon of fuel versus the total energy required to match the fuel energy difference between biodiesel and diesel or the fuel consumption of the SynGas system.

For the SynGas rig, the energy cost of glycerin was determined to equal \$0.11/kW-hr or \$3.29/kW. This was found by combining the energy balances of system and the lower heating value of the reformate mixture in order to solve for the required mass flow rate of reformate. The first equation links the energy output by the generator to the engine required energy:

$$\eta_{Gen} E_{Gen} = \eta_f E_{Engine} \quad (45)$$

where, η_{Gen} is the efficiency of the generator, which is assumed to be 100%; E_{Gen} is the maximum electrical output from the generator, which is assumed to be 30kW; η_f is the fuel conversion efficiency, estimated as 33.3%; and the E_{Engine} is the required engine energy. This indicates that the engine will require 90 kW of energy to produce 30 kW of electrical power as commonly assumed through the 1/3rd rule of engines.

With the energy required for the engine known, the mass flow rate of glycerin can be determined by using the solved lower heating value of the reformate presented in a later section. Estimates of the conversion of glycerin to a reformate mixture composition of 57% H_2 and 43% CO results in a lower heating value of 19,554 kJ/kg. From this, the following equation solves for the mass flow rate:

$$E_{Engine} = \dot{m}_{reformate} Q_{lhv} \quad (46)$$

where, $\dot{m}_{reformate}$ is the required mass flow rate of the reformate and the lower heating value $\left(Q_{lhv}\right)$ of the reformate resulting in a mass flow rate of 4.603 g/s for glycerin. Dividing the mass flow rate by the density of glycerin will obtain the volumetric flow rate of the glycerin:

$$\dot{Q}_{glycerin} = \frac{\dot{m}_{reformate}}{\rho_{glycerin}} \quad (47)$$

where, $\dot{Q}_{glycerin}$ is the volumetric flow of the glycerin and $\rho_{glycerin}$ is the density of glycerin, which is assumed to be 1261 kg/m^3 (see paper 1). This results in a volumetric flow rate of 3.47 US Gallon/hour. By using the price of glycerin at \$0.09/pound or \$0.95/US Gallon [21], the energy cost was found to be \$3.29/kW or \$0.11/kW-hr.

For the reformate system, the energy cost analysis was completed as a price additive to biodiesel in order to obtain equal energy content compared to diesel. In January 2011, the price of diesel was approximately \$3.45/US Gallon and biodiesel was approximately \$4.05/US Gallon [22]. The energy content (or lower heating value) of diesel is approximately 44,700 kJ/kg [23] and the energy content of 100 percent biodiesel is approximately 37,000 kJ/kg [24]. Converting the energy content to a volume basis allows the determination of the total available energy per gallon of fuel source::

$$EC_{Fuel} = \frac{Q_{lhv}}{\rho_{fuel}} \quad (48)$$

where, EC_{Fuel} is the energy content of the fuel; Q_{lhv} is the lower heating value of the fuel; and ρ_{fuel} is the density of the fuel, with diesel approximately 832 kg/m^3 [23] and biodiesel at 880 kg/m^3 [24]. This results in energy content for diesel to be 140,780.95 kJ and for biodiesel to be 123,252.99 kJ; or a difference of 17,527.97 kJ. In order to determine the added fuel cost for glycerin, the energy difference was divided by the energy content of reformate (or the 57% H_2 and 43% CO), which is 93,339.13 kJ/US Gallon:

$$V_{glycerin} = \frac{\Delta E}{EC_{reformate}} \quad (49)$$

where, $V_{glycerin}$ is the required volume of glycerin added to the one gallon of biodiesel, ΔE is the energy difference between diesel and biodiesel, and $EC_{reformate}$ is the energy content of reformate. This results in an added cost of \$0.18/US Gallon for a total fuel cost of \$4.23/US Gallon.

4. Conclusion

This researcher has reached his ultimate goal for the graduate level experience by working on three major University of Kansas research projects. These projects were the Feedstock-to-Tailpipe Initiative's Synthesis Gas Reforming Rig and Single-Cylinder Biodiesel Test Stand, along with a novel Reformate Assistive Biodiesel Combustion system. Each of these projects provided the experience of real-world scenarios and practice with data acquisition systems, equipment control and hydrogen combustion. Using the PMBOK method of project management, each of the projects presented different starting points, ending points, and skills needed to complete the tasks. The PMBOK divides a project up

into five phases: Initiating, Planning, Executing, Monitoring/Controlling, and Closing. Within each of these phases, there are several tasks that PMI requires to be completed in order to ensure a successful project.

For the Synthesis Gas Reforming Rig system, this researcher was tasked to develop a project plan for implementation of a data acquisition and controls system and completed the first two phases of the PMBOK method. This system will be comprised of a variety of different sensors that will obtain the needed research data. In addition to the physical system, two models were developed that relate the flow rates of glycerin and air to the required power output. The second project involved implementing the data acquisition hardware and controls for the Single-Cylinder Biodiesel Test Stand. This researcher was brought in during the execution phase of the project, thereby giving the experience of jumping into the middle of a project and completing the last three phases. This effort provided the necessary tools and experience to learn the proper method of implementation of a data acquisition system. Even though all of the work done on this system will be seen in later papers with the author indicated as a co-author, the work accomplished here is critical in order for the Feedstock-to-Tailpipe Initiative to publish accurate results. The last project included a unique reformate assisted biodiesel combustion project completed from start to finish through all five phases of the project. This entailed developing a fuel additive system and testing a reformate mixture derived from an understanding of the SynGas rig. The results demonstrate the potential of a hydrogen/carbon monoxide mixture as a fuel additive for increased fuel economy of biodiesel fuels. This research is being submitted for a journal publication indicating the in-depth nature of the analysis. It was only through an understanding of the first two projects that the third project could be accomplished successfully.

Nomenclature

Abbreviations:	Description:
2D	Two-Dimensions
AC	Alternating Current
AFV	Air-Fuel Value
BEC	Biomass Energy Company
CEAE	Civil, Environmental, and Architectural Engineering
CO	Carbon Monoxide
CO_2	Carbon Dioxide
CPE	Chemical and Petroleum Engineering
cRIO	CompactRIO
DC	Direct Current

DCM	Department of Construction Management
ECU	Engine Control Unit
EGR	Exhaust Recirculation Gas
FPGA	Field-programmable Gate Array
FTT	Feedstock-to-Tailpipe
GC	Gas Chromatograph
H_2	Hydrogen
H_2O	Water
KU	University of Kansas
LFE	Laminar Flow Element
ME	Mechanical Engineering
N_2	Nitrogen
NI	National Instruments
OH	Hydroxide
PMBOK	Project Management Book of Knowledge
PMI	Project Management Institute
PTO	Power-Take Off
RFP	Request for Proposal
RPM	Revolutions Per Minute
TV	Throttle Valve
VI	Virtual Instrument

Variables	Description:	Units:
β	Ratio of Orifice Hole to Pipe Diameter	[1]
ρ	Density	[kg/m^3]
$\dot{Q}$	Volumetric Flow Rate	[cfm]
μ	Viscosity	[Micropoise]
η_f	Conversion Efficiency	[1]
η_{th}	Thermal Efficiency	[1]
η_c	Combustion Efficiency	[1]
τ	Torque	[N-m]

$\dot{m}$	Mass Flow Rate	[g/s]
A	Cross-Sectional Area	[m^2]
AF	Air Fuel Ratio	[1]
b	Bore	[m]
BSE	Brake Specific Emission	[g/kW-hr]
$BSFC$	Brake Specific Fuel Consumption	[g/kW-hr]
C	Orifice Coefficient	[1]
E	Energy	[J or J/s]
EC	Energy Content	[kJ/m^3]
f	Frequency	[Hz]
GF	Gas Factor	[1]
I	Current Signal	[Amps]
k	Ratio of Specific Heat	[1]
$\dot{m}$	Mass Flow Rate	[g/s]
MW	Molar Weight	[kg/kmol
N	Engine Speed	[rpm]
P	Pressure	[N/m^2],[psi]
P	Power	[Watts]
Q_{in}	Total Energy	[Watts]
Q_{lhv}	Lower Heating Value	[MJ/kg]
R	Gas Constant	[J/kg-K]
r	Pressure Ratio of the Orifice	[1]
RH	Relative Humidity	[1]
s	Stroke	[m]
T	Temperature	[Kelvin]
V	Voltage Signal	[Volts]
V_d	Displacement Volume	[m^3]
W	Work	[Watts]
X	Mass Fraction	[1]
Y	Volume/Mole Fraction	[1]

References

1. *Project Management Institute*. 2011; Available from: http://www.pmi.org/.
2. Duncan, W.R., *A Guide to te Project Management Body of Knowledge (PMBOK)*. 1996: Newtown Square, PA.
3. *Spark Gap*. 2011; Available from: http://en.wikipedia.org/wiki/Spark_gap.
4. Omega, *EWS-BP-A Barometric Pressure Sensor Manual*.
5. Omega, *EWS-RH Temperature and Relative Humidity Sensor Manual*.
6. Omega, *PX227 Differential Pressure Sensor Data Sheet*.
7. A.T. Ashcroft, A.K.C., M.L.H. Green, P.D.F. Vernon *Partial oxidation of methane to synthesis gas using carbon dioxide.* Nature, 1991. **352**: p. 225-226.
8. Meriam, *Laminar Flow Elements - Installation & Operation Instructions*.
9. Emerson, *Elite CMF-010 Flow Meter and Transmitter Manual and Data Sheets*.
10. Heywood, J.B., *Internal Combustion Engine Fundamentals.* . 1988, New York: McGraw-Hill, Inc.
11. Omega, *PX309 Series Pressure Sensor Data Sheets*.
12. Omega, *TC-K Data Sheet*.
13. Futek, *TRS705 Manual and Data Sheet*.
14. Woodward, *Woodward Power Meter Manual*.
15. M.J. Moran, H.N.S., *Fundamentals of Engineering Thermodynamics*. 5th ed. 2004, Danvers: Wiley & Sons, Inc.
16. Beckwith, T.G., *Mechanical Measurements*. 6th ed. 2006, New York, NY: Prentice Hall.
17. Brooks, *5800S Thermal Mass Flow Controller Manual*: Brooks Instruments.
18. Brooks, *SLA5800 Thermal Mass Flow Controller Manual and Data Sheet*: Brooks Instruments.
19. Gas, M., *Matheson Gas Product Guide*.
20. Gardner, R.M.G.D.G.L.C.N.T., *A Super-Extended Zel'dovich Mechanism for NOx Modeling and Engine Calibration.* Society of Automotive Engineering, 1998(980781): p. 85-96.
21. Hass, M.J., *A process model to estimate biodiesel production costs.* Bioresource Technology, 2006. **97**: p. 671-678.
22. DOE. *Alternative Fuel Price Reports*. 2011.
23. Energy, D.o. *Fuel Data Sheet*. www.afdc.energy.gov/afdc/pdfs/fueltable.pdf 2010.
24. Board, N.B. (2011) *Energy Content*.

Control and Data Acquisition System for a Synthesis Gas Generator Rig

Eric Cecrle
Department of Mechanical Engineering
University of Kansas, Lawrence, Kansas, USA

Abstract

This report summarizes the analysis and solution of building a controls and data acquisition system for the University of Kansas Synthesis Gas (SynGas) rig. The SynGas rig is comprised of three sections: the reformer, the engine, and the generator. Each of these sections has a variety of sensors that collect data while also providing control of equipment. The report begins with an analysis of the sensors and their availability. There are two types of sensors: general and special. General sensors measure temperatures, pressures, and flow rates. Special sensors find single unique properties such as density and tank elevation. With an understanding of the needed sensors, the placement of these components was determined. When all sensors were identified and the placement resolved, the selection of a data acquisition and control system (DAQC) was accomplished, and a National Instruments compact reconfigurable input/output (cRIO) system was chosen. Finally, models were developed that related the engine performance to the reformation levels of SynGas from glycerin. Overall, the total cost for the system was determined to be $7,900, and implementation is currently underway.

1. Introduction

The Synthesis Gas (SynGas) reformer rig provided by Bill Ayres of R^3 Sciences of Overland Park, Kansas has brought a unique opportunity to the University of Kansas (KU) for the "Feedstock to Tailpipe" Initiative. This initiative is a multidisciplinary research project that is investigating future alternative fuels. The SynGas rig is an addition to this initiative allowing the university to reform glycerin, the byproduct of biodiesel into a hydrogen rich mixture for subsequent combustion. Originally, KU was promised a completed rig, but due to the economic crisis of 2008, Biomass Energy Company (BEC) of Golden, Colorado (the original manufacturer of the rig), was allowed to remove equipment. The components removed include the following: the reformer catalytic material along with the controls and data acquisition equipment. As a result, the task of this researcher was to analyze and develop a plan to rebuild the controls and data acquisition system for reliability and accuracy. This report also briefly describes current efforts of rebuilding the SynGas rig.

2. Background

Before building the controls and data acquisition system, an understanding of the SynGas rig was required. This rig is comprised of three major components: the reformer, the engine, and the generator as indicated by Figure 1 in Appendix A.

2.1. Reformer

The reformer system is comprised of many different apparatuses (sub-systems). It uses propane pre-heating in order to warm the reformer to an adequate temperature, as glycerin does not vaporize and combust easily. This is due to a high amount of energy required for combustion, as glycerin cannot normally be used in an engine without requiring the chamber to first reach a temperature of 3000°F [1]. This system uses the temperature from propane combustion in order to vaporize and reform the glycerin to produce a hydrogen-rich fuel (Note: another method is to use a combustion enhancer, such as nitrating glycerin to and from a nitroglycerin species). The pre-heating system uses a custom direct current (DC) pump to transport the glycerin to the reformer, where it goes through two heating elements in order to raise its temperature making it easier to vaporize. To reform the glycerin, the system needs to operate at a rich to an ultra rich fuel-to-air mixture to create single-oxygen molecules (e.g., CO, OH, etc.) and non-oxygen molecules (e.g., H_2). Based on the stoichiometry of partial-oxidized glycerin ($C_3H_5(OH)_3$), this mixture can be up to 57% hydrogen (H_2) and 43% carbon monoxide (CO). Both of these components have an associated heating value that can be used to fuel the engine in the system. To aid in the understanding of glycerin in the system, the majority of its properties are presented in Appendix B, Figure 2 through Figure 6.

2.2. Engine

The engine is a General Motors (GM) V-8 that has a total displacement volume of 350 cubic inches and a compression ratio of 8.2:1. Currently it is naturally aspirated with electronic spark timing. It uses a Woodward Air-Fuel Valve (AFV) to regulate the fuel-to-air mixture by monitoring a Bosch oxygen sensor in the engine exhaust system. The engine speed is controlled by a Woodward Throttle Valve (TV) that regulates the amount of air entering into the engine. The engine uses a custom propane carburetor that provides enough restriction with the TV in order to regulate the flow of air to maintain 1,800 revolutions per minute (rpm) needed for the generator. The current setup allows for all of the fluid flows of the engine to be operated independent of each other. Placing the TV ahead of the AFV allows for the flow of SynGas to adjust to the variable flow of air at different engine speeds and power requirements.

2.3. Generator

The generator was to be based on a 30 kilowatt (kW) alternating-current (AC) three-phase motor, which is monitored by a Woodward voltage and current sensor. During talks with experts in this field, it was found that this motor could be used as a generator by first requiring an input of 30 kW of power to the motor. The engine would then be run slightly faster than the motor's powered operating speed, changing the flow of electrons, effectively converting the motor to an induction generator and sending generated electricity back into the electric grid. However, this was not feasible with the current setup, because the rig location on the university property does not have 30 kW of 208 VAC 3-phase capabilities. Therefore, a standalone power take-off (PTO) generator will be used to replace the motor. The PTO purchased for this system is a Mecc Alte ECO32-2L/4 PTO alternator, and installation will be completed in the near future.

2.4. Elements to monitor or control

Of the three major components, only the reformer and engine need to be controlled and monitored; whereas, the PTO generator will act as a self-reliant device with electrical outlets used to plug in electrical loads. There are two reasons to use a generator to load the system. The first reason is to simulate a real-life scenario, such as using in an industrial plant or farm irrigation system in order to provide power. The second reason is that a generator is cheaper than a dynamometer, and the current location is not capable of implementing a more traditional dynamometer setup.

The rationale to load this system is to understand how the hydrogen and carbon monoxide mixture perform under different situations using a spark-ignition (SI) engine. Research has shown that hydrogen combustion is preferred in a SI engine because of its high auto-ignition temperature. Values that can be obtained by loading the engine are glycerin flow rate and intake airflow rate that help prove its viability for power generation across multiple platforms. In other words, by creating a map of power output versus glycerin flow rate (and other variables), the information can be scaled for a multitude of different power generation options. A brief synopsis of the control of the reformer and engine is provided below.

2.4.1. Reformer

The reformer is comprised of many different components that require control and monitoring via a data acquisition system. Those components are the reformer pre-heating system, glycerin pump control, glycerin heating system, reformer air control, and SynGas process line monitoring. Each of these items can have various temperature, pressure, and flow inputs along with an assortment of control outputs. An example of this is a glycerin pump controller where a flow meter, pressure sensor, and temperature sensor are used to regulate the injection of glycerin into the reformer.

2.4.2. Engine

For safety reasons, the engine is designed to be remotely shutdown from a secondary building. In addition, the engine was originally configured with a four-stage fuel system:

(1) The start-up stage, which started the engine on propane and allowed the reformer to begin producing SynGas;
(2) The transitional stage, where propane and SynGas are mixed to provide smooth engine operation;
(3) SynGas mixture only stage, where the engine is running solely on the SynGas mixture;
(4) The propane engine clean out stage, where propane assists in the combustion of soot and char in the engine that accumulates during the SynGas operation.

Efforts to start the engine on SynGas without the use of propane as a startup and transitional fuel have been attempted and proven successful. However, soot and char were found in the fuel line when running on just SynGas alone. This is not a major issue, but it needs to be regularly checked in order to prevent excessive backpressure through clogging. The soot and char can act as a fuel source, similar to coal; therefore, not immediately removing it from the stream by filtration or gasification will not significantly affect operation of the system.

3. Methods of control

There will be two types of control methods implemented. These methods are a simple on/off control and a mathematical model input. An example is turning on and off the glycerin pre-heating tape relays based on the temperature of the glycerin entering the reformer. The second method, the mathematical model input, uses inputs from different devices to regulate a selected apparatus. The mathematical alternative is the most common method to use for a system that does not require a significant amount of input from a sensor/computer. An example is the glycerin flow control where the glycerin reformer inlet temperature, density, and volumetric flow rate will be used to regulate the flow controller using the theory presented in a later section.

4. Equipment

Throughout the SynGas rig is a variety of sensors and control units that monitor data and regulate fuel flows. The following subsections explain the different types of sensors, their placement and purpose.

4.1. General Sensors

The SynGas rig has three general sensors that will be placed throughout the rig. These are temperature probes, pressure sensors, and flow meters or controllers. Each of these sensors registers vital information to assist with the production of SynGas and utilization as a fuel and the control of the engine.

4.1.1. Temperature Probes

Temperature probes come in three different options: resistance thermometer (RTD), thermocouple (TC), or thermistor. Each of these probes has their own unique measurement qualities. The RTD is a resistance based temperature sensor that is calibrated to narrow ranges of temperatures and can read a maximum temperature of 1,800°F. It has a fast response to temperature changes with an accuracy of +/- 0.2°C. The next probe is the TC that has a wider range of temperatures than the RTD, but can be much slower to respond and has a reduced accuracy of +/- 3%. However, the TC has a maximum temperature of 4,200°F allowing for higher temperature applications. The last probe is the thermistor, which has the same accuracy and temperature bandwidth traits of the RTD, but it has a slightly higher maximum temperature of 2,300°F. For most of the tests, the data will be taken over a significant duration of time allowing temperatures to stabilize (steady state) indicating that time-response is not an issue. Moreover, the TC has the widest collection bandwidth of the three temperature probes. Therefore, the TC is the best option for the SynGas rig given its relatively low cost. The TC selected for the SynGas rig is the Omega KQXL for its collection bandwidth, durability, and resistance to oxidation, carburization, and chlorination while costing only $30 each. A NI-9213 module with a resolution around 0.02°C will monitor the thermocouples. Note: for more information about these modules, see Section 5: Data Collection and Control Device.

4.1.2. Pressure Sensors

Pressure sensors are not as general as temperature probes; they are designed specially for a given purpose. There are two types of pressure sensors: the manometer and the diaphragm. The manometer is used where a process device has a pressure differential. The diaphragm sensor is used to measure the gage or absolute pressure of a process line. Throughout the SynGas rig, pressure sensors will be placed between process devices to monitor changes in pressure. An example is before and after a pressure regulator, which reduces the tank pressure of propane to a lower pressure for use in the reformer. For the SynGas rig, Omega PX-319 pressure transducers (PT) were selected in order to obtain either absolute or gage pressure. The PX-319 offers a wide range of calibrated pressure transducers with an accuracy of +/- 0.25% of full-scale output and costs $240 each. A NI-9203 module with 12-bit resolution will monitor these pressure transducers; for example, the resolution for a 30 psia PT is 5.68E-04 psia.

4.1.3. Flow Meters/Controllers

A flow meter or controller measures either the volumetric flow rate or the mass flow rate of a given fluid. There are wide ranges of different available options on the market and they can be categorized into three groups: pressure differential flow meters, volumetric flow meters, and mass flow meters. Each category has a variety of different measurement techniques as illustrated in Figure 7 in Appendix C. Each device has different performance parameters that make them unique to their

application. On average, a low-cost flow meter is approximately $1,000-$2,000; mid-cost flow meters are about $2,000-$4,000; and high-cost flow meters are in the range of $4,000-$6,000+. The flow meter types that have been selected for this project are the turbine, positive displacement, and thermal mass. In later subsections, the type and purpose of these selections will be given.

Using these three general sensors, the properties of a fluid can be found and recorded. With enough data collected, a second-generation of the SynGas rig can be developed for any given real-world application such as agricultural irrigation systems, emergency power systems, and energy-recovery for biodiesel production plants.

4.2. Points of Data Collection and/or Control

With an understanding of the available general sensors, a more detailed explanation of placement and purpose can be given. As explained before, the SynGas rig is delineated into three sections: reformer, engine, and generator. Each section will be described according to its corresponding inlet to outlet methodology in order to assist with the understanding of the purpose and the placement of the sensors.

4.2.1. Reformer System to Engine

The reformer system has four inlets that serve a unique purpose: glycerin, propane, air, and ignition. The glycerin inlet involves the source of alternative test fuels that create the hydrogen enriched fuel stream. The propane inlet is the source of pre-heating that is required to achieve and maintain the necessary reforming temperature and aid in the warm-up of the engine. The air inlet is required for the combustion of propane in the pre-heating process, along with performing partial-oxidation during reforming. The ignition inlet provides the required energy in order to start the pre-heating combustion for this application.

4.2.1.1. Glycerin

The glycerin inlet is comprised of three components: tank, pump/flow meter, and the heat exchanger and heat tape. The tank is used to store the glycerin mixture to reform. The pump/flow meter is the system that will regulate the flow to the reformer for research values. The heat exchanger and heat tape are used to assist in the vaporization of the glycerin for the reformer. More information about each of these parts are given in their respective section.

4.2.1.1.1. Glycerin Tank

The reformer system starts with the glycerin tank. This tank can store up to 60 gallons of crude, refined or diluted glycerin. In the tank, a PT and an ultrasonic tank level sensor are used. The ultrasonic tank level sensor sends a pulse through the liquid and analyzes the time to receive the signal back in order to determine the height of the glycerin. By knowing the height of the glycerin, a warning light can be used

to ensure enough glycerin is available to run long-duration tests. The height can also be used to solve for the density of the glycerin using hydrostatic principles by utilizing a pressure sensor. By placing the sensor at a given height in the glycerin, the hydrostatic pressure will be known, which then can be used to solve for the density of the glycerin via the following equation [2]:

$\rho = \frac{p}{gh}$	(1)

where ρ is the density of glycerin [kg/m^3], g is the gravitational constant [9.81 m/s^2], h is the height of the glycerin in the tank measured by the ultrasonic tank level sensor [m] and p is the pressure read by the PT [Pa]. By obtaining the density of the glycerin, the mass flow rate can be determined by using a volumetric flow meter, which will be explained later.

An Omega LVU-31 ultrasonic level sensor was selected for the tank level sensor. It needs to be placed a minimum of four inches away from the fluid and can measure up to a distance of fifty inches with a resolution of 0.01 inches. It allows the user to calibrate the analog output signal and costs $350. Assuming the glycerin tank is four feet (1.2192 m) high and contains pure glycerin (density of 1.26415 kg/m^3), the maximum pressure of the tank would be 15,119.68 Pa (2.192 psig). Therefore, a 5 psig Omega PX-319-005GI pressure sensor would be adequate. The resolution for this sensor is 9.54E-05 psig using the 0.01 inch resolution characteristics of the LVU-31 sensor. Therefore, the determined density change will be accurate to ±0.061 kg/m^3 (solved using the root-sum-square error method) if both temperature and pressure changed by the resolution of the sensors. The pressure change from the height resolution would be 0.0461 psig. A NI-9203 module will monitor the pressure sensor, and a NI-9205 module will monitor the LVU-31 sensor.

4.2.1.1.2. Pump Transport System and Flow Meter

To be able to transport the glycerin to the reformer, a high viscosity oval-gear pump is used. This pump is attached to a 12VDC motor with a variable speed controller in order to regulate the reforming process. In order to determine needed adjustments to the speed of the pump, an oval-gear flow meter with a PT and TC are placed after the pump to calculate glycerin mass flow rate. Using this system allows for the use of a higher glycerin-to-water ratio than other pump systems could offer. The reason why a high viscosity pump and flow meter are needed is because pure glycerin can have up to a viscosity of 1,410 centipoise (cps) at room temperature. Most flow meters and controllers are-designed for 200 cps liquids. The flow meter selected was an Omega FPD1001B-A, costing $975 that can handle 1,000 cps of viscosity with an accuracy of ± 1.0% of the reading. A NI-9203 module will monitor the flow meter and is good enough for a 98% glycerin-to-water mixture at room temperature as indicated by Figure 4 in Appendix B.

A question that arises is how to measure pure glycerin if the recommended flow meter can only handle 1,000 cps? In order to test pure glycerin, a different flow meter would be required, and there exists an Omega flow meter that can be purchased with the capability of a 1,000,000 cps fluid. However, this will result in a reduced accuracy as oval-gear flow meters are most accurate closer to their maximum viscosity. Since it is anticipated that water will be added to the glycerin to aid in the production of hydrogen through steam reforming and the water gas shift reaction (discussed later), it was more prudent to purchase the lower viscosity flow meter. Tests will be done using the installed meter in order to explore its tolerances according to different water-to-glycerin ratios and when pure glycerin is added.

4.2.1.1.3. Glycerin Heat Exchanger and Heat Tape

With the transport system explained, the glycerin pre-heating system can be discussed. The first device that the glycerin encounters is a heat exchanger (HE). The HE uses the outlet heat from the reformer to assist in the heating of the glycerin as it requires a temperature greater than approximately 500-600°F to vaporize [3]. Placing TCs at the inlet and outlet of the HE allows monitoring of the heat transfer from the HE in order to regulate the flow rate of the glycerin. After the glycerin HE, Omega heat tape wrapped around the pipe further assists in the heating process. With a TC placed at the outlet of the HE (just before the heat tape) and a TC at the inlet to the reformer (just after the heat tape), a better understanding of heat transfer characteristics can be obtained. Finally, a PT placed before the reformer will provide all reformer inlet conditions of the glycerin.

4.2.1.2. Propane

Propane is used in order to pre-heat the reformer to the necessary temperature for glycerin reformation. To be able to regulate the propane source, a thermal mass flow controller will be used. This device measures the temperature difference of the fluid in order to determine its flow rate. The determined temperature difference controls a solenoid valve that regulates the flow into the reformer. A thermal mass flow controller is used to maintain constant combustion during the pre-heating process by matching the airflow rate to a specified air-fuel ratio. A second thermal mass flow controller can be added in order to test gaseous-based reforming, such as propane and natural gas in comparison to glycerin. The selection of the thermal mass flow meter has not been completed because at the current state of the SynGas rig, flow rates for propane have not been obtained.

A question that has arisen regarding this system involves the necessity of installing a propane thermal mass flow controller if the propane regulators are set to a pre-set value and the controllers use a solenoid to turn on or off the flow when needed. The vaporization of propane varies with its liquefied temperature; the result of this temperature will vary the outlet pressure and consequently change the amount of gaseous propane flow rate. Therefore, with any changes in environmental conditions, the initial

conditions will vary through the regulators and require a continuous readjustment of the regulators in order to maintain the same mass flow rate for combustion. Hence, if propane is only being used to perform pre-heating of the reformer, a thermal mass flow controller is not necessary. If research data needs to be collected on propane reforming, this is because as the environmental conditions change, the propane properties might not necessarily remain constant throughout the test. Collecting this data will provide an exact volumetric flow rate value versus an assumed value using an air-fuel ratio calculation through a lambda sensor on the system.

4.2.1.3. Air

The air inlet is a critical element for proper optimization of the reformer. The regulation of air is required in order to provide for combustion pre-heating and the correct fuel-air levels for reforming. Originally, the reformer was driven by the vacuum of the engine based on piston movement. Now, with the reformer decoupled from the engine, the air inlet requires a positive supply pressure to force flow through the system. To accomplish this, either a variable flow blower/pump with a flow meter or a constant flow pump with a mass flow controller was required. The best option of the two would be the latter as it is more repeatable in nature and can maintain a uniform airflow. In the updated setup, a high volumetric flow rate air compressor is being used as the constant flow pump. The air compressor is an Industrial Air Super Hi-Flo Single-Stage that can output 18.1 scfm (standard cubic feet per minute) at 90 psi and costs $1,000. In order to measure the mass flow rate, experiments are being performed with a low cost mass flow controller of a second student's design. However, if the low cost alternative is found not to be feasible, a thermal mass flow controller will be purchased instead. This controller is a Brooks SLA5853 that can regulate between 100 slpm (standard liters per minute) to 2500 slpm of nitrogen (3.53 scfm to 88.29 scfm) or 99.8 slpm to 2495 slpm of air (3.52 scfm to 88.11 scfm); accurate to ± 1.0% of the rate, ± 0.2% of the full-scale and costs $3,200. The mass flow controller can be monitored via RS-485 to USB connection for higher accuracy control.

4.2.1.4. Ignition

The last reformer component is the ignition source. As mentioned previously, in order to pre-heat the reformer, the combustion of propane must occur. The original system on the rig used a glide-arc setup, but it had issues with carbon bridging and irregular arcing. In order to solve this issue, a more traditional spark-plug transformer system was implemented that provides a continuous energy discharge and its functionality will be controlled remotely through a relay. The spark plug used was a Bosch Platinum+4 spark plug and the transformer used was a Franceformer (9030 P4) 9,000 volt transformer.

4.2.1.5. Propane Heat Exchanger

Once reforming has occurred, the SynGas passes through the glycerin HE and into the propane HE. The purpose of the propane HE is to vaporize the propane and cool down the SynGas mixture to prevent the engine from knocking due to a hotter inlet mixture. The vaporization of propane involves its transition from a liquid to a gas in order to mix with air for combustion and can happen by two methods: either evaporation or boiling. Evaporation occurs at a given pressure and temperature below its boiling point where the surface only goes through the phase change. Boiling occurs when the liquid is brought above its boiling point and the entire the entire mixture goes through the phase change. In the current setup, the propane goes through both methods in order to ensure a constant pressure and complete vaporization. The propane HE has TCs placed at the inlet and outlet of the process line in order to obtain the temperature drop of the SynGas mixture as this will capture heat transfer characteristics and be used to tune overall efficiency of the system.

4.2.1.6. Cyclones

In this setup, cyclones are used to remove any large particles of soot from the reformate stream that might hinder engine operation. In this device, cyclonic separation uses rotational effects and gravity in order to remove the particles. It takes the relatively dirty stream entering at the top of the container and forces it through a spiral downward motion. As the speed dissipates, the particles begin to fall to the base of the cyclone with the warm gas rising to the top. As a result, it separates the particles from the stream without requiring filtration that would add a substantial pressure drop. In order to calculate heat transfer characteristics and monitor reformate flow, TCs were placed on the inlets of both cyclones in the system.

4.2.2. Engine

The engine section has relatively fewer components to monitor. In particular, only the fuel source to the engine and the control of the engine need to be observed. This section provides a brief discussion of the examination of the inlet stream and the engine itself.

4.2.2.1. Inlet Stream

For research purposes, the fuel flow rate and other fuel process properties will be obtained using PTs, TCs, and a volumetric flow meter. The fuel properties that can be found are density, temperature, and the mass flow rate of the reformed mixture. With respect to measuring the inlet fuel flow rate, a turbine flow meter is one of the most accurate flow meters on the market. Moreover, it has a negligible pressure drop preventing any excessive backpressure on the system. At this time, a turbine flow meter has not been selected for the reason that there are too many uncertainties in the current setup to size it appropriately. This researcher recommends using a Cameron NuFlo/Barton turbine flow meter. Specifically, the Barton 7400 series flow meter is designed for industrial applications similar to this

project. In order to take an accurate reading, the following parameters are required: system pressure range, system temperature, mixture concentrations, and maximum flow rate. Again, because of the current state of the project, the exact turbine flow meter cannot be selected without making significant assumptions. Of interest, there is a current NuFlo turbine flow meter on this setup leftover from BEC efforts. It is designed for liquid metering; however, the weatherproof box and board can be reused reducing the cost of the system. Furthermore, throughout the fuel line, PTs and TCs will be placed before and after any device that can cause pressure drops or temperature losses. The last set of PT and TC is placed right before the Woodward AFV to monitor the engine inlet conditions. The Barton 7400 series flow meter is accurate to 0.2% of the flow rate and output will be determined when the flow meter is purchased.

4.2.2.2. Engine Components

The last two components for engine control are the Woodward AFV and TV previously mentioned. Each of these valves was designed to provide independent control of the system. The AFV is used to control the flow of SynGas into the engine, whereas, the TV is used to adjust the speed of the engine. These valves also allow external control in order to adjust the pre-set constants for optimization of the system. Specifically, each of these valves has valve position outputs that will be monitored by the DAQC system presented in the following section.

4.3. Summary

This explanation of placement and sensor selection finishes this analysis for the SynGas rig with an engineering drawing of the overall system presented in Appendix A: Figure 1. In order to view basic electrical schematics how these components come together, refer to Appendix D: Figure 8. A cost estimate of the different items required is presented in Appendix E: Table 1 and Table 2. Of interest, the total cost to purchase all the needed sensors for the SynGas rig will be $3,900. In order to monitor and control these sensors, the next section describes the data acquisition hardware.

5. Data Collection and Control Device

For this project, a National Instruments (NI) compact RIO (cRIO) chassis (cRIO-9072) was chosen to collect and record all data. This equipment was selected for its real-time (RT) data acquisition (DAQ) capabilities, RT controllability, and its interchangeable input and output modules. These modules are devices that collect and monitor analog or digital signals or can output a necessary signal to control another piece of equipment. An example module is an analog voltage collection device (NI-9205) that can capture 32x single-line voltages or 16x differential voltages. The modules selected are as follows: 1x 32-channel voltage input module (NI-9205), 1x 16-channel voltage output module (NI-9264), 2x 8-channel

current input module (NI-9203), 1x 16-channel TC module (NI-9213), and 1x 32-channel digital input/output (DIO) module (NI-9403).

The NI-9205 module can read up 32 channels of voltage signals. Each channel can be set to read a ± 200 mVDC, ± 1VDC, ± 5VDC, or a ± 10VDC signal with the resolution at 16-bit or 65536 segments of the set scale. For example, the resolution of a ± 10VDC signal is 3.05E-04 VDC or 0.305 mVDC. The voltage input module will read all the engine sensors, ultrasonic tank level, Woodward valves, flow meters, flow controllers, and oxygen sensor.

The NI-9264 module can control up to 16 voltage-controlled devices. It can output a signal ranging from -10 VDC to 10 VDC with a resolution of 16-bit. The controllable voltage change is 3.05E-04 VDC or 0.305 mVDC and the current it uses is 16 mA. The voltage output module will be used to control the motor controller, Woodward valves, and flow controllers.

The NI-9203 module measures current signals through eight-channels at 0-20 mA or ±20 mA. It is a 16-bit module; therefore, the resolution is 6.10E-04 mA for the ±20 mA or 3.05E-04 mA for the 0-20 mA settings. The current input modules will be used to read the PT, flow meters, and flow controllers.

The NI-9213 module is a sixteen-channel thermocouple reader that is accurate to 0.02°C. It will be used to collect all the TC probes while incoporating the built-in cold-junction compensation (CJC) to normalize the signal. A TC normally has two junction points and two output wires with the typical signal on the millivolt (mV) range as it measures the voltage differential between two dissimilar metals in the probe. One junction point measures the desired piece of equipment and the other is the cold bath or reference point which allows the voltage differential to occur. However, TCs normally do not have a reference point junction and instead use a digitalized CJC to act as the cold bath.

The last module is the NI-9403 that is a 32-channel digital input output device. It outputs a value between zero and five VDC in order to control equipment or it can read a similar signal. This module can be used to read the speed from the ignition coil, control the Woodward valves, and control any solid-state relays.

The total cost of the cRIO system is $4,000 with the estimate presented in Appendix E, Table 1. At this point, the physical system is specified and theoretical models are now necessary in order to relate the hardware signals to engineering properties and controls.

6. Reformer Predictor Model

This model is comprised of four major parts: reactions, mass flow rates, thermodynamic properties, and the fuel energy balancing equation. Each part is necessary in order to use the flow rates from the glycerin and air flow meters and the reforming temperature in order to predict the species concentrations leaving the reformer along with its respective energy content. The model balances the feedstock molar amounts to the syngas levels by utilizing the water-gas shift (WGS) reaction. The WGS

relates the interaction between water vapor (H_2O), carbon monoxide (CO), hydrogen (H_2), and carbon dioxide (CO_2) at a given temperature and pressure. The mass flow rates relate the flow meters to the model with thermodynamic properties used to calculate physical properties (like molar weight and gas constant) from the molar fractions, temperature, and pressure. The fuel energy balancing equation links the energy input from a standard fuel source of propane in order to predict the potential energy available from the reformate and the required input flow rates necessary.

6.1. Reactions

This model uses thermodynamics and the stoichiometric balance present from chemistry along with the WGS chemical equilibrium reaction. It can provide an estimate of reforming levels with later validation through a collaborative effort with the Chemical and Petroleum Engineering Department. Specifically, a Gas Chromatograph and Mass Spectrometer (GC-MS) device is available to measure CO and H_2 levels after the SynGas rig control is finalized.

A generalized stoichiometric balance based on a fuel with carbon, hydrogen and oxygen components is as follows:

$f\left(\mathrm{C}_\alpha\mathrm{H}_\beta\mathrm{O}_\gamma\right)+\left(\mathrm{O}_2+3.76\mathrm{N}_2\right)\rightarrow a\mathrm{CO}_2+b\mathrm{H}_2+c\mathrm{CO}+d\mathrm{H}_2\mathrm{O}+e\mathrm{N}_2$	(2)

Note that in order to create hydrogen, the reformer must run "rich" which involves an excess of fuel through limiting air. In this situation, the right hand side of the stoichiometric balance does not include oxygen. Given this balance, the governing equations of atoms can be written as follows:

C:	$\alpha f = a + c$	(3)
H:	$\beta f = 2b + 2d$	(4)
O:	$\gamma f + 2 = 2a + c + d$	(5)
N:	$3.76 * 2 = 2e$	(6)

However, this only provides four equations; whereas, there are five unknowns (note: the component *f* will be used as an input variable). Similar to the lessons learned in the Internal Combustion Engines course (ME 636), the chemical equilibrium equation for the water-gas shift reaction can be used:

$K_{eq} = \log_{10}(C) = \frac{c^1 d^1}{a^1 b^1}\left(\frac{p}{p^0}\right)^{1+1-1-1} = \frac{cd}{ab}$	(7)

By using a temperature base curved-fit from the JANAF Thermochemical Table [4] for the WGS reaction in the range of 298 K to 1400 K,

$K_{eq} = -2.31719599\times10^{-12}T^4 + 7.97773201\times10^{-9}T^3 - 7.14355823\times10^{-6}T^2$ $+ 2.4713825\times10^{-3}T - 2.94930280\times10^{-1}$	(8)

the model can adapt to a changing reforming temperature.

Now, the predictor model has all of the necessary equations to solve for the moles of the products as indicated in Appendix F. In particular, the solution for the moles of hydrogen is found as:

$b = \frac{-\left\{ f\left[\gamma + 2 - \beta - 2\alpha + K_{eq}\left(a + \frac{\beta}{2} - \gamma\right)\right] - 2K_{eq}\right\}}{2\left(1 - K_{eq}\right)} - \frac{\sqrt{\left\{ f\left[\gamma + 2 - \beta - 2\alpha + K_{eq}\left(a + \frac{\beta}{2} - \gamma\right)\right] - 2K_{eq}\right\}^2 - 4\left(1 - K_{eq}\right)\left[\beta f^2\left(\alpha + \frac{\beta}{4} - \frac{\gamma}{2} - \frac{1}{f}\right)\right]}}{2\left(1 - K_{eq}\right)}$	(9)

with the rest of the moles determined as:

$d = \frac{\beta}{2} f - b$	(10)
$c = 2\alpha f + \frac{\beta}{2} f - \gamma f - 2 - b$	(11)
$a = \alpha f - c$	(12)
$e = 3.76$	(13)

In order to demonstrate the model usage, Appendix G:

Table 4 presents the predictions of output reformate species at 101325 Pa and 800K. This pressure and temperature were chosen because (a) the reformate chamber is at atmospheric conditions and (b) research accomplished on the WGS reaction for the Catalyst Modeling course (ME 790) found that keeping the temperature around 1000°F (810K) would assist in the reduction of char and soot formation during the reforming process. In

Table 4, propane's fuel-to-air molar ratio was chosen to be 2/3 (mass air-fuel ratio of 4.73) as this represents the last value before the reforming process lacks enough O_2 to form CO for the WGS equilibrium reaction. Once the ratio goes below this, the formation of soot and other hydrocarbon-based species will start being present in the reforming process. In order to view the influence of different air-fuel ratios on output species, refer to Figure 9 in Appendix H.

Since glycerin contains the necessary oxygen needed to form CO without added O_2, a much larger fuel-air molar ratio (almost zero air-fuel ratio) can be tested. For glycerin reforming, the fuel-air molar ratio of 25 (mass air-fuel ratio of 0.024) was used to demonstrate the most restrictive reforming level. The benefit of testing propane versus glycerin is that both gases contain the same amount of carbon and hydrogen atoms, so the H_2/CO ratio will remain the same between tests (1.34:1, as seen in

Table 4). The only difference will be the presence of Exhaust Gas Recirculation (EGR) species in the product. As the table elucidates, H_2O and CO_2 are now present since additional oxygen is being added to the mixture through the fuel, but the magnitude of H_2 and CO is much larger than the remaining species demonstrating the potential of glycerin reformation.

Of significant interest, the H_2O, CO_2 and N_2 species that result from the reforming process must be considered as EGR species entering the engine. EGR acts as a dilute used to change the specific

properties of the mixture via acting as a thermal heat sink that draws potential energy away from the available work in order to reduce the in-cylinder peak pressure and temperature. Diminishing this temperature lowers the formation of NO_x emissions and is a key control method by engine manufacturers. They introduce EGR into the engine through a redirection of exhaust gases from the exhaust manifold(s) into the intake manifold displacing air. The disadvantage of using EGR is that it decreases engine performance and volumetric efficiency. Ideally, for maximizing the potential fuel economy of glycerin, the system would not utilize any EGR; however, since glycerin cannot be used as a fuel directly and must go through this reformation process, EGR is effectively created as a side product that cannot be eliminated from the intake stream to the engine. However, for a fuel mixture containing purely H_2 and CO (our SynGas), EGR does not affect combustion significantly because the flammability limit of this mixture is from 12.5% to 74% per volume; whereas, gasoline is only 1.4% to 7.6% per volume. Therefore, a gasoline engine can only run up to a maximum amount of approximately 30% EGR by volume. It has been found that hydrogen combustion is capable of 50% EGR by volume as hydrogen is more tolerant because of its significantly large laminar flame speed (1.85 m/s) [5]. Of interest, carbon monoxide has a laminar flame speed of 0.19 m/s. Therefore, it is feasible that the engine can run on SynGas even up to 50% EGR by volume. For further investigation, air-fuel ratio sweeps are presented in Figure 11 in Appendix I as a demonstration of how the model will be used in the control process.

This model can also be used to include the addition of water to the glycerin mixture. Adding water to glycerin promotes a higher H_2/CO ratio as it shifts chemical equilibrium in the WGS reaction (indicated in

Table 4 in Appendix G, Figure 13 and Figure 15 in Appendix I). Moreover, water reduces the freezing temperature of glycerin to more amenable conditions since pure glycerin can freeze at 62.6°F (see Figure 3 in Appendix B). The addition of water does promote more CO_2 and H_2O creation as the oxygen in the water helps complete combustion. This is a negative influence as it effectively creates more EGR; however, this is offset somewhat by the increased heating value due to more H_2 that is present.

6.2. SynGas Reformer Fuel Mass Flow Rate Equation

In order to determine the fuel-to-air molar ratio as input to the predictor model, the mass flow rates of the fuel and air sources will be obtained from the flow meters/controllers. By knowing the fuel and air mass flow rates, they can be used to solve for the fuel-to-air molar ratio by dividing the mass flows rates by their respective molar weights:

$$f = \frac{\dot{m}_f / M_f}{\dot{m}_a / M_a} \qquad (14)$$

where M_f is the molar weight of the fuel and M_a is the molar weight of the air. Hence, the DAQC system will include this mathematical model in order to determine the target H_2/CO levels leaving the reformer based on flow rates and temperatures.

6.3. SynGas Properties Equations

In addition to molar species values, the gas properties of the SynGas mixture can be found by using the predictor model. This allows for solution of the required reforming mass flow rate in order to achieve the same engine power output produced by propane. In order to accomplish this, the researchers must first test the system on propane and record the fuel mass flow rates by using the propane carburetors pre-set air-fuel ratio and the air mass flow rate from an engine sensor. The propane carburetor is pre-set to an air-to-fuel ratio of 15.7 (by mass) and can be verified by checked it with a lambda (wideband oxygen) sensor. The airflow rate can be found by using of a Laminar Flow Element (LFE) connected to the engine intake air stream or use a mass airflow (MAF) sensor that is used on modern-day cars for redundancy and increased fuel control.

The LFE requires differential pressure sensors and upstream air temperature, pressure, and density sensors to find the mass flow rate. These sensors will be monitored between two NI modules: NI-9203 and NI-9205. The MAF sensor requires an intake air temperature sensor (IAT) and manifold absolute pressure (MAP) sensor to solve for the intake air mass flow rate. These sensors will be monitored by differential modules depending on the output of the sensor. For frequency outputs, the NI-9304 module will be used. For voltage sensors, the NI-9205 module will be used. This will be synched to the power output by monitoring a power meter, such as using a Woodward GenSet Controller. The GenSet Controller uses a voltage and current analyzer to solve for the load power draw and frequency. These terms can be monitored using the NI-9203 module. With the load and propane mass flow rate calculated, a map can be produced and the DAQC will be able to self adjust the reforming flow rates based on the model.

The first SynGas mixture property that is required in order to accomplish this is the mixture molecular weight. To solve for this value, the molar weights of the products must be factored by the number of moles (n_i) and subsequently divided by total moles of the SynGas mixture as follows [2]:

$$MW_{mix} = \frac{\sum n_i MW_i}{\sum n_i} \quad (15)$$

Given the molar weight of the SynGas mixture, its gas constant can be found using the universal gas constant (R_u = 8.314 kJ/kmol·K) [2]:

$$R_{mix} = \frac{R_u}{MW_{mix}} \quad (16)$$

Utilizing this value with a pressure transducer (p) and a temperature (T) probe, the density of the mixture can be found through the ideal gas law [2]:

$$\rho_{mix} = \frac{p}{R_{mix}T} \quad (17)$$

Another important property that is required is the lower heating value (Q_{LHV}) of the SynGas mixture. By knowing this value, the researchers can relate the engine load (or power) to the required fuel mass flow rate of reforming as explained in the next section. To solve for this, the summation of the molar lower heating values must be multiplied by the mole fractions of the products [2]:

$$\bar{Q}_{LHV,mix} = \sum Q_{LHV,i} MW_i X_i \quad (18)$$

where $Q_{LHV,i}$ are the respective heating values of all components that act as a fuel and X_i are the mole fractions of these species in the mixture. Then, by taking the molar lower heating value divided by the mixture's molar weight, the lower heating value for the SynGas mixture can be found as [2]:

$$Q_{LHV,mix} = \frac{\bar{Q}_{LHV,mix}}{MW_{mix}} \quad (19)$$

The properties for the three different mixture types that can be reformed are given in

Table 4 in Appendix G. In the case of propane, the molar weight and lower heating value of the mixture are lower because of the larger amount of EGR present in the mixture. Even though there is no presence of CO_2 and H_2O at a mass air-fuel ratio of 4.73, the EGR level remains high because of the N_2 present during this process. Further demonstration of the influence of EGR can be seen via Figure 10 in Appendix H. The pure glycerin mixture shows the most potential because of its lower EGR value. This is because of the larger amount of glycerin that can be used during the reforming process and the negligible air required to reform. The addition of water reduces the glycerin potential because of the presence of extra EGR from the water promoting the presence of H_2O and CO_2 as products in the WGS equilibrium reaction. For the reader's benefit, the results from the pure glycerin and glycerin with water reforming are present in Figure 12, Figure 14 and Figure 16 in Appendix I.

One important item to note is that a second lower heating value (or complete mixture lower heating value: $CQ_{LHV,mix}$) is presented in

Table 4 as it includes an estimated value of the mixture through inclusion of the EGR fraction and not just the fuel alone. In order to obtain the lower heating value of a fuel, the volume fractions of the fuel species has to be computed [2]:

$$X_{\mathrm{H_2}\text{-fuel}} = \frac{X_{\mathrm{H_2}}}{X_{\mathrm{H_2}} + X_{\mathrm{CO}}} \quad (20)$$

$$X_{\mathrm{CO}\text{-fuel}} = \frac{X_{\mathrm{CO}}}{X_{\mathrm{H_2}} + X_{\mathrm{CO}}} \quad (21)$$

Then, using equations (15), (18), and (19) the lower heating value can be found. For propane, glycerin, and glycerin with water, the following fuel lower heating values were found: 19,720 kJ/kg, 19,958 kJ/kg, and 21,911 kJ/kg (also seen in
Table 4 in Appendix G). In order to understand how the influence of air-fuel ratio impacts the potential energy output, refer to Figure 10 for propane in Appendix H; Figure 12 for pure glycerin; and Figure 14 and Figure 16 for glycerin with water in Appendix I.

For the complete mixture lower heating value, equations (15), (18), and (19) are used. For H_2O, CO_2, and N_2, their lower heating values are zero; therefore, this causes a reduced lower heating value in comparison to just the fuel alone. The following equation represents the link between the lower heating values calculated from equation (19) and the modified complete mixture lower heating value:

$$CQ_{LHV,mix} = Q_{LHV,mix(all\ species)} \quad (22)$$

The reason the complete mixture is being considered is that it simplifies the link between fuels and an approximate energy input that can be found using a flow meter. If the fuel lower heating value is used to approximate the energy input, the model will under predict the amount of fuel needed to obtain the same power as the engine is running on propane (46,350 kJ/kg) as described in further detail in the next section. The complete mixture lower heating values found for propane, glycerin, and glycerin with water reforming are the following: 7247 kJ/kg, 18,389 kJ/kg, and 16,700 kJ/kg (as seen in

Table 4 in Appendix G). As a result, with these gas properties, the SynGas mixture can be analyzed in real-time through the cRIO device in order to help control equipment. For further investigation how the air-fuel ratio influences the complete mixture lower heating value, refer to Figure 10 for propane in Appendix H; Figure 12 for pure glycerin; and Figure 14 and Figure 16 for glycerin with water in Appendix I.

6.4. SynGas Reformer Fuel Energy Balancing Equation

Setting the fuel source mass flow rate needed to run the SynGas mixture in the engine requires use of basic fluid mechanics and thermodynamics. In particular, running the engine on propane only through its initial calibration provides the following heat input as a function of power needed:

$$Q_{add} = \dot{m}_{propane} Q_{LHV,propane} \quad (23)$$

where the mass flow rate of propane will be provided by the DAQC. In order to achieve the same engine power just using glycerin requires an understanding of the reforming process. The heating value after the reforming process was determined in the previous section; therefore, in order to obtain the same energy input to the engine, the energy addition must be equated as follows:

$$Q_{add} = \dot{m}_{propane} Q_{LHV,propane} = \dot{m}_{mix} CQ_{LHV,mix} \quad (24)$$

Hence, the flow rate of the mixture can be calculated by the DAQC setup as:

$\dot{m}_{mix} = \dot{m}_{propane} \frac{Q_{LHV,propane}}{CQ_{LHV,mix}}$	(25)

Once the power output versus mass flow rate map is complete, the system is configured and ready to run on the reformate mixture. Note that if the fuel-only mixture lower heating value is used, the denominator in the above equation will be too large. Hence, the DAQC would predict a lower reformate flow rate than is needed.

7. Predictor Model with Continuous Propane Heating

The reason why a predictor model with continuous propane heating was developed was to investigate how the stoichiometric combustion of propane would influence the reformate mixture composition. In particular, continuous propane heating would be beneficial in reforming as it can provide a constant source of energy during the process. Model development followed along the same lines as the previous models illustrated with the only difference in that the air is balanced with propane in order to provide stoichiometric combustion; therefore, five moles of air are present versus one mole. Moreover, water is included and, if desired, the model can be made more basic to allow for variations in air depending on future research needs. In particular, if the reformer cannot be operated only on glycerin, then the researchers can revisit this model development.

This model begins utilizing the stoichiometric balance equations

$f*\left((1-x)*C_3H_8O_3 + x*H_2O\right) + C_3H_8 + 5*(O_2 + 3.76*N_2) \rightarrow a*CO_2 + b*H_2 + c*H_2O + 3.76*N_2$ $f\left[(1-x)(C_3H_8O_3) + xH_2O\right] + C_3H_8 + 5\left(O_2 + 3.76N_2\right) \rightarrow aCO_2 + bH_2 + cCO + dH_2O + eN_2$	(26)

with the atom balance as follows:

C:	$3f(1-x)+3 = a+c$	(27)
H:	$8f(1-x)+2fx+8 = 2b+2d$	(28)
O:	$3f(1-x)+fx+10 = 2a+c+d$	(29)
N:	$18.8 = e$	(30)

Using the WGS chemical equilibrium equation from before, the following equations were developed:

See Appendix J equation (J14) for *b*.	(31)
$d = -b+4f-3fx+4$	(32)
$c = 7f-7fx-b$	(33)
$a = -c+3f-3fx+3$	(34)
$e = 18.8$	(35)

As Table 5 in Appendix K (and Figure 17, Figure 19, and Figure 21 in Appendix L) shows, glycerin reforming with continuous propane heating is not desired. It is infeasible to develop a hydrogen-enriched mixture, even after the addition of water to promote CO conversion. The model demonstrates a

reduced lower heating value because of the extra CO_2 and H_2O formed (further evident in Figure 18, Figure 20, and Figure 22 in Appendix L). Hence, by continuously injecting propane into the reformer, an adequate temperature for partial oxidation reforming will be maintained, but the mixture potential as a SynGas is severely compromised.

8. Conclusion

The Synthesis Gas reforming rig allows the University of Kansas to reform the byproduct of biodiesel and glycerin, into a hydrogen rich mixture. Originally, KU was promised a completed rig, but upon inspection after delivery, it was found that significant work was needed in order to get the system running. The task of this paper was to formulate a plan in order to implement data acquisition and control equipment while efforts were underway to get the system functional. To achieve this design goal, the ideal placement of pressure transducers, thermocouples and flow meters was indicated. Sensors were selected in order to calculate the properties of a SynGas mixture while additionally regulating the glycerin flow rate based on the power needs of the engine. In order to accomplish this, a predictor model was developed in order to connect the reforming process to engine combustion. Moreover, a solution has been presented for the DAQC system and work is underway as to its implementation.

9. Nomenclature

Abbreviations:	Description:
AC	Alternating Current
AFV	Air-Fuel Value
BEC	Biomass Energy Company
CEAE	Civil, Environmental, and Architectural Engineering
CJC	Cold-Junction Compensation
CO	Carbon Monoxide
CO_2	Carbon Dioxide
CPE	Chemical and Petroleum Engineering
cRIO	CompactRIO
DACQ	Data Acquisition and Control System
DAQ	Data Acquisition
DC	Direct Current
ECU	Engine Control Unit
EGR	Exhaust Recirculation Gas

FPGA	Field-programmable Gate Array
FTT	Feedstock-to-Tailpipe
GC-MC	Gas Chromatograph
H_2	Hydrogen
H_2O	Water
HE	Heat Exchanger
KU	University of Kansas
LFE	Laminar Flow Element
MAF	Mass Air Flow Sensor
MAP	Manifold Absolute Pressure Sensor
ME	Mechanical Engineering
N_2	Nitrogen
NI	National Instruments
OH	Hydroxide
PT	Pressure Transducer
PTO	Power-Take Off
RPM	Revolutions Per Minute
RT	Real-Time
RTD	Resistance Therometer
SI	Spark Ignition
TC	Thermocouple
TV	Throttle Valve
WGS	Water-Gas Shift

Variable:	Description:	Units:
$\dot{m}_{propane}$	Mass flow rate of propane	[kg/s]
$\dot{m}_{mix}$	Mass flow rate of mixture	[kg/s]
$Q_{LHV,propane}$	Lower heating value of propane	[kJ/kg]
$CQ_{LHV,mix}$	Lower heating value of SynGas mixture	[kJ/kg]
a	Carbon Dioxide moles	[kmol]
b	Hydrogen moles	[kmol]
c	Carbon Monoxide moles	[kmol]

d	Water Vapor moles	[kmol]
e	Nitrogen moles	[kmol]
f	Fuel-to-Air molar ratio	[1]
g	Gravitational constant = 9.81	[m/s^2]
h	Tank height	[m]
K_{eq}	Chemical Equilibrium constant	[1]
M	Molar Weight	[kg/kmol]
n_i	Mole Fraction	[1]
p	Pressure	[Pa]
R	Gas Constant	[J/kg-K]
R_u	Universal Gas Constant = 8314	[J/kg-K]
T	Temperature	[K]
X	Volume Fraction	[1]
α	Fuel source carbon atom count	[1]
β	Fuel source hydrogen atom count	[1]
γ	Fuel source oxygen atom count	[1]
ρ	Fluid density	[kg/m^3]

10. References

1. *MK Glycerin Burner Technology*. 2011; Available from: http://www.glycerinburners.com/glycerin_burning.php.
2. M.J. Moran, H.N.S., *Fundamentals of Engineering Thermodynamics*. 5th ed. 2004, Danvers: Wiley & Sons, Inc.
3. Dow. *Glycerin Properties*. 2010; Available from: http://www.dow.com/glycerine/resources/physicalprop.htm.
4. Cengel, M.B.Y.A., *JANAF Tables*. 5th ed. Thermodynamics: An Engineering Approach. 2006: McGraw-Hill.
5. C. M. White, R.R.S., A. E. Lutz, *The hydrogen-fuel internal combustion engine: a technical review.* International Journal of Hydrogen Energy, 2006. **31**: p. 1292-1305.
6. Beckwith, T.G., *Mechanical Measurements*. 6th ed. 2006, New York, NY: Prentice Hall.

Appendix A: Engineering Drawings

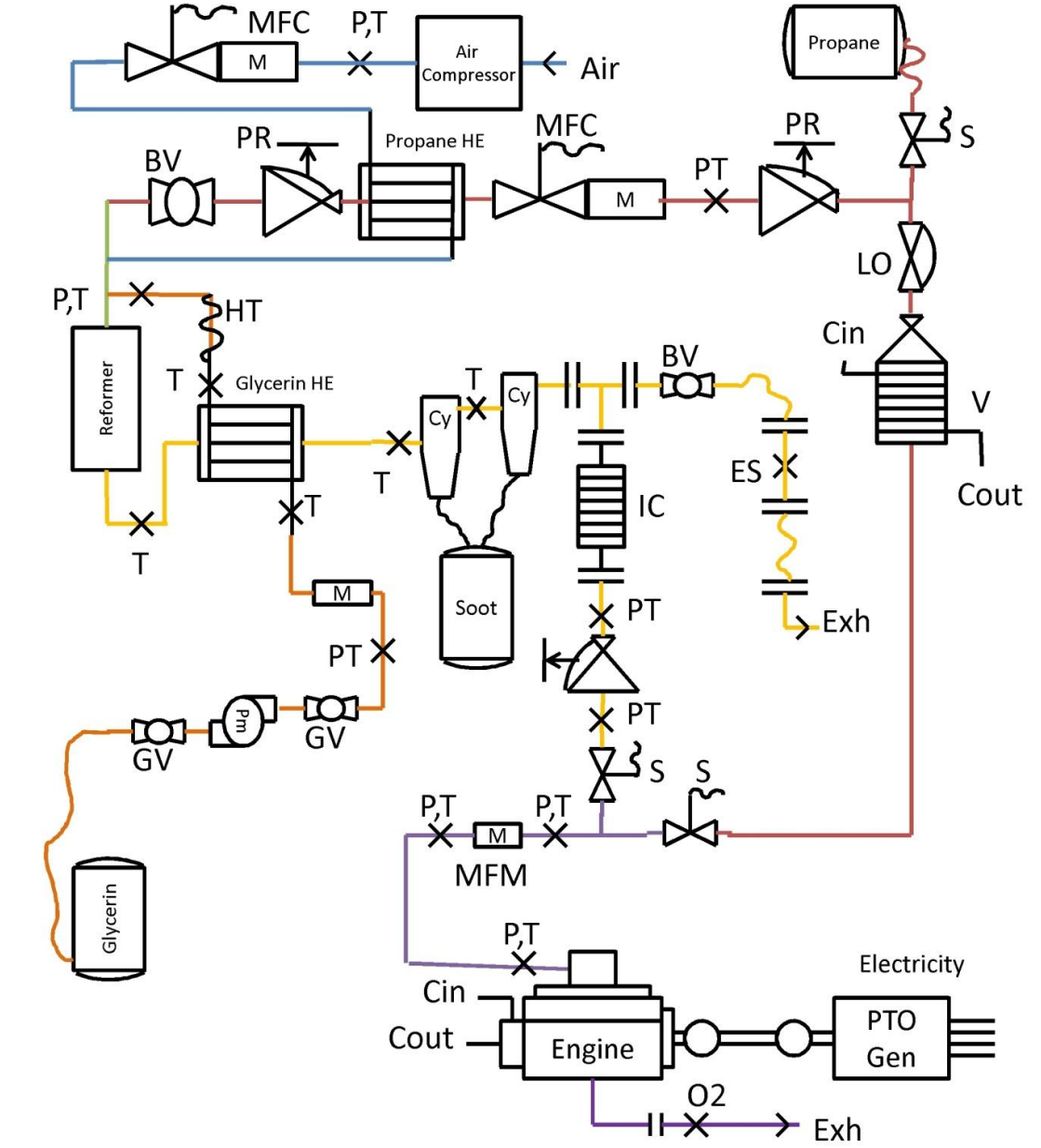

B= Blower	HE = Heat Exchanger	Pm= Pump
BV = Ball Valve	HT = Heat Tape	PR = Pressure Regulator
C = Coolant	IC = Intercooler	S = Solenoid
Cy = Cyclone	LO = Vacuum Lock-off	T = Thermocouple
ES = Emissions Sampling	MFC = Mass Flow Controller	V = Vaporizer
Exh = Exhaust	MFM = Mass Flow Meter	
Gen = Generator	O2 = Oxygen Sensor	
GV = Global Valve	P = Pressure Transducer	

Figure 1. Engineering Schematic for the Transportation Researches Institute (TRI) – Feedstock-to-Tailpipe Initiatives Glycerin Reforming Rig (aka. SynGas Rig).

Appendix B: Glycerin Properties

Glycerine (%)	Density (g/cm ^{3}) 15°C	15.5°C	20°C	25°C	30°C	Glycerine (%)	Density (g/cm ^{3}) 15°C	15.5°C	20°C	25°C	30°C
100	1.26415	1.26381	1.26108	1.25802	1.25495	50	1.12870	1.12845	1.12630	1.12375	1.12110
99	1.26160	1.26125	1.25850	1.25545	1.25235	49	1.12600	1.12575	1.12360	1.12110	1.11845
98	1.25900	1.25865	1.25590	1.25290	1.24975	48	1.12325	1.12305	1.12090	1.11840	1.11580
97	1.25645	1.25610	1.25335	1.25030	1.24710	47	1.12055	1.12030	1.11820	1.11575	1.11320
96	1.25385	1.25350	1.25080	1.24770	1.24450	46	1.11780	1.11760	1.11550	1.11310	1.11055
95	1.25130	1.25095	1.24825	1.24515	1.24190	45	1.11510	1.11490	1.11280	1.11040	1.10795
94	1.24865	1.24830	1.24560	1.24250	1.23930	44	1.11235	1.11215	1.11010	1.10775	1.10530
93	1.24600	1.24565	1.24300	1.23985	1.23670	43	1.10960	1.10945	1.10740	1.10510	1.10265
92	1.24340	1.24305	1.24035	1.23725	1.23410	42	1.10690	1.10670	1.10470	1.10240	1.10005
91	1.24075	1.24040	1.23770	1.23460	1.23150	41	1.10415	1.10400	1.10200	1.09975	1.09740
90	1.23810	1.23775	1.23510	1.23200	1.22890	40	1.10145	1.10130	1.09930	1.09710	1.09475
89	1.23545	1.23510	1.23245	1.22935	1.22625	39	1.09875	1.09860	1.09665	1.09445	1.09215
88	1.23280	1.23245	1.22975	1.22665	1.22360	38	1.09605	1.09590	1.09400	1.09180	1.08955
87	1.23015	1.22980	1.22710	1.22400	1.22095	37	1.09340	1.09320	1.09135	1.08915	1.08690
86	1.22750	1.22710	1.22445	1.22135	1.21830	36	1.09070	1.09050	1.08865	1.08655	1.08430
85	1.22485	1.22445	1.22180	1.21870	1.21565	35	1.08800	1.08780	1.08600	1.08390	1.08165
84	1.22220	1.22180	1.21915	1.21605	1.21300	34	1.08530	1.08515	1.08335	1.08125	1.07905
83	1.21955	1.21915	1.21650	1.21340	1.21035	33	1.08265	1.08245	1.08070	1.07860	1.07645
82	1.21690	1.21650	1.21380	1.21075	1.20770	32	1.07995	1.07975	1.07800	1.07600	1.07380
81	1.21425	1.21385	1.21115	1.20810	1.20505	31	1.07725	1.07705	1.07535	1.07335	1.07120
80	1.21160	1.21120	1.20850	1.20545	1.20240	30	1.07455	1.07435	1.07270	1.07070	1.06855
79	1.20885	1.20845	1.20575	1.20275	1.19970	29	1.07195	1.07175	1.07010	1.06815	1.06605
78	1.20610	1.20570	1.20305	1.20005	1.19705	28	1.06935	1.06915	1.06755	1.06560	1.06355
77	1.20335	1.20300	1.20030	1.19735	1.19435	27	1.06670	1.06655	1.06495	1.06305	1.06105
76	1.20060	1.20025	1.19760	1.19465	1.19170	26	1.06410	1.06390	1.06240	1.06055	1.05855
75	1.19785	1.19750	1.19485	1.19195	1.18900	25	1.06150	1.06130	1.05980	1.05800	1.05605
74	1.19510	1.19480	1.19215	1.18925	1.18635	24	1.05885	1.05870	1.05720	1.05545	1.05350
73	1.19235	1.19205	1.18940	1.18650	1.18365	23	1.05625	1.05610	1.05465	1.05290	1.05100
72	1.18965	1.18930	1.18670	1.18380	1.18100	22	1.05365	1.05350	1.05205	1.05035	1.04850
71	1.18690	1.18655	1.18395	1.18110	1.17830	21	1.05100	1.05090	1.04950	1.04780	1.04600
70	1.18415	1.18385	1.18125	1.17840	1.17565	20	1.04840	1.04825	1.04690	1.04525	1.04350
69	1.18135	1.18105	1.17850	1.17565	1.17290	19	1.04590	1.04575	1.04440	1.04280	1.04105
68	1.17860	1.17830	1.17575	1.17295	1.17020	18	1.04335	1.04325	1.04195	1.04035	1.03860
67	1.17585	1.17555	1.17300	1.17020	1.16745	17	1.04085	1.04075	1.03945	1.03790	1.03615
66	1.17305	1.17275	1.17025	1.16745	1.16470	16	1.03835	1.03825	1.03695	1.03545	1.03370
65	1.17030	1.17000	1.16750	1.16475	1.16195	15	1.03580	1.03570	1.03450	1.03300	1.03130
64	1.16755	1.16725	1.16475	1.16200	1.15925	14	1.03330	1.03320	1.03200	1.03055	1.02885
63	1.16480	1.16445	1.16205	1.15925	1.15650	13	1.03080	1.03070	1.02955	1.02805	1.02640
62	1.16200	1.16170	1.15930	1.15655	1.15375	12	1.02830	1.02820	1.02705	1.02560	1.02395
61	1.15925	1.15895	1.15655	1.15380	1.15100	11	1.02575	1.02565	1.02455	1.02315	1.02150
60	1.15650	1.15615	1.15380	1.15105	1.14830	10	1.02325	1.02315	1.02210	1.02070	1.01905
59	1.15370	1.15340	1.15105	1.14835	1.14555	9	1.02085	1.02075	1.01970	1.01835	1.01670
58	1.15095	1.15065	1.14830	1.14560	1.14285	8	1.01840	1.01835	1.01730	1.01600	1.01440
57	1.14815	1.14785	1.14555	1.14285	1.14010	7	1.01600	1.01590	1.01495	1.01360	1.01205
56	1.14535	1.14510	1.14280	1.14015	1.13740	6	1.01360	1.01350	1.01255	1.01125	1.00970
55	1.14260	1.14230	1.14005	1.13740	1.13470	5	1.01120	1.01110	1.01015	1.00890	1.00735
54	1.13980	1.13955	1.13730	1.13465	1.13195	4	1.00875	1.00870	1.00780	1.00655	1.00505
53	1.13705	1.13680	1.13455	1.13195	1.12925	3	1.00635	1.00630	1.00540	1.00415	1.00270
52	1.13425	1.13400	1.13180	1.12920	1.12650	2	1.00395	1.00385	1.00300	1.00180	1.00035
51	1.13150	1.13125	1.12905	1.12650	1.12380	1	1.00155	1.00145	1.00060	0.99945	0.99800
						0	0.99913	0.99905	0.99823	0.99708	0.99568

Figure 2. Density of Glycerin-Water Solution provided by Dow Chemical Company [3].

Glycerine by Wt. (%)	Water (%)	Freezing Points (°C)	(°F)	Glycerine by Wt. (%)	Water (%)	Freezing Points (°C)	(°F)
0.0	100.0	0.0	32.0	65.0	35.0	-43.0	-45.4
5.0	95.0	-0.6	30.9	65.6 (1)	34.4	-44.5	-48.1
10.0	90.0	-1.6	29.1	66.0 (1)	34.0	-44.7	-48.5
11.5 (1)	88.5	-2.0	28.4	66.7 (1)	33.3	-46.5	-51.7
15.0	85.0	-3.1	26.4	67.1 (1)	32.9	-45.5	-49.9
20.0	80.0	-4.8	23.4	67.3 (1)	32.7	-44.5	-48.1
22.6 (1)	77.4	-6.0	21.2	68.0 (1)	32.0	-44.0	-47.2
25.0	75.0	-7.0	19.4	70.0	30.0	-38.9	-38.0
30.0	70.0	-9.5	14.9	70.9 (1)	29.1	-37.5	-35.5
33.3 (1)	67.0	-11.0	12.2	75.0	25.0	-29.8	-21.6
35.0	65.0	-12.2	10.0	75.4 (1)	24.6	-28.5	-19.3
40.0	60.0	-15.4	4.3	79.0 (1)	21.0	-22.0	-7.6
44.5 (1)	55.5	-18.5	-1.3	80.0	20.0	-20.3	-4.5
45.0	55.0	-18.8	-1.8	84.8 (1)	15.2	-10.5	13.1
50.0	50.0	-23.0	-9.4	85.0	15.0	-10.9	12.4
53.0 (1)	47.0	-26.0	-14.8	90.0	10.0	-1.6	29.1
55.0	45.0	-28.2	-18.8	90.3 (1)	9.7	-1.0	30.2
60.0	40.0	-34.7	-30.5	95.0	5.0	7.7	45.9
60.4 (1)	39.6	-35.0	-31.0	95.3 (1)	4.7	7.5	45.5
64.0 (1)	36.0	-41.5	-42.7	98.2 (1)	1.8	13.5	56.3
64.7 (1)	35.3	-42.5	-44.5	100.0	0.0	17.0	62.6

(1) Actual determination. Remaining values were interpolated from curve.

Figure 3. Freezing Point of Glycerin-Water Solution provided by Dow Chemical Company [3].

Glycerine per cent weight	Temperatur e (°C)										
	0	10	20	30	40	50	60	70	80	90	100
0 [1]	1.792	1.308	1.005	0.8007	0.6560	0.5494	0.4688	0.4061	0.3565	0.3165	0.2838
10	2.44	1.74	1.31	1.03	0.826	0.680	0.575	0.500	–	–	–
20	3.44	2.41	1.76	1.35	1.07	0.879	0.731	0.635	–	–	–
30	5.14	3.49	2.50	1.87	1.46	1.16	0.956	0.816	0.690	–	–
40	8.25	5.37	3.72	2.72	2.07	1.62	1.30	1.09	0.918	0.763	0.668
50	14.6	9.01	6.00	4.21	3.10	2.37	1.86	1.53	1.25	1.05	0.910
60	29.9	17.4	10.8	7.19	5.08	3.76	2.85	2.29	1.84	1.52	1.28
65	45.7	25.3	15.2	9.85	6.80	4.89	3.66	2.91	2.28	1.86	1.55
67	55.5	29.9	17.7	11.3	7.73	5.50	4.09	3.23	2.50	2.03	1.68
70	76	38.8	22.5	14.1	9.40	6.61	4.86	3.78	2.90	2.34	1.93
75	132	65.2	35.5	21.2	13.6	9.25	6.61	5.01	3.80	3.00	2.43
80	255	116	60.1	33.9	20.8	13.6	9.42	6.94	5.13	4.03	3.18
85	540	223	109	58	33.5	21.2	14.2	10.0	7.28	5.52	4.24
90	1310	498	219	109	60.0	35.5	22.5	15.5	11.0	7.93	6.00
91	1590	592	259	127	68.1	39.8	25.1	17.1	11.9	8.62	6.40
92	1950	729	310	147	78.3	44.8	28.0	19.0	13.1	9.46	6.82
93	2400	860	367	172	89	51.5	31.6	21.2	14.4	10.3	7.54
94	2930	1040	437	202	105	58.4	35.4	23.6	15.8	11.2	8.19
95	3690	1270	523	237	121	67.0	39.9	26.4	17.5	12.4	9.08
96	4600	1580	624	281	142	77.8	45.4	29.7	19.6	13.6	10.1
97	5770	1950	765	340	166	88.9	51.9	33.6	21.9	15.1	10.9
98	7370	2460	939	409	196	104	59.8	38.5	24.8	17.0	12.2
99	9420	3090	1150	500	235	122	69.1	43.6	27.8	19.0	13.3
100	12070	3900	1410	612	284	142	81.3	50.6	31.9	21.3	14.8

[1]Viscosity of water taken from "Properties of Ordinary Water-Substance." N.E. Dorsey, p. 184. New York (1940)

Figure 4. Viscosity of Aqueous Glycerin-Water Solution (Units: cP/mPa-s) provided by Dow Chemical Company [3].

		Specific Heats, Cal/g/°C or Btu/lb/°F								
		Glycerine								
°F	°C	25%	30%	35%	40%	45%	50%	55%	60%	65%
35.0	1.7	0.88	0.87	0.86	0.84	0.82	0.80	0.77	0.74	0.71
30.0	-1.1	0.88	0.86	0.85	0.83	0.81	0.79	0.76	0.73	0.70
25.0	-3.9	0.87	0.86	0.84	0.82	0.80	0.78	0.75	0.72	0.69
20.0	-6.7	0.86	0.85	0.83	0.82	0.79	0.77	0.74	0.71	0.68
19.0 (1)	-7.2	6.8 (1)	–	–	–	–	–	–	–	–
15.0 (1)	-9.4	4.1	4.8 *	0.82	0.80	0.78	0.76	0.73	0.70	0.67
10.4 (1)	-12.0	–	–	3.7 (1)	–	–	–	–	–	–
10.0	-12.2	2.7	3.2	3.6	0.80	0.78	0.75	0.72	0.69	0.66
5.0	-15.0	2.1	2.4	2.7	0.79	0.77	0.74	0.71	0.67	0.65
4.6 (1)	-15.2	–	–	–	2.9 (1)	–	–	–	–	–
0.0	-17.8	1.7	1.9	2.1	2.4	0.76	0.73	0.70	0.66	0.63
-1.8 (1)	-18.8	–	–	–	–	2.4 (1)	–	–	–	–
-5.0	-20.6	1.4	1.6	1.8	2.0	2.2	0.72	0.69	0.65	0.62
-9.6 (1)	-23.1	–	–	–	–	–	2.0 (1)	–	–	–
-10.0	-23.3	1.2	1.4	1.6	1.7	1.9	2.0	0.68	0.64	0.61
-15.0	-26.1	1.1	1.2	1.3	1.5	1.6	1.7	0.67	0.63	0.60
-18.9 (1)	-28.3	–	–	–	–	–	–	1.7 (1)	–	–
-20.0	-28.9	1.0	1.1	1.2	1.3	1.4	1.5	1.6	0.62	0.59
-25.0	-31.7	0.9	1.0	1.1	1.2	1.25	1.3	1.4	0.61	0.58

(1)Estimated freezing point, and maximum specific heat for mixture of this composition.

The horizontal lines in each column mark the lower limit of the one-phase systems.

Figure 5. Specific Heat of Glycerin-Water Solution provided by Dow Chemical Company [3].

°C	195	185	175	165	155	145	135	125
L = cal/mol	18170	18780	18610	18740	19740	19810	19430	18925
°C	115	105	95	85	75	65	55	
L = cal/mol	19530	19300	19910	20840	21170	21120	21060	

L is the molar heat of vaporization.

Figure 6. Heat of Vaporization for Glycerin provided by Dow Chemical Company [3] .

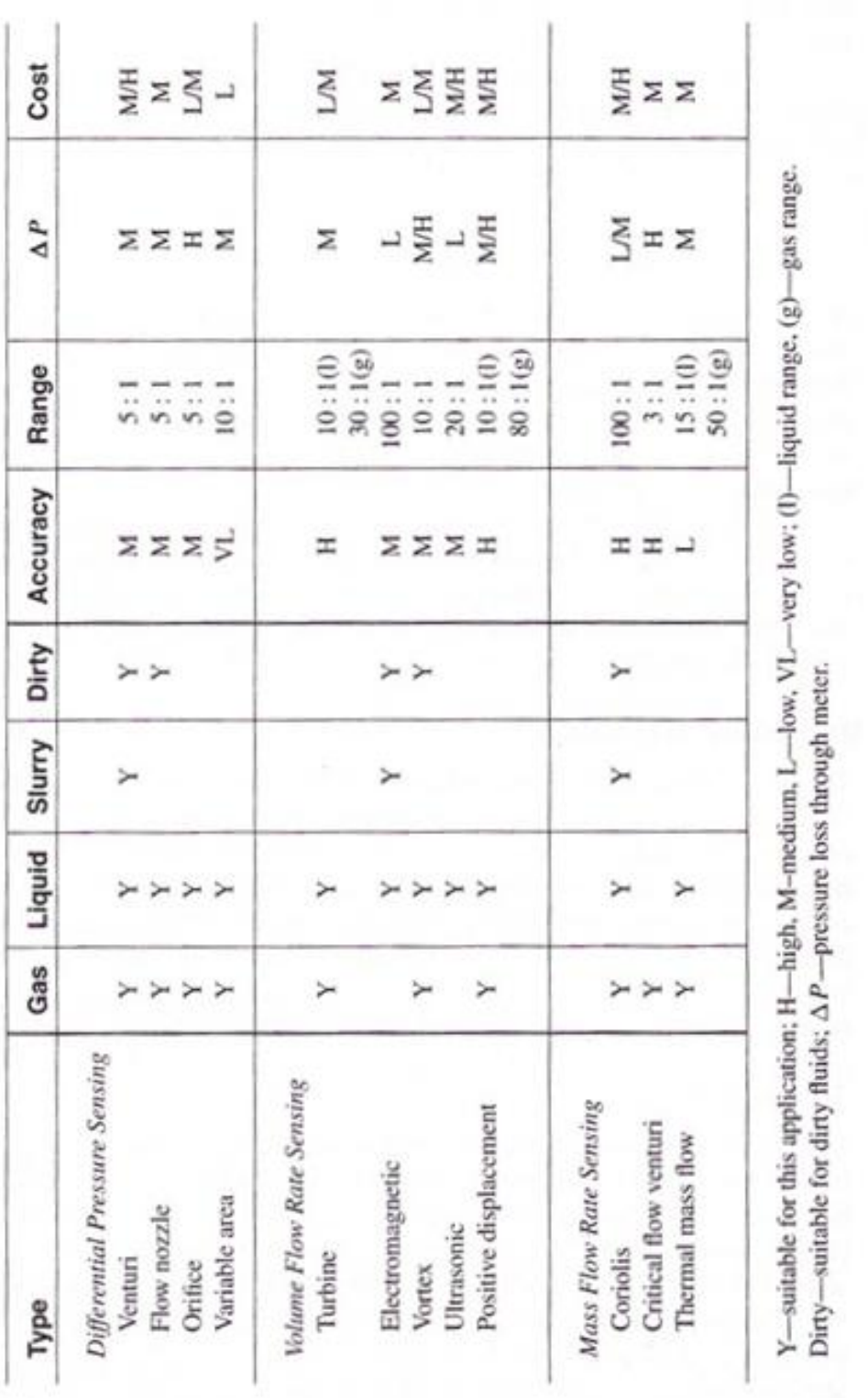

Type	Gas	Liquid	Slurry	Dirty	Accuracy	Range	ΔP	Cost
Differential Pressure Sensing								
Venturi	Y	Y	Y	Y	M	5 : 1	M	M/H
Flow nozzle	Y	Y		Y	M	5 : 1	M	M
Orifice	Y	Y			M	5 : 1	H	L/M
Variable area	Y	Y			VL	10 : 1	M	L
Volume Flow Rate Sensing								
Turbine	Y	Y			H	10 : 1(l)	M	L/M
						30 : 1(g)		
Electromagnetic		Y	Y	Y	M	100 : 1	L	M
Vortex	Y	Y		Y	M	10 : 1	M/H	L/M
Ultrasonic		Y			M	20 : 1	L	M/H
Positive displacement	Y	Y			H	10 : 1(l)	M/H	M/H
						80 : 1(g)		
Mass Flow Rate Sensing								
Coriolis	Y	Y	Y	Y	H	100 : 1	L/M	M/H
Critical flow venturi	Y				H	3 : 1	H	M
Thermal mass flow	Y	Y			L	15 : 1(l)	M	M
						50 : 1(g)		

Y—suitable for this application; H—high, M–medium, L—low, VL—very low; (l)—liquid range, (g)—gas range.
Dirty—suitable for dirty fluids; ΔP—pressure loss through meter.

Figure 7. Flow Meter/Controller Options compiled and published in *Mechanical Measurements 6th edition* by Beckwith [6].

Appendix D: Electric Schematics

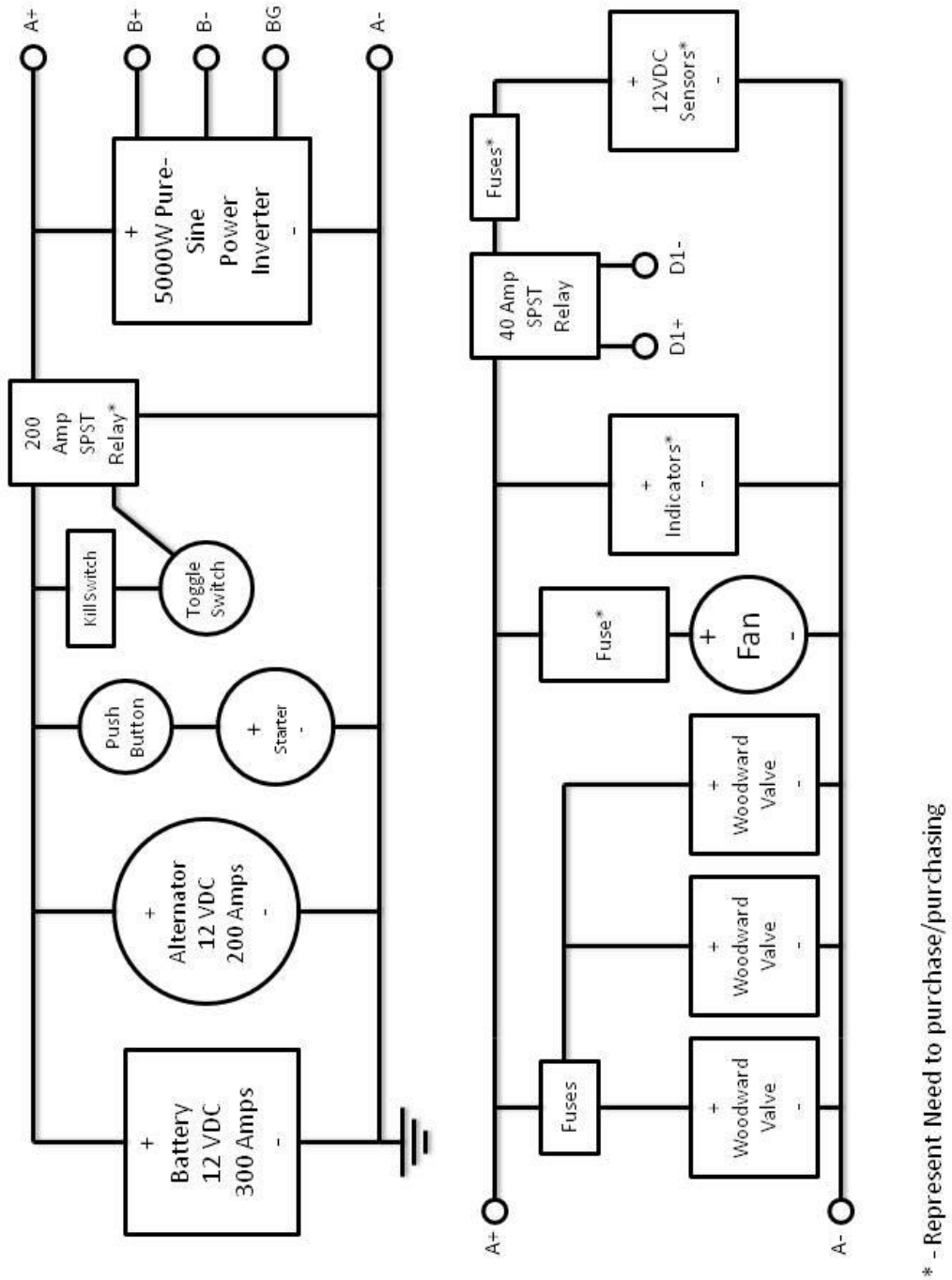

Figure 8. Electronic Schematic for the Transportation Researches Institute (TRI) – Feedstock-to-Tailpipe Initiatives Glycerin Reforming Rig (aka. SynGas Rig). (Continues on Next Two Pages via Right Hand Side of Diagram)

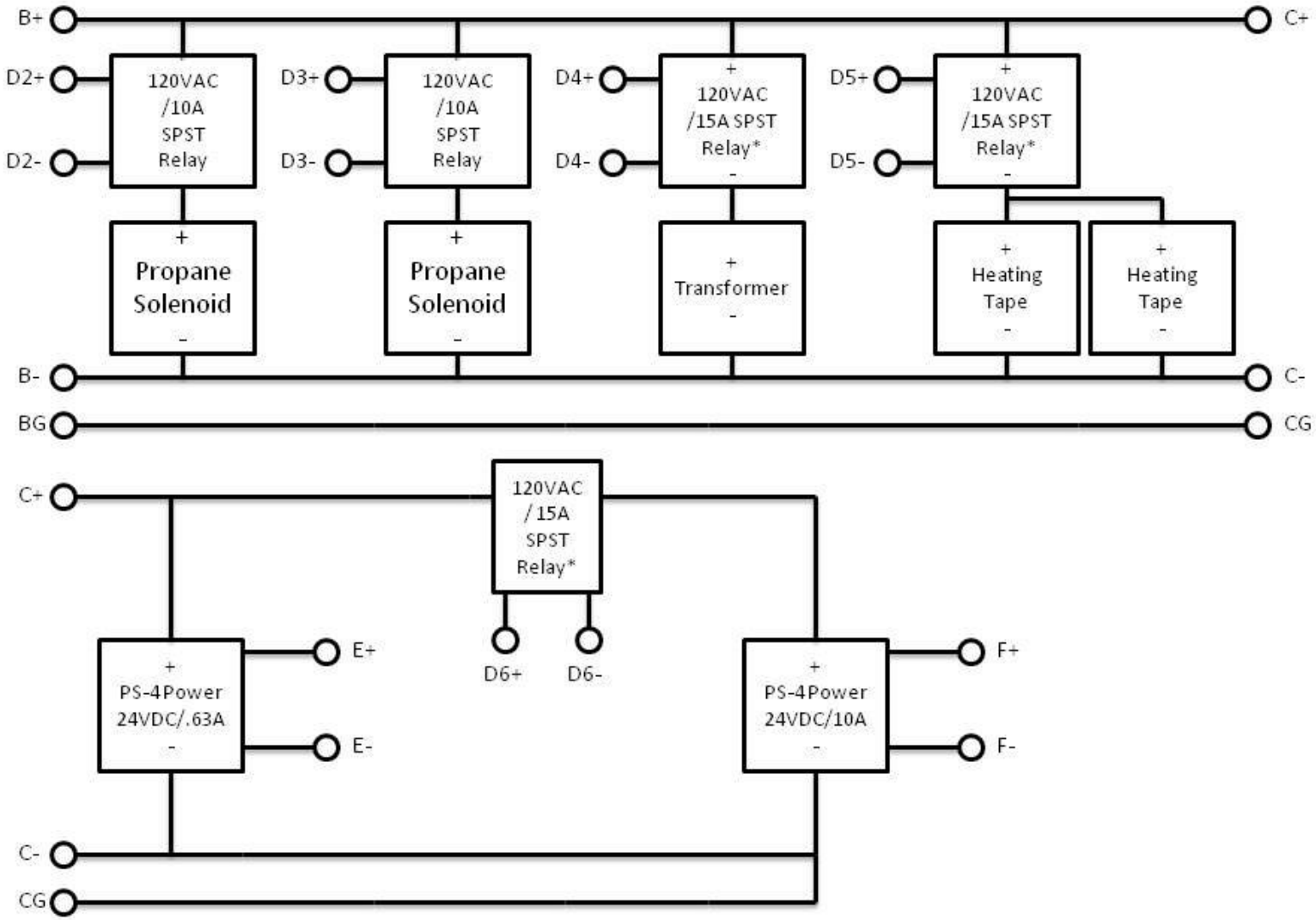

* - Represent Need to purchase/purchasing

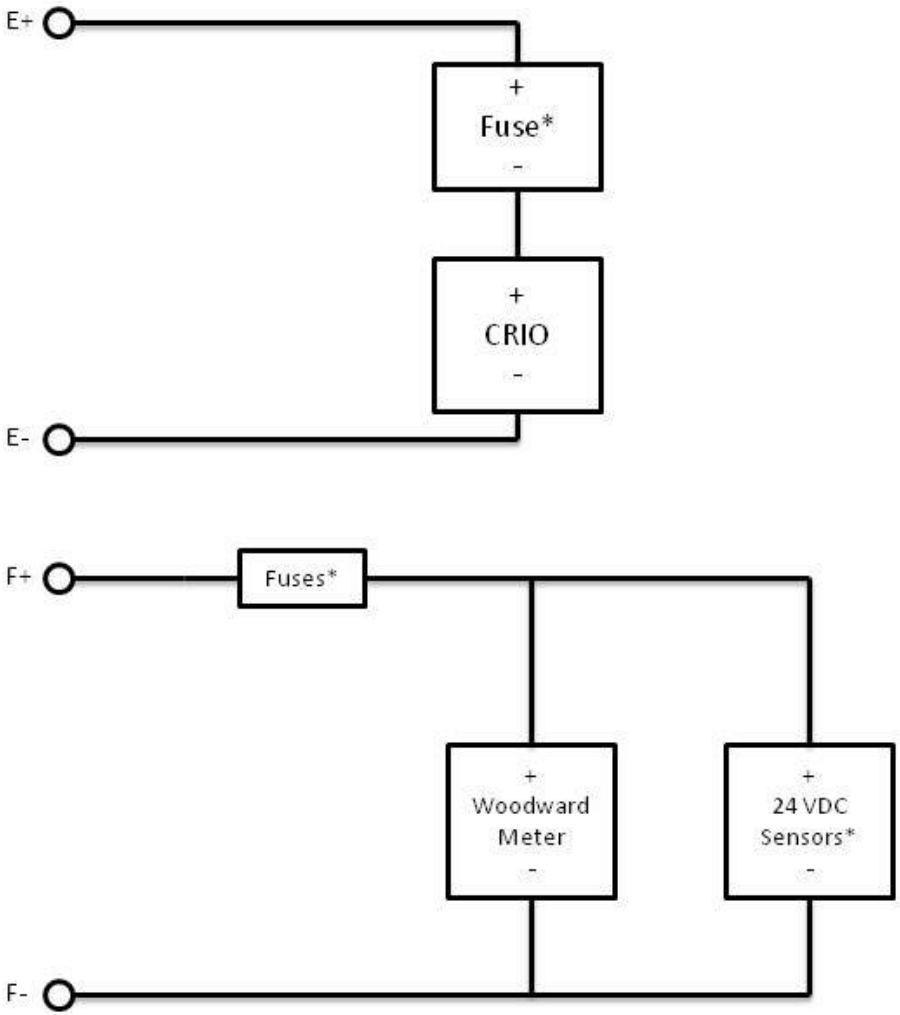

* - Represent Need to purchase/purchasing

Appendix E: Cost Estimates

Table 1. Cost Estimate for Control and Data Acquisition System on the Transportation Researches Institute (TRI) – Feedstock-to-Tailpipe Initiatives Glycerin Reforming Rig (aka. SynGas Rig).

Item:	Company:	Product Number:	Description:	Qty:	Price:	Cost:
1	National Instruments	cRIO-9073	CompactRIO 8-Modules	1	$ -	$ -
2	National Instruments	NI 9205	32-Channel Analog Voltage Input Module	1	$ 720.00	$ 720.00
3	National Instruments	NI 9264	16-Channel Analog Voltage Output Module	1	$ 810.00	$ 810.00
4	National Instruments	NI 9203	8-Channel Analog Current Input Module	2	$ 440.00	$ 880.00
5	National Instruments	NI 9213	16-Channel Thermocouple Module	1	$ 900.00	$ 900.00
6	National Instruments	NI 9403	32-Channel Digital I/O Module	1	$ 440.00	$ 440.00
7			Additional Equipment			
-	Mouser Electronics	709-DRP240-24	Linear & Switching Power Supplies 240W 24V 10A	1	$ 153.50	$ 153.50
		802-586-902	General Purpose / Industrial Relays SPNO 12VDC	1	$ 47.01	$ 47.01
		881-STH24D12	Solid State Relays 12A 12-280VAC 3-32VDC Zero Cross	3	$ 15.86	$ 47.58
					Total:	$ 3,998.09

Table 2. Cost Estimate for Measuring Equipment on the Transportation Researches Institute (TRI) – Feedstock-to-Tailpipe Initiatives Glycerin Reforming Rig (aka. SynGas Rig). (Continues on Next Four Pages)

Item:	Company:	Product Number:	Description:	Qty:	Necessary:	Connection:	Price:	Cost:
1	Omega	FPD1001 B-A	1/8" Oval Gear Pulse Meter	1	X	Current	$ 975.00	$ 975.00
2	Omega	KQXL-18U-12	K-Type Thermocouple - 6" Length, 1/8" Diameter, Ungrounded Junction					
-			After the large heat exchanger & before the reformer (propane)		Have	TC	$ 30.00	$ -
-			After the glycerin pump & before the glycerin flowmeter for MFR	1	X	TC	$ 30.00	$ 30.00
-			After the Glycerin flow meter & before small heat exchanger	1		TC	$ 30.00	$ 30.00
-			After the small heat exchanger & before the heat tape	1		TC	$ 30.00	$ 30.00
-			After the reformer & before the small heat exchanger		Have	TC	$ 30.00	$ -
-			After the small heat exchanger & before big exchanger		Have	TC	$ 30.00	$ -
-			After the big heat exchanger & before the first cyclone		Have	TC	$ 30.00	$ -
-			After the first cyclone & before the second cyclone	1		TC	$ 30.00	$ 30.00
-			After the second cyclone & before the process tee	1		TC	$ 30.00	$ 30.00

-			After the process tee & before the intercooler		Have	TC	$ 30.00	$ -
-			After the intercooler & before the pressure regulator	1		TC	$ 30.00	$ 30.00
3	Omega	KQXL-18E-12	K-Type Thermocouple - 6" Length, 1/8" Diameter, Exposed Junction					
-			After the pressure regulator & before the solenoid	1		TC	$ 27.00	$ 27.00
-			After the solenoid & before the engine flowmeter for MFR	1	X	TC	$ 27.00	$ 27.00
-			After the engine flowmeter & before the ZPR	1		TC	$ 27.00	$ 27.00
-			After the ZPR & before the Woodward A/F Valve	1	X	TC	$ 27.00	$ 27.00
4	Omega	PX319-200GI	Pressure Transducer - 200 PSI gauge - Din Connection					
-			After the Glycerin pump & before the Glycerin Flowmeter for MFR	1	X	Current	$ 225.00	$ 225.00
-			After the heat tape & before the reformer nozzle	1	X	Current	$ 225.00	$ 225.00
5	Omega	PX319-030AI	Pressure Transducer - 30 PSI absolute - Din Connection					
-			Reform Inlet Air Pressure	1			$ 245.00	$ 245.00

-			After the pressure regulator & before the solenoid	1		Current	$ 245.00	$ 245.00
-			After the solenoid & before the engine flowmeter for MFR	1	X	Current	$ 245.00	$ 245.00
-			After the engine flowmeter & before the ZPR	1		Current	$ 245.00	$ 245.00
-			After the ZPR & before the Woodward A/F Valve	1	X	Current	$ 245.00	$ 245.00
6	Omega	PX319-200AI	Pressure Transducer - 200 PSI absolute - Din Connection					
-			On the process tee	1		Current	$ 245.00	$ 245.00
-			After the intercooler & before the pressure regulator	1		Current	$ 245.00	$ 245.00
7	Omega	LVU31	Ultrasonic level transmitter/switch 1.2 m (4') range	1		Voltage	$ 350.00	$ 350.00
8	Swagelok	SS-200-1-4BT	SS Swagelok Tube Fitting, Bored-Through Male Connector, 1/8 in. Tube OD x 1/4 in. Male NPT					
-			After the pressure regulator & before the solenoid		Have		$ -	$ -
-			After the solenoid & before the engine flowmeter for MFR		Have		$ -	$ -
-			After the engine flowmeter & before the ZPR		Have		$ -	$ -
-			After the ZPR & before the		Have		$	$

			Woodward A/F Valve				-	-
-			After the intercooler & before the pressure regulator	1			$ 25.00	$ 25.00
9	Swagelok	SS-200-1-2BT	SS Swagelok Tube Fitting, Bored-Through Male Connector, 1/8 in. Tube OD x 1/8 in. Male NPT					
-			After the large heat exchanger & before the reformer (propane)		Have		$ -	$ -
-			After the glycerin pump & before the glycerin flowmeter for MFR	1	X		$ 25.00	$ 25.00
-			After the Glycerin flow meter & before small heat exchanger		Have		$ -	$ -
-			After the small heat exchanger & before the heat tape		Have		$ -	$ -
-			After the reformer & before the small heat exchanger		Have		$ -	$ -
-			After the small heat exchanger & before big exchanger		Have		$ -	$ -
-			After the big heat exchanger & before the first cyclone		Have		$ -	$ -
-			After the first cyclone & before the second cyclone		Have		$ -	$ -
-			After the second cyclone & before the process tee		Have		$ -	$ -

-			After the process tee & before the intercooler		Have		$ -	$ -
10			Oil Pressure		Have	Voltage	$ -	$ -
11			Coolant Temperature		Have	Voltage	$ -	$ -
12	Woodward		Speed		Have	Serial	$ -	$ -
13	Summit Racing	A054E051N	Tachometer, Digital, 0-9,900 rpm, 2 1/16 in., 8-Cylinder, Electrical, Red, Each	1	X	Voltage	$ 61.95	$ 61.95
			Total:	24				$ 3,889.95

Appendix F: Predictor Model

The governing stoichiometric balance for the reformation of a hydrocarbon and oxygen containing fuel equals:

$$f\left(\mathrm{C}_{\alpha}\mathrm{H}_{\beta}\mathrm{O}_{\gamma}\right)+\left(\mathrm{O}_2+3.76\mathrm{N}_2\right)\rightarrow a\mathrm{CO}_2+b\mathrm{H}_2+c\mathrm{CO}+d\mathrm{H}_2\mathrm{O}+3.76\mathrm{N}_2$$

with the atom balances represented as:

C:	$\alpha f = a + c$	(F1)
H:	$\beta f = 2b + 2d$	(F2)
O:	$\gamma f + 2 = 2a + c + d$	(F3)
N:	$3.76 = e$	(F4)

To solve for the five variables, the model requires a fifth equation. This comes from chemical equilibrium according to the Water-Gas Shift Reaction as discussed in ME 636 Internal Combustion Engines: $a\mathrm{CO}_2+b\mathrm{H}_2\leftrightarrow c\mathrm{CO}+d\mathrm{H}_2\mathrm{O}$ with the equilibrium constant derived from fundamentals as:

$$K_e=\log_{10}\left(C\right)=\frac{c^1d^1}{a^1b^1}\left(\frac{P}{a+b+c+d}\right)^{1+1-1-1}=\frac{cd}{ab} \qquad \text{(F5)}$$

By using Microsoft Excel 2007 polynomial equation solver, an equation can be found for K_e as a function of temperature (K) using the data from Table 3:

$$K_{eq}=-2.31719599\times10^{-12}T^4+7.97773201\times10^{-9}T^3-7.14355823\times10^{-6}T^2 +2.4713825\times10^{-3}T-2.94930280\times10^{-1} \qquad \text{(F6)}$$

Table 3. Log Base 10 Equilibrium Constant for Water Gas Shift Reaction provide in *Thermodynamics: An Engineering Approach* by Cengel. [4]

Temperature [K]	C	K_e	Solved	Difference
298	-5.018	9.594E-06	9.59424E-06	-2.34253E-10
500	-2.139	0.00726106	0.007261059	1.99351E-10
1000	-0.159	0.69342581	0.6934258	6.01657E-09
1200	0.135	1.36458314	1.364583125	1.13729E-08
1400	0.333	2.15278173	2.152781715	1.92684E-08

The equilibrium equation can then be used to solve for *b* as follows:

Solving (F1) for a:	$a = \alpha f - c$	(F7)
Solving (F2) for d:	$d = \frac{\beta}{2} f - b$	(F8)

Solving (F3) for c:	$c = \gamma f + 2 - 2a - d$	(F9)
Plugging (F7,F8) into (F9)	$c = \gamma f + c - c(\alpha f - c) - \left(\frac{\beta}{2} f - b\right)$	
	$c = \gamma f + 2 - 2\alpha f + 2c - \frac{\beta}{2} f + b$	(F10)
Solving (F10) for c:	$c = 2\alpha f + \frac{\beta}{2} f - \gamma f - 2 - b$	(F11)

By substituting equations (F7, F8, and F11) into (F5), we obtain the following for the chemical equilibrium constant:

$$K_e = \frac{\left(2\alpha f + \frac{\beta}{2} f - \gamma f - 2 - b\right)\left(\frac{\beta}{2} f - b\right)}{(\alpha f - c)b}$$

$$K_e = \frac{b^2(1) + b\left(\gamma f + 2 - \beta f - 2\alpha f\right) + \left(2\alpha \frac{\beta}{2} f^2 + \frac{\beta^2}{4} f^2 - \frac{\beta}{2}\gamma f^2 - \beta f\right)}{b^2(1) + b\left(-\alpha f - \frac{\beta}{2} f + \gamma f + 2\right) + (0)}$$

$$K_e\left(b^2(1) + b\left(-\alpha f - \frac{\beta}{2} f + \gamma f + 2\right) + (0)\right) =$$

$$\left(b^2(1) + b\left(\gamma f + 2 - \beta f - 2\alpha f\right) + \left(2\alpha \frac{\beta}{2} f^2 + \frac{\beta^2}{4} f^2 - \frac{\beta}{2}\gamma f^2 - \beta f\right)\right)$$

$$\left(b^2(K_e) + b\left(-\alpha K_e f - \frac{\beta}{2} K_e f + \gamma K_e f + 2K_e\right)\right)$$

$$= \left(b^2(1) + b\left(\gamma f + 2 - \beta f - 2\alpha f\right) + \left(2\alpha \frac{\beta}{2} f^2 + \frac{\beta^2}{4} f^2 - \frac{\beta}{2}\gamma f^2 - \beta f\right)\right)$$

$$b^2(1 - K_e) + b\left(\gamma f + 2 - \beta f - 2\alpha f - \left(-\alpha K_e f - \frac{\beta}{2} K_e f + \gamma K_e f + 2K_e\right)\right)$$

$$+ \left(2\alpha \frac{\beta}{2} f^2 + \frac{\beta^2}{4} f^2 - \frac{\beta}{2}\gamma f^2 - \beta f\right) = 0$$

$$b^2(1 - K_e) + b\left(\gamma f + 2 - \beta f - 2\alpha f + \alpha K_e f + \frac{\beta}{2} K_e f - \gamma K_e f - 2K_e\right)$$

$$+ \left(2\alpha \frac{\beta}{2} f^2 + \frac{\beta^2}{4} f^2 - \frac{\beta}{2}\gamma f^2 - \beta f\right) = 0$$

$b^2\left(1-K_e\right)+b\left(f\left(\gamma-\beta-2\alpha+K_e\left(\alpha+\frac{\beta}{2}-1\right)\right)+2-2K_e\right)+\left(f^2\beta\left(\alpha+\frac{\beta}{4}-\frac{\gamma}{2}-\frac{1}{f}\right)\right)=0$	(F12)

Then, by using the quadratic equation, *b* can be found from (F12):

$b=-\frac{\left(f\left(\gamma-\beta-2\alpha+K_e\left(\alpha+\frac{\beta}{2}-1\right)\right)+2-2K_e\right)}{\left(1-K_e\right)}$ $+\frac{\sqrt{\left(f\left(\gamma-\beta-2\alpha+K_e\left(\alpha+\frac{\beta}{2}-1\right)\right)+2-2K_e\right)^2-4\left(1-K_e\right)\left(f^2\beta\left(\alpha+\frac{\beta}{4}-\frac{\gamma}{2}-\frac{1}{f}\right)\right)}}{\left(1-K_e\right)}$ $b=-\frac{\left(f\left(\gamma-\beta-2\alpha+K_e\left(\alpha+\frac{\beta}{2}-1\right)\right)+2-2K_e\right)}{\left(1-K_e\right)}$ $-\frac{\sqrt{\left(f\left(\gamma-\beta-2\alpha+K_e\left(\alpha+\frac{\beta}{2}-1\right)\right)+2-2K_e\right)^2-4\left(1-K_e\right)\left(f^2\beta\left(\alpha+\frac{\beta}{4}-\frac{\gamma}{2}-\frac{1}{f}\right)\right)}}{\left(1-K_e\right)}$	(F13)

Using equation (F13), the molar amounts can be found for each of the species leaving the reformer:

$d=\frac{\beta}{2}f-b$	(F8)
$c=2\alpha f+\frac{\beta}{2}f-\gamma f-2-b$	(F11)
$a=\alpha f-c$	(F7)
$e=3.76$	(F4)

Appendix G: Predictor Model Table for Propane and Glycerin Reforming

Table 4. Predictor Model Results of Propane (C_3H_8), Glycerin ($C_3H_8O_3$), and Glycerin with 33% Water Reformation at a Reformer Temperature of 800K and 101325 Pa.

	Propane		*Glycerin*		*Glycerin with 33% Water*	
Fuel/Air molar ratio		2/3		25		25
Air/Fuel ratio		4.73		0.024		.0546
Carbon dioxide	*a*	0.00	*a*	0.95	*a*	10.28
Hydrogen	*b*	2.68	*b*	98.95	*b*	108.28
Carbon monoxide	*c*	2.00	*c*	74.05	*c*	64.72
Water vapor	*d*	0.00	*d*	1.05	*d*	4.22
Nitrogen	*e*	3.76	*e*	3.76	*e*	3.76
H_2/CO ratio		1.34		1.34		1.67
EGR%		44.55		3.22		9.55
M_{mix} [kg/kmol]		19.76		13.65		13.93
R_{mix} [J/kg·K]		402.80		609.18		596.70
$Q_{LHV,mix}$ [kJ/kg]		19,720		19,958		21,911
$CQ_{LHV,mix}$ [kJ/kg]		7247		18,389		16,700

Appendix H: Propane Results from the Predictor Model

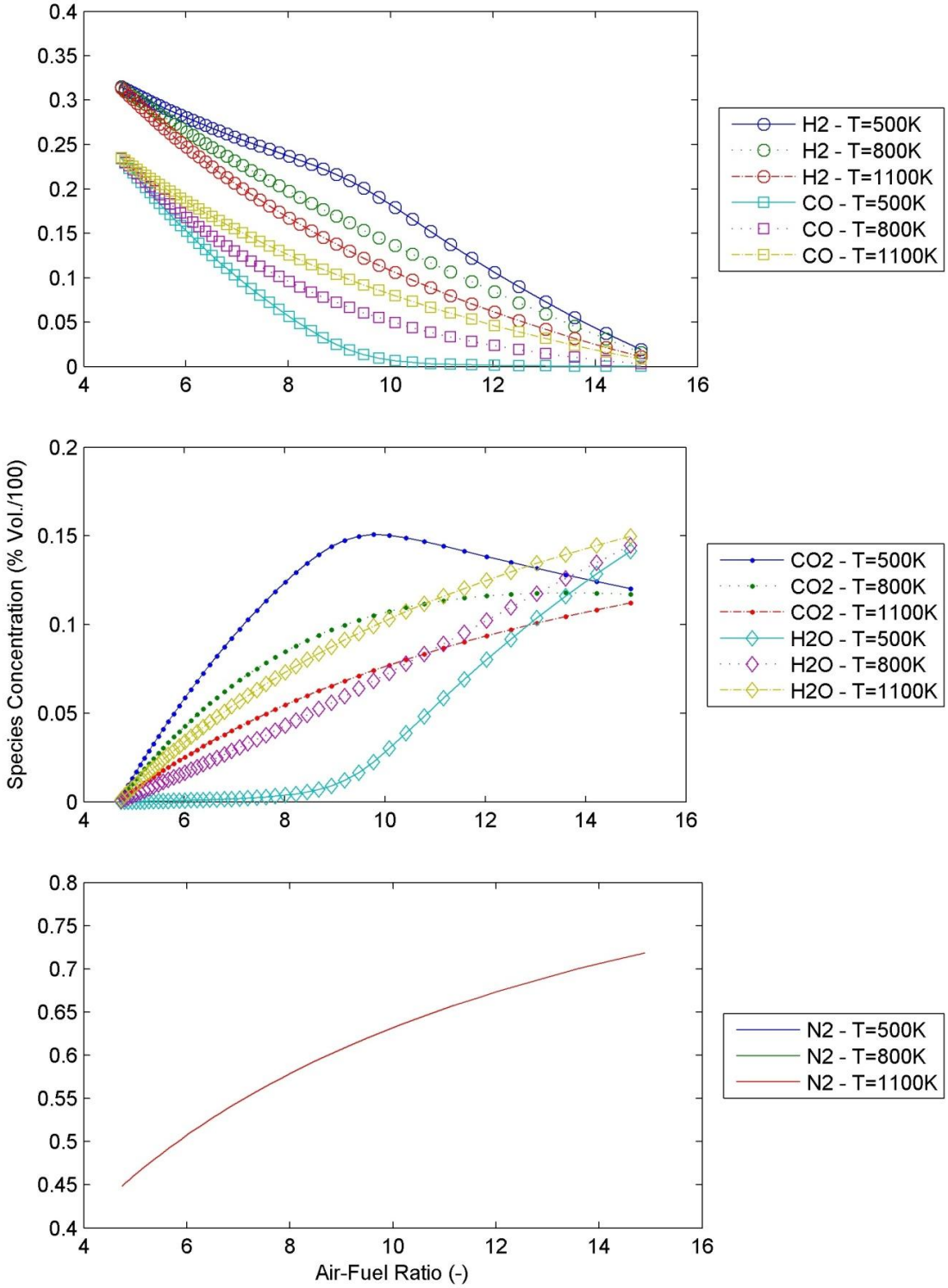

Figure 9. Species Concentration for Propane Reforming at any pressure and multiple temperatures with *x*-axis given as a function of mass air-to-fuel ratio.

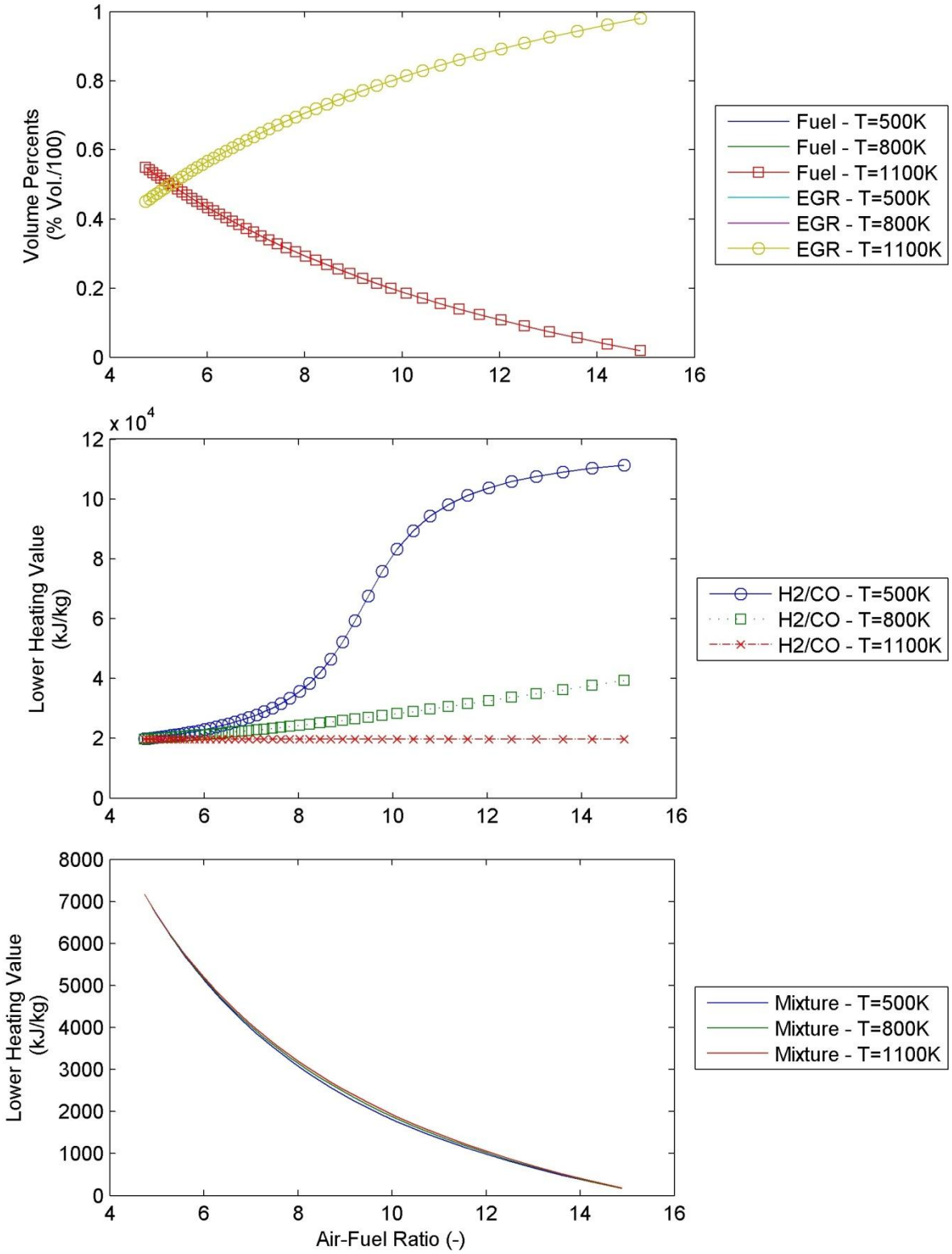

Figure 10. Properties for Propane Reforming at any pressure and multiple temperatures with *x*-axis given as a function of mass air-to-fuel ratio.

Appendix I: Glycerin Results from the Predictor Model

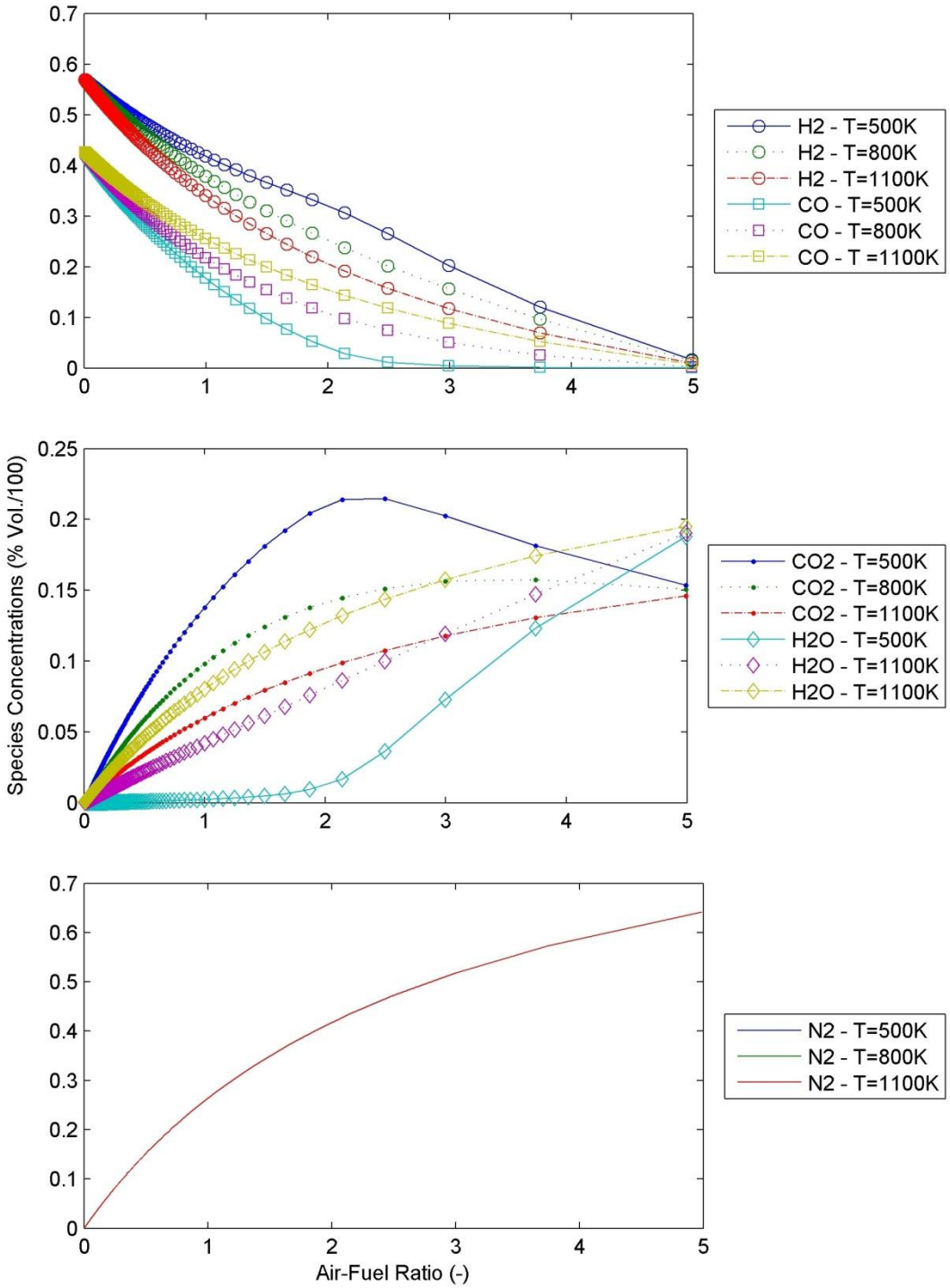

Figure 11. Species Concentration for Glycerin Reforming with 0% Water at any pressure and multiple temperatures with *x*-axis given as a function of mass air-to-fuel ratio.

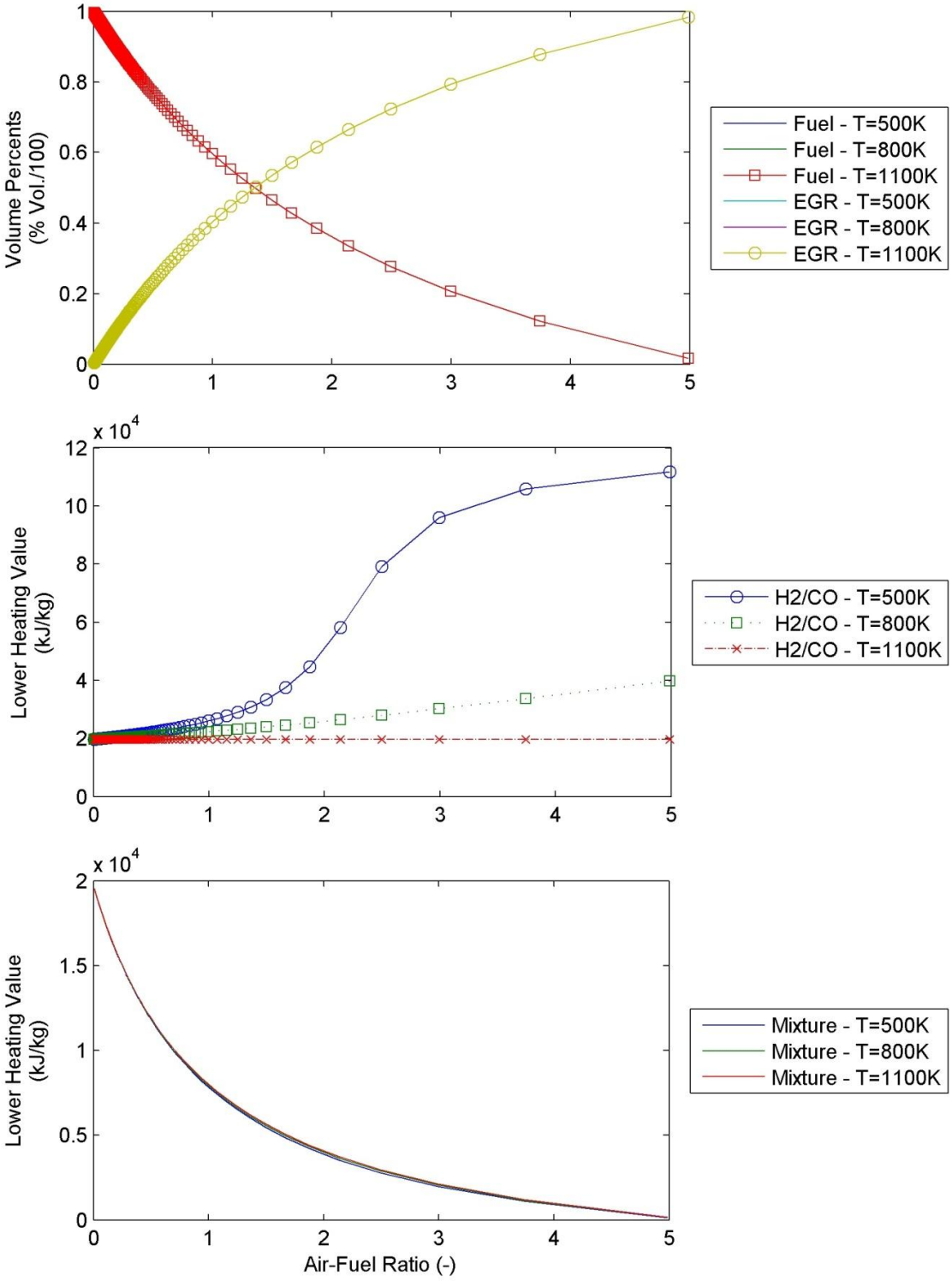

Figure 12. Properties for Glycerin Reforming with 0% Water at any pressure and multiple temperatures with *x*-axis given as a function of mass air-to-fuel ratio.

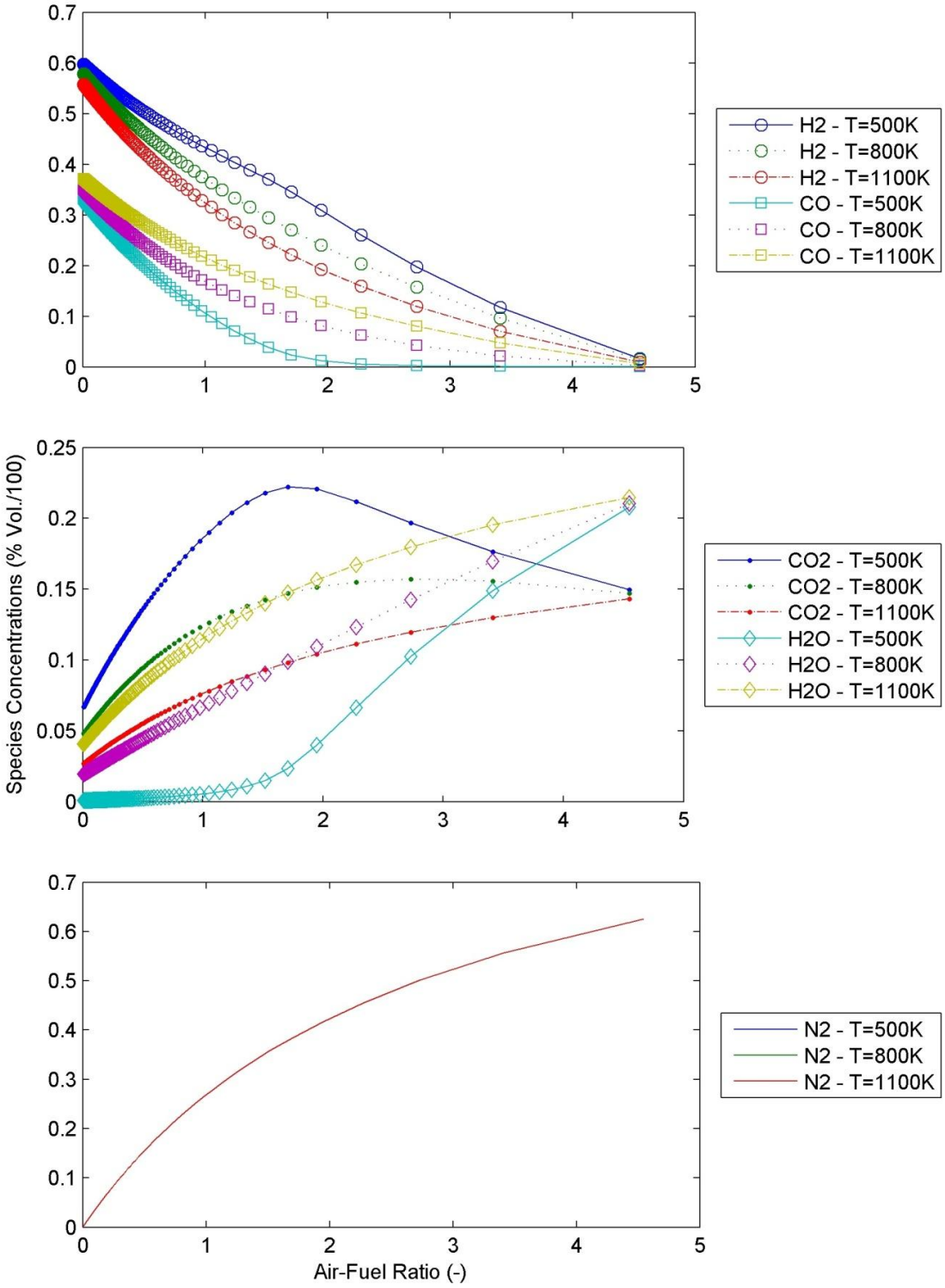

Figure 13. Species Concentration for Glycerin Reforming with 33% Water at any pressure and multiple temperatures with *x*-axis given as a function of mass air-to-fuel ratio.

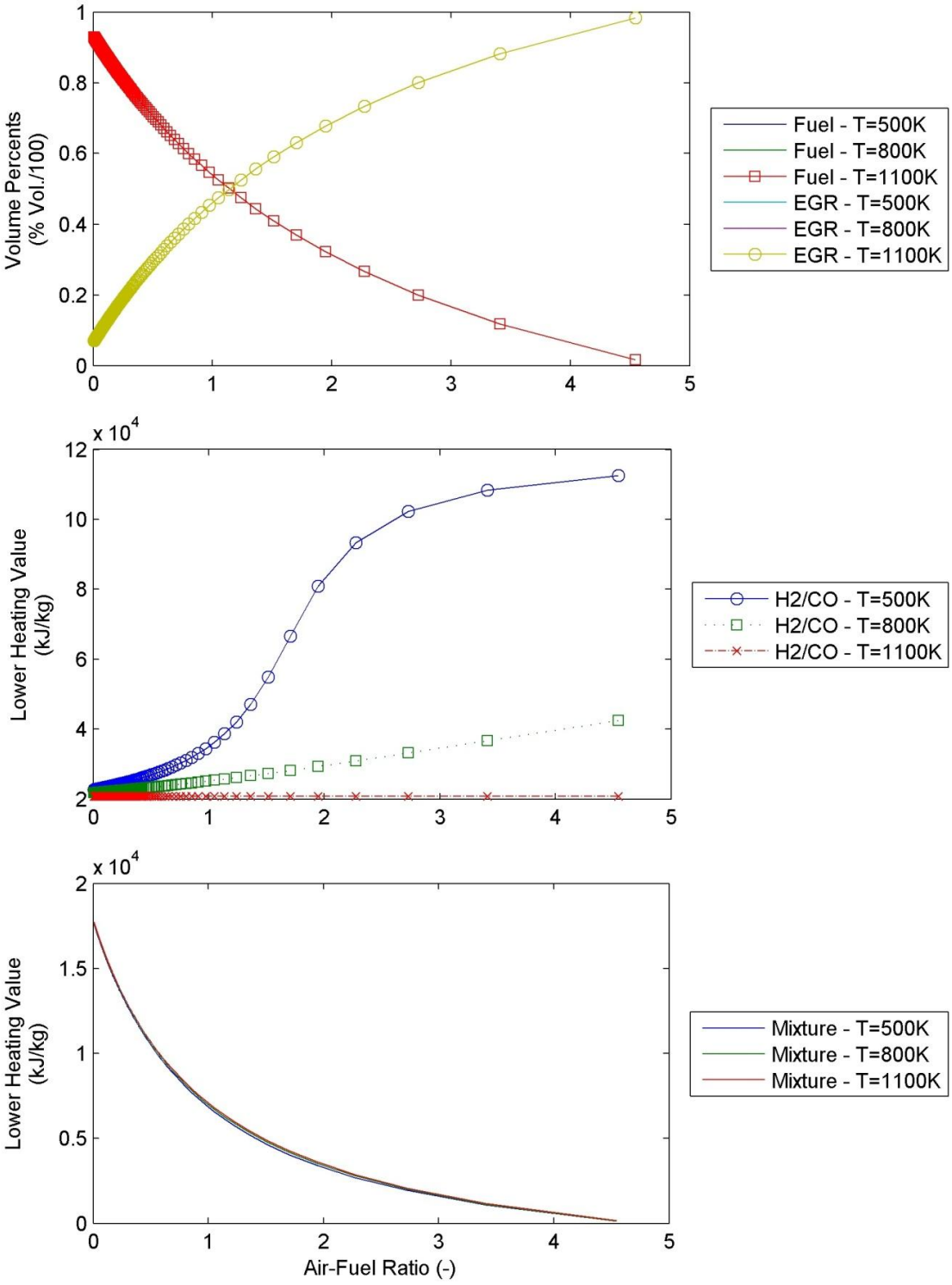

Figure 14. Properties for Glycerin Reforming with 33% Water at any pressure and multiple temperatures with *x*-axis given as a function of mass air-to-fuel ratio.

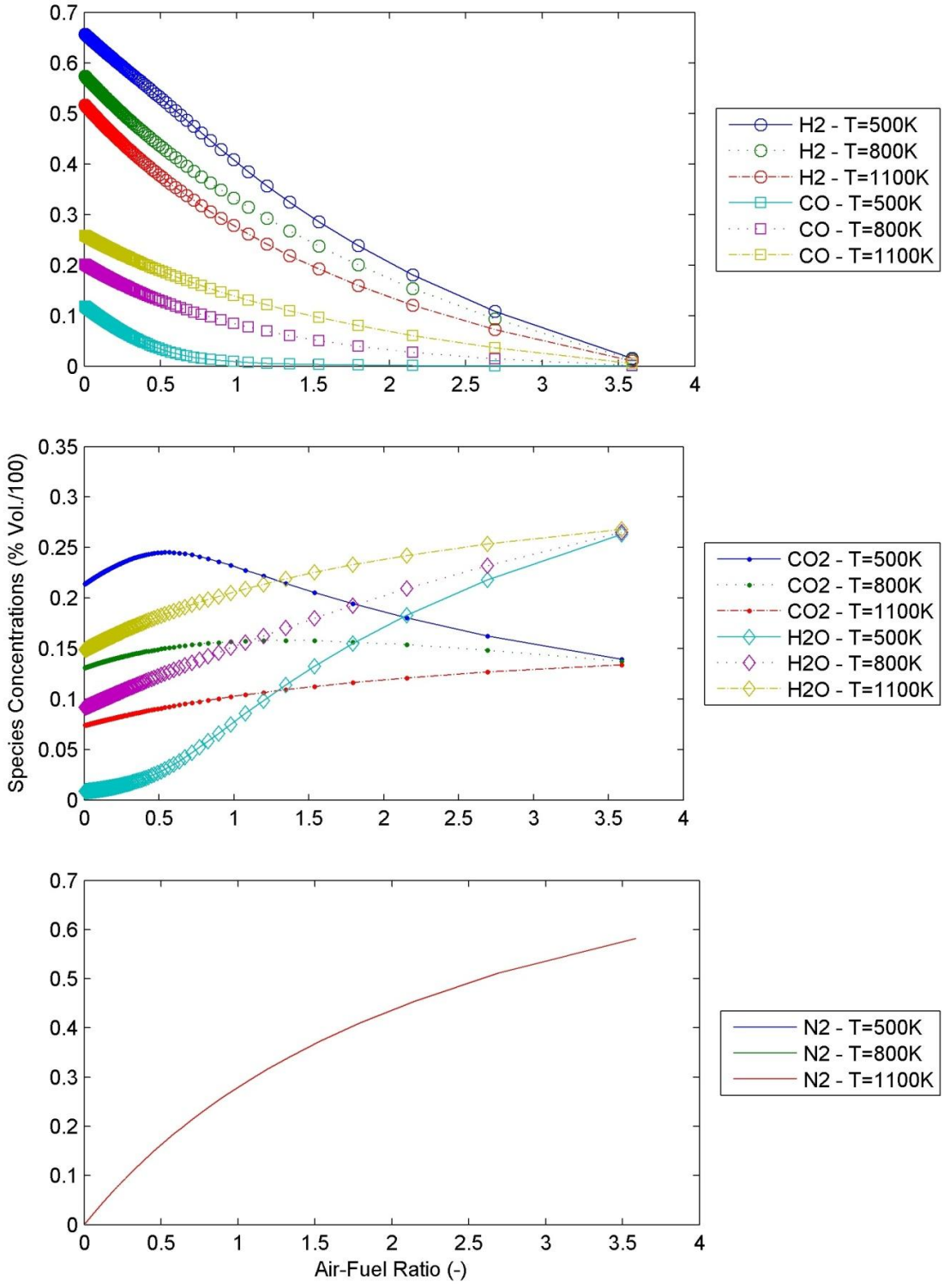

Figure 15. Species Concentration for Glycerin Reforming with 67% Water at any pressure and multiple temperatures with *x*-axis given as a function of mass air-to-fuel ratio.

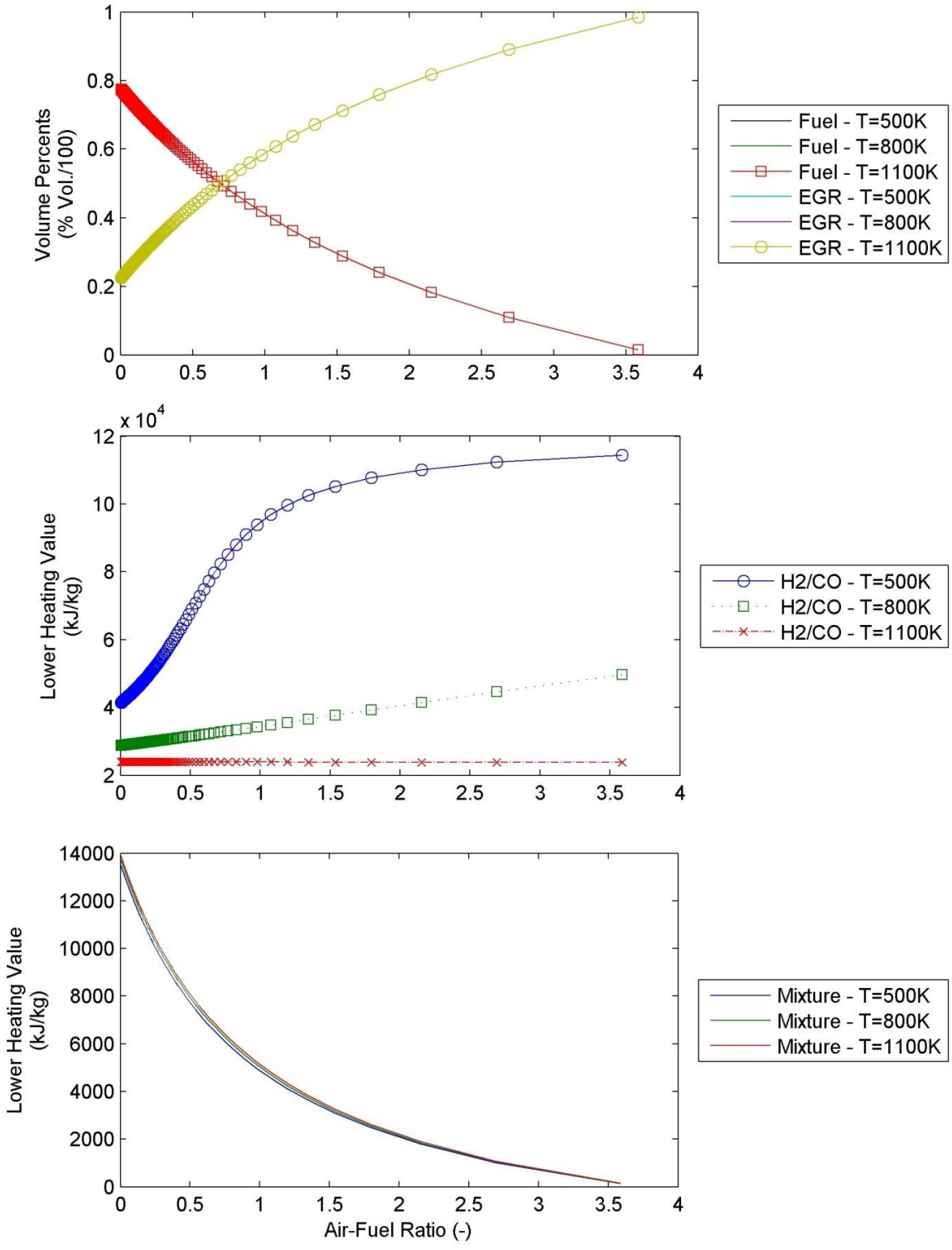

Figure 16. Properties for Glycerin Reforming with 67% Water at any pressure and multiple temperatures with *x*-axis given as a function of mass air-to-fuel ratio.

Appendix J: Glycerin Reforming with Continuous Propane Heating Equations

The governing stoichiometric balance for the reformation of a hydrocarbon and oxygen containing fuel equals:

$$f\left[(1-x)\left(\mathrm{C}_{\alpha}\mathrm{H}_{\beta}\mathrm{O}_{\gamma}\right)+x\mathrm{H}_2\mathrm{O}\right]+\mathrm{C}_3\mathrm{H}_8+5\left(\mathrm{O}_2+3.76\mathrm{N}_2\right)\rightarrow a\mathrm{CO}_2+b\mathrm{H}_2+c\mathrm{CO}+d\mathrm{H}_2\mathrm{O}+18.8\mathrm{N}_2$$

with the atom balances represented as:

C:	$f(1-x)\alpha+3=a+c$	(J1)
H:	$f(1-x)\beta+2fx+8=2b+2d$	(J2)
O:	$f(1-x)\gamma+x+10=2a+c+d$	(J3)
N:	$18.8=e$	(J4)

To solve for the five variables, the model requires a fifth equation. This comes from chemical equilibrium according to the Water-Gas Shift Reaction as discussed in ME 636 Internal Combustion Engines: $a\mathrm{CO}_2+b\mathrm{H}_2\leftrightarrow c\mathrm{CO}+d\mathrm{H}_2\mathrm{O}$ with the equilibrium constant derived from fundamentals as:

$K_e=\log_{10}(C)=\dfrac{c^1d^1}{a^1b^1}\left(\dfrac{P}{a+b+c+d}\right)^{1+1-1-1}=\dfrac{cd}{ab}$	(J5)

By using Microsoft Excel 2007 polynomial equation solver, an equation can be found for K_e as a function of temperature (K) using the data from Table 3 in Appendix F:

$K_{eq}=-2.31719599\times10^{-12}T^4+7.97773201\times10^{-9}T^3-7.14355823\times10^{-6}T^2$ $+2.4713825\times10^{-3}T-2.94930280\times10^{-1}$	(J6)

The equilibrium equation can then be used to solve for *b* as follows:

Solving (J1) for a:	$a=-c+3f-3fx+3$	(J7)
Solving (J2) for d:	$d=-b+4f-3fx+4$	(J8)
Solving (J3) for c:	$c=-2a+10-d+3f-2fx$	(J9)
Plugging (J7,I8) into (J9)	$c=-2(-c+3f-3fx+3)+10-(-b+4f-3fx+4)+3f-2fx$ $c=2c-7f+b-7fx$	(J10)
Solving (J10) for c:	$c=7f-7fx-b$	(J11)
Plugging (J11) into (J7):	$a=-7f+7fx+b+3f-3fx+3$ $a=-4f+4fx+b+3$	(J12)

By substituting equations (J8, J1, and J12) into (J5), we obtain the following for the chemical equilibrium constant:

$K_e = \frac{(7f - 7fx - b)(-b + 4f - 3fx + 4)}{(-4f + 4fx + b + 3)b}$ $K_e = \frac{b^2(1) + b(-11f + 10fx - 4) + (281f^2 - 49f^2x + 28f - 28fx + 21f^2x^2)}{b^2(1) + b(3 + 4fx - 4f) + (0)}$ $K_e\left(b^2(1) + b(3 + 4fx - 4f) + (0)\right)$ $= \left(b^2(1) + b(-11f + 10fx - 4) + (281f^2 - 49f^2x + 28f - 28fx + 21f^2x^2)\right)$ $\left(b^2(K_e) + b(K_e(3 + 4fx - 4f))\right)$ $= \left(b^2(1) + b(-11f + 10fx - 4) + (281f^2 - 49f^2x + 28f - 28fx + 21f^2x^2)\right)$ $b^2(1 - K_e) + b\left(f(10x - 11) - 4 - K_e(3 + 4f(x - 1))\right)$ $+ \left(f(281f - 49fx + 28 - 28x + 21fx^2)\right) = 0$	(J13)

Then, by using the quadratic equation, *b* can be found from (J13):

$b = -\frac{\left(f(10x - 11) - 4 - K_e(3 + 4f(x - 1))\right)}{(1 - K_e)}$ $+ \frac{\sqrt{\left(f(10x - 11) - 4 - K_e(3 + 4f(x - 1))\right)^2 - 4(1 - K_e)\left(f(281f - 49fx + 28 - 28x + 21fx^2)\right)}}{(1 - K_e)}$ $b = -\frac{\left(f(10x - 11) - 4 - K_e(3 + 4f(x - 1))\right)}{(1 - K_e)}$ $- \frac{\sqrt{\left(f(10x - 11) - 4 - K_e(3 + 4f(x - 1))\right)^2 - 4(1 - K_e)\left(f(281f - 49fx + 28 - 28x + 21fx^2)\right)}}{(1 - K_e)}$	(J13)

Using equation (J13), the molar amounts can be found for each of the species leaving the reformer:

$d = -b + 4f - 3fx + 4$	(J8)
$c = 7f - 7fx - b$	(J11)
$a = -c + 3f - 3fx + 3$	(J7)
$e = 18.8$	(J4)

Appendix K: Glycerin Reforming with Continuous Propane Reforming Results Table

Table 5. Glycerin Reforming without Water with Continuous Propane Heating at 101325 Pa and 800K.

Fuel/air molar ratio		25
Air/Fuel ratio		0.0023
Carbon dioxide	*a*	3.30
Hydrogen	*b*	100.30
Carbon monoxide	*c*	74.70
Water vapor	*d*	3.70
Nitrogen	*e*	18.80
H_2/CO ratio		1.34
EGR%		12.83
M_{mix} [kg/kmol]		15.11
R_{mix} [J/kg·K]		550.41
$Q_{LHV,mix}$ [kJ/kg]		20,563
$CQ_{LHV,mix}$ [kJ/kg]		14,948

Appendix L: Glycerin Reforming with Continuous Propane Results from the Predictor Model

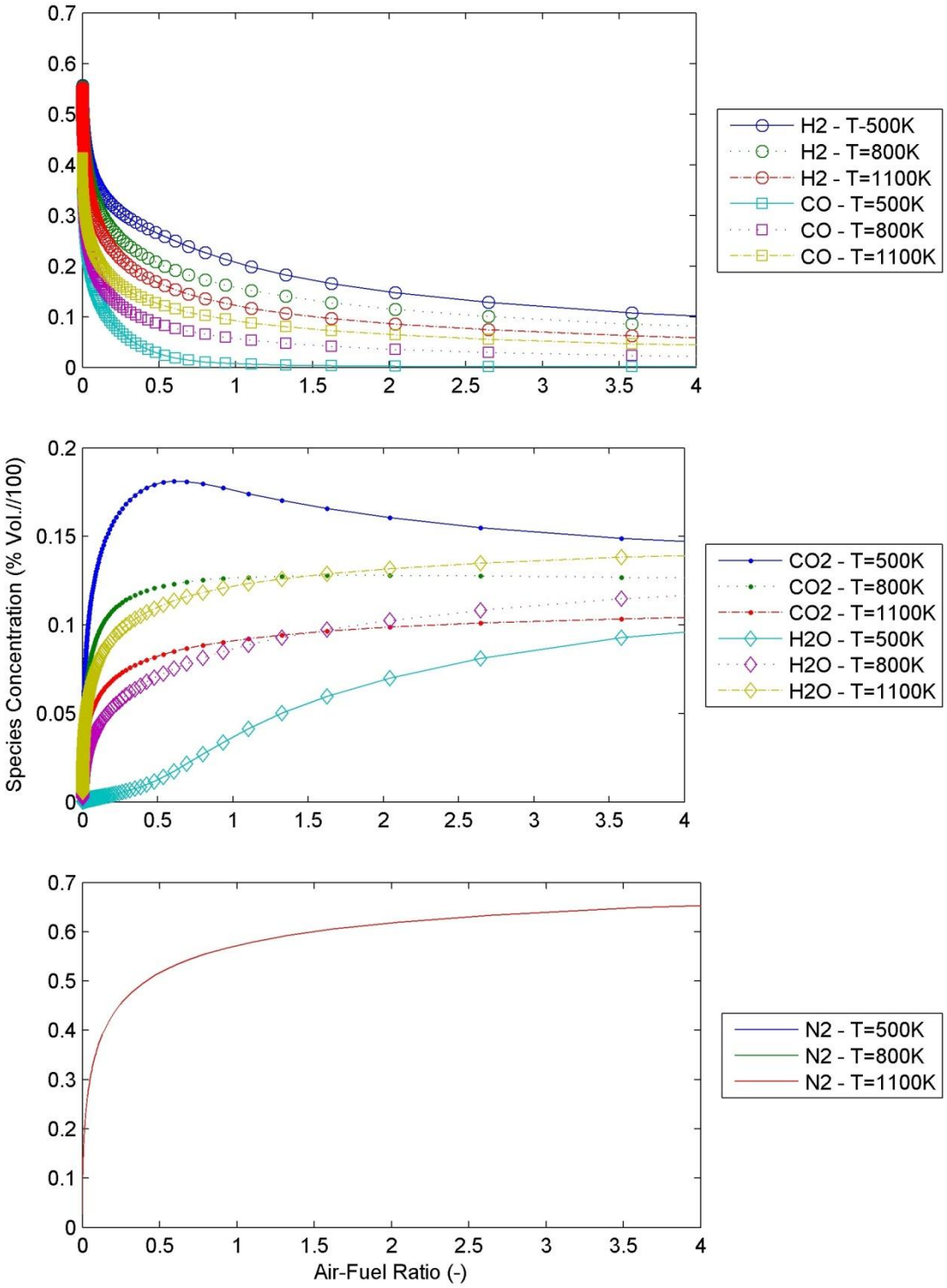

Figure 17. Species Concentration for Glycerin Reforming 0% Water and Propane Heating at any pressure and multiple temperatures with *x*-axis given as a function of mass air-to-fuel ratio.

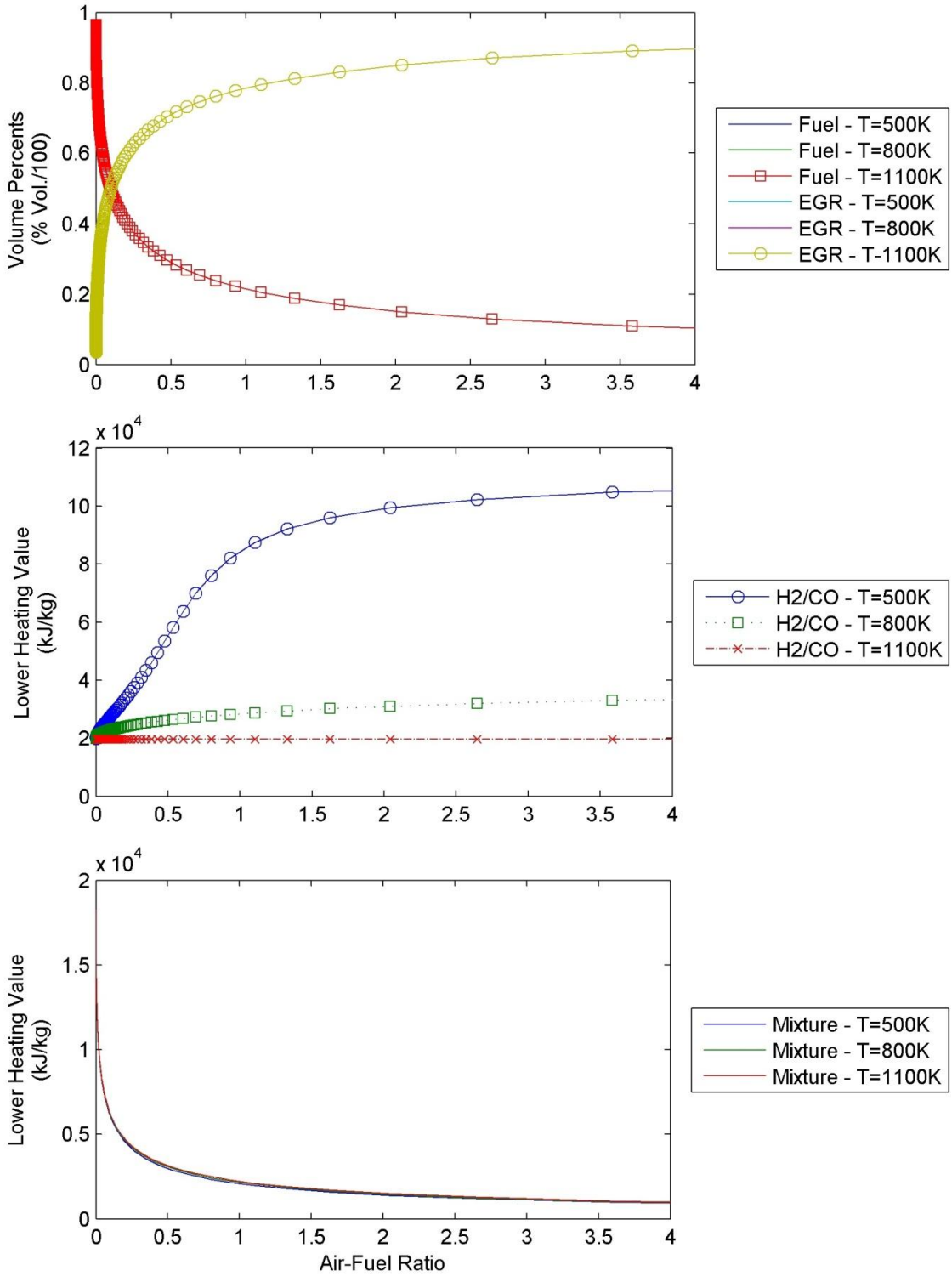

Figure 18. Properties for Glycerin Reforming with 0% Water and Propane heating at any pressure and multiple temperatures with *x*-axis given as a function of mass air-to-fuel ratio.

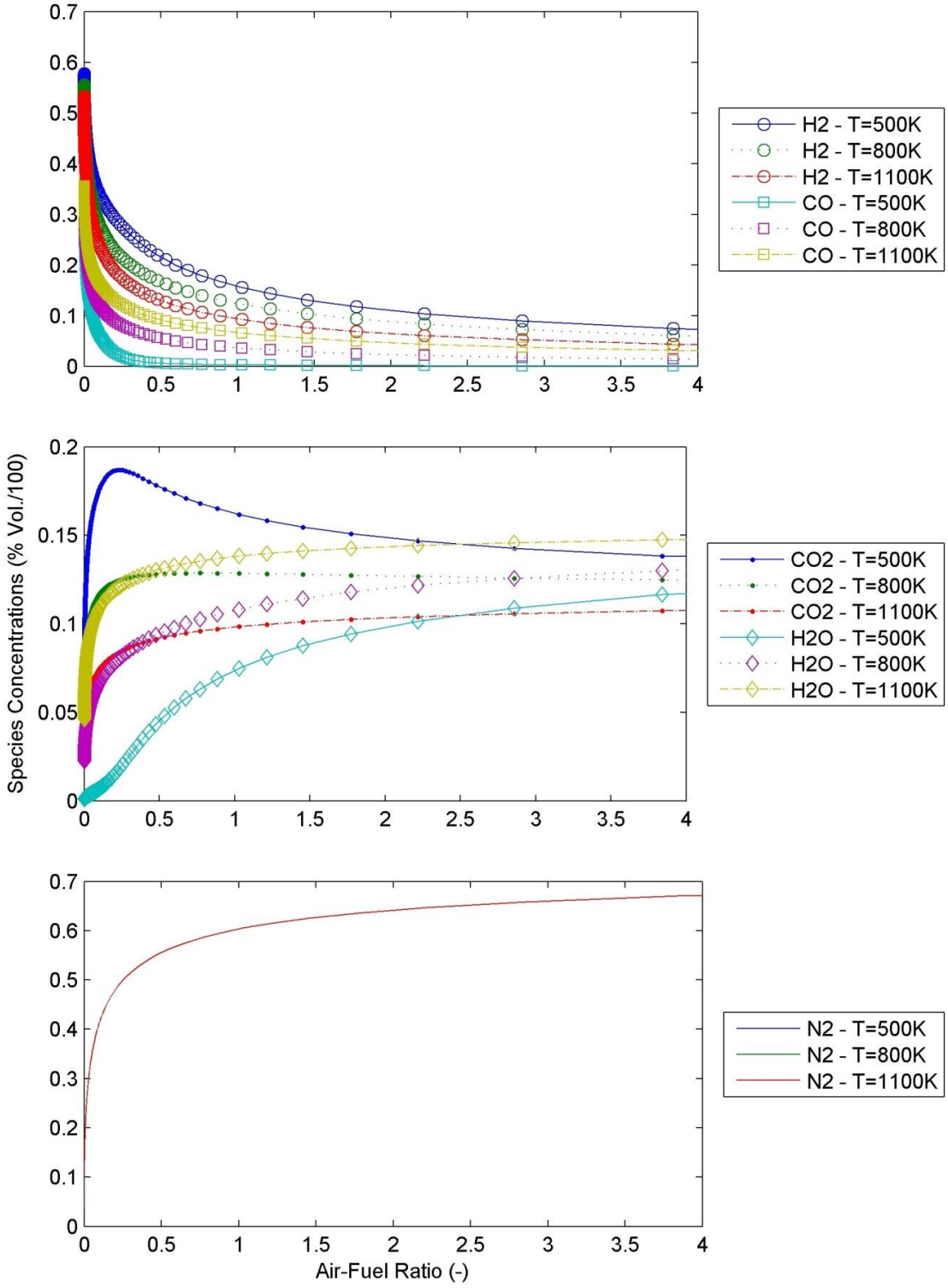

Figure 19. Species Concentration for Glycerin Reforming with 33% Water and Propane Heating at any pressure and multiple temperatures with *x*-axis given as a function of mass air-to-fuel ratio.

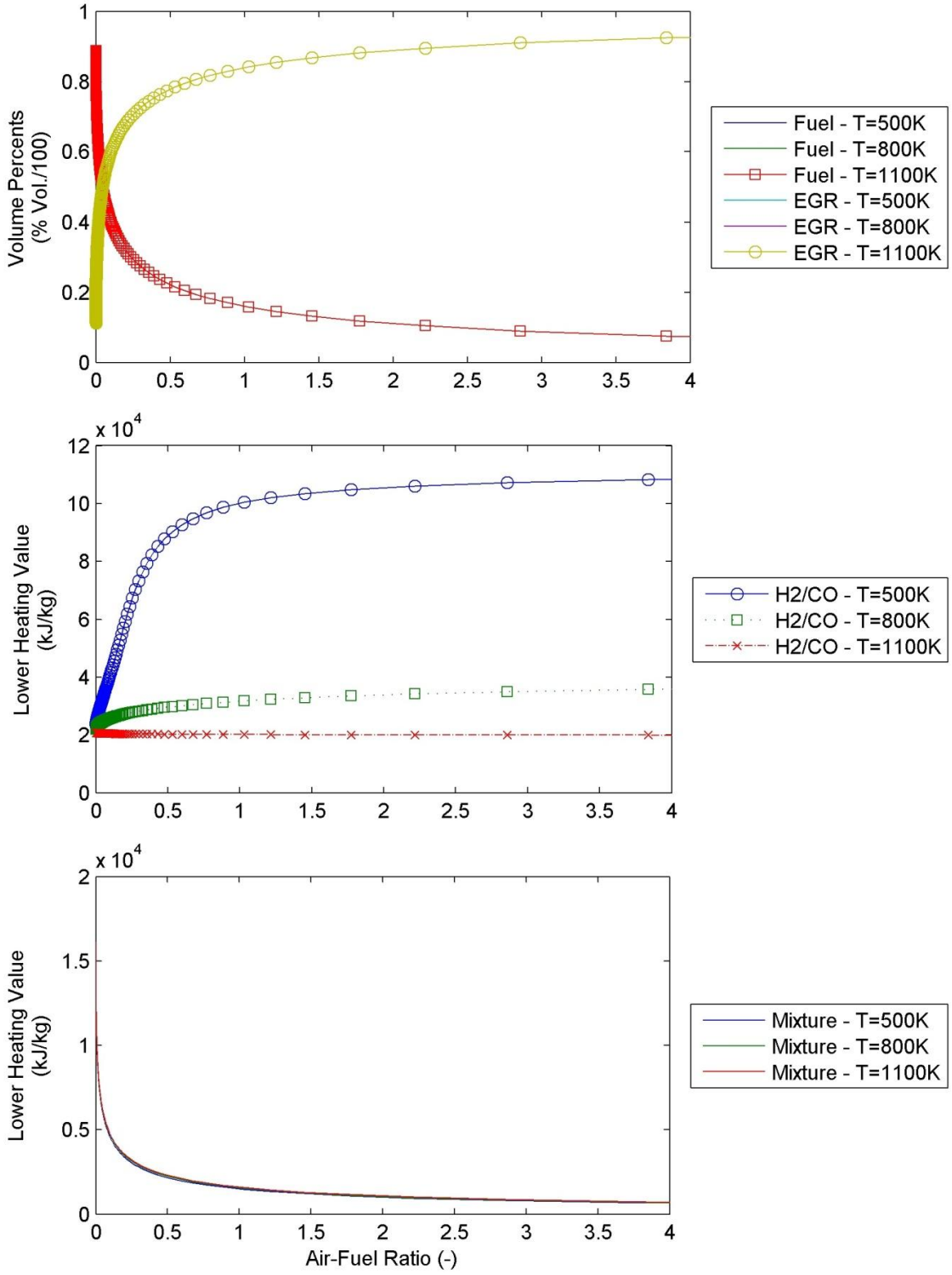

Figure 20. Properties for Glycerin Reforming with 33% Water and Propane Heating at any pressure and multiple temperatures with *x*-axis given as a function of mass air-to-fuel ratio.

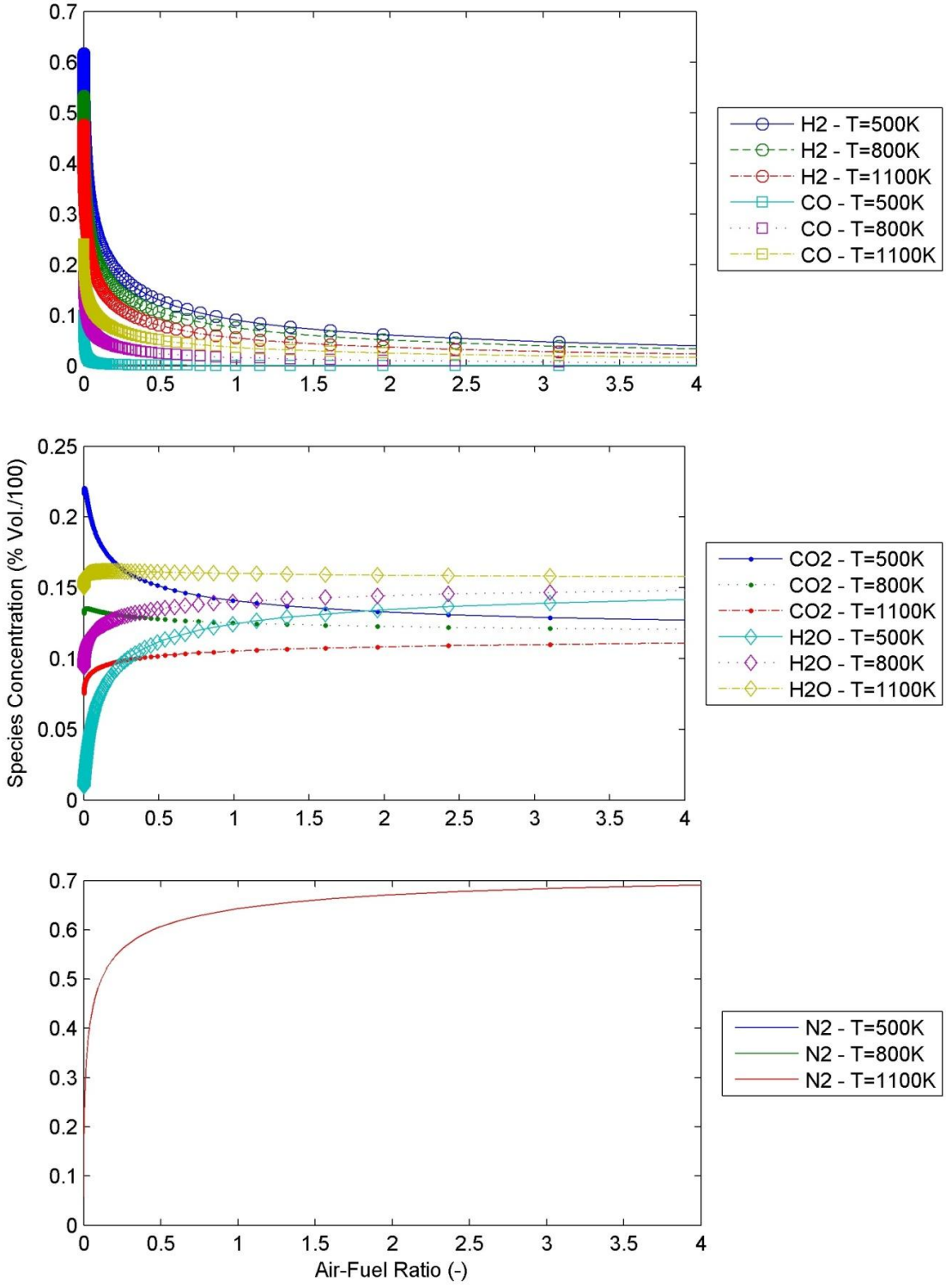

Figure 21. Species Concentration of Glycerin Reforming with 67% Water and Propane Heating at any pressure and multiple temperatures with *x*-axis given as a function of mass air-to-fuel ratio.

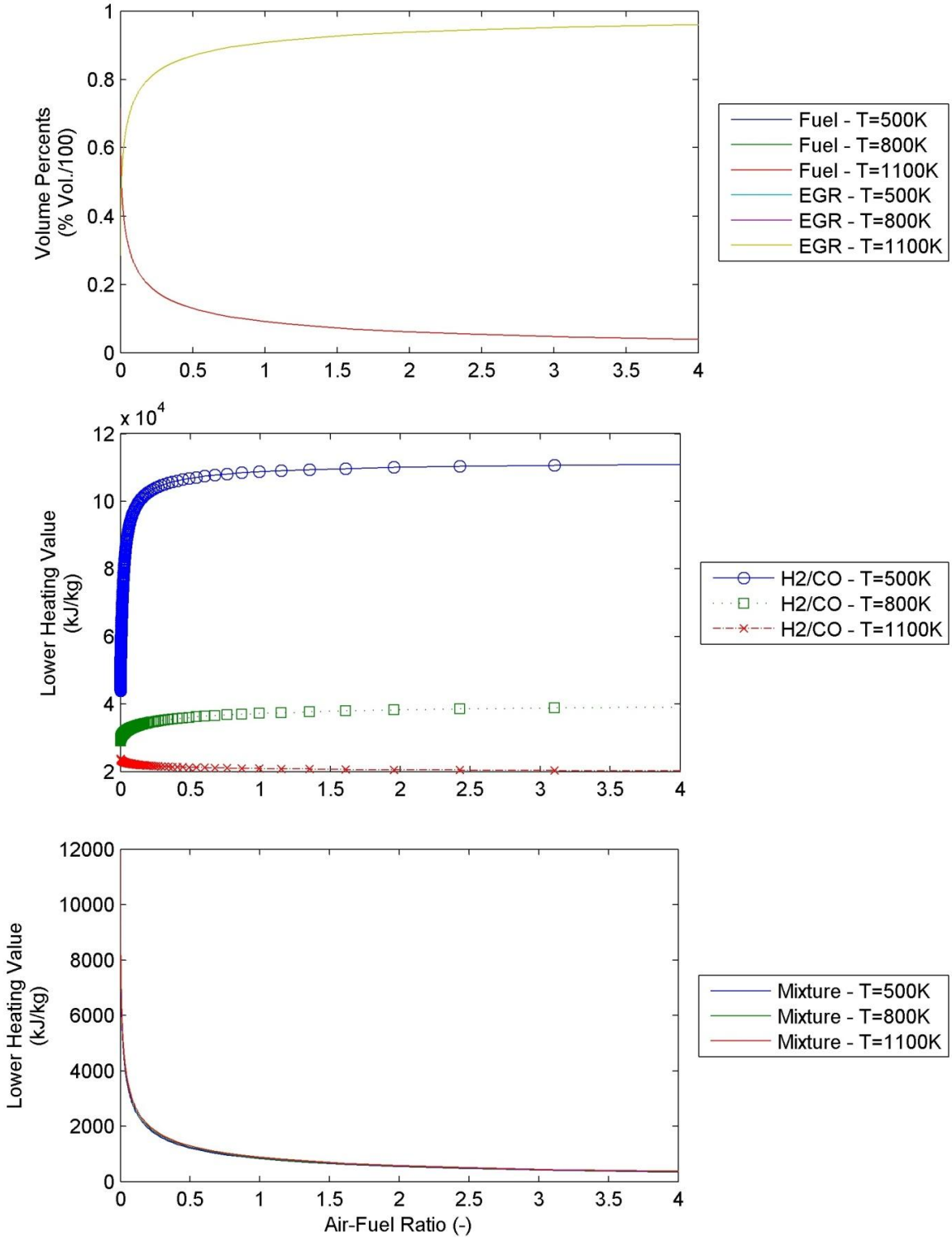

Figure 22. Properties for Glycerin Reforming with 67% Water and Propane Heating at any pressure and multiple temperatures with *x*-axis given as a function of mass air-to-fuel ratio.

Investigation of Biodiesel Feedstock Properties on Engine Performance and Emissions
[INITIAL DRAFT]

E. Cecrle[1], C. Depcik[1], A. Duncan[2], J. Guo[3], M. Mangus[1], E. Peltier[3], S. Stagg-Williams[2]

[1] University of Kansas, Department of Mechanical Engineering
[2] University of Kansas, Department of Chemical and Petroleum Engineering
[3] University of Kansas, Department of Civil, Environmental and Architectural Engineering
1530 W. 15th Street, Lawrence, KS 66045-4709

---

1. Introduction

The global energy supply currently relies heavily on petroleum-based fuels in order to meet consumer demand. However, the finite resources of these fuels cannot supply the world with energy indefinitely. Estimates indicate that the world liquid fuel consumption will increase from 86.1 million barrels per day to 110.6 million barrels per day in 2035. For this fuel consumption, projections of the transportation sector indicate that it will account for more than 60% of the total liquid fuel usage in 2035, up from its current level of 46% [1]. Logic dictates that researchers must find alternative and renewable fuel sources that augment, and possibly even replace conventional sources in order to meet future energy needs. Specifically, the transportation sector requires practical and sustainable sources of renewable supplies that can replace today's petroleum-based fuels.

Most of the energy used in the transportation sector is in the form of liquid fuels, such as gasoline and diesel [2]. Researchers have shown that compression ignition engines that burn diesel fuel can be operated successfully using fuels derived from renewable sources, hereto referred as biodiesel [3, 4]. Common creation of biodiesel occurs by converting feedstocks, such as vegetable oils or animal fats, into mono-alkyl esters of long chain fatty acids using methanol or ethanol catalysis. Of interest, the biodiesel fuels derived in this manner show significant promise as they do not require any engine hardware modifications while retaining a similar energy content as diesel [4-6]. However, before biodiesel can replace petroleum diesel, there are a number of issues to consider.

The first obstacle of biodiesel use is the feedstock for production. Ideally, this source must be abundant in order for production in quantities large enough to meet the previously indicated demand. Moreover, researchers must consider the source of this fuel based on economic and social factors. Articles in the press illustrate a perception, true or not, that first-generation biodiesel fuels created from feedstock typically used for human consumption may result in higher consumer prices and a decreased global supply of food [3, 4, 7]. In addition, biodiesel intended for today's infrastructure must have similar

performance in engines as the petroleum-based diesel it is replacing. This includes factors such as engine power, fuel consumption and emission levels.

To address some of these issues, this paper presents biodiesel research that investigates how biodiesel affects engine fuel consumption, power output and emission levels. While engine power generated during the combustion of biodiesel remains comparable to that of diesel operation in most cases [8], fuel consumption tends to increase. This is a function of biodiesel's lower energy content and higher density [8]. Simply put, it requires more biodiesel to perform the same amount of work. However, this result is partially offset by biodiesel's often higher cetane number (CN) and better lubricity characteristics [9, 10]. The higher CN promotes a better quality combustion and thermal efficiency while biodiesel's higher lubricity reduces frictional losses. While biodiesel CN and lubricity do offset somewhat the energy penalty in using a lower energy dense fuel, research demonstrates that an engine running on 100% biodiesel may have an increase of up to 12% in brake-specific fuel consumption [8].

Part of this increase in fuel consumption may additionally relate to the impact biodiesel has on fuel injection timing. Biodiesel fuel has a higher bulk modulus of compressibility than diesel fuel. This causes pressure waves in an engine's pump-line-nozzle system to move more rapidly in biodiesel [3, 6, 11, 12]. Therefore, the fuel injector will open earlier in the engine cycle when it is injecting biodiesel. This injection can be on the order of $1\text{-}2^0$ for pump-line-nozzle systems; however, this effect is not as prevalent for high-pressure common rail injections systems [11, 12]. As a result, researchers must consider the relative influence of fuel injection timing when comparing performance to diesel fuel. Moreover, because of the non-linearity of engine combustion, both injection timing and fuel composition characteristics affect exhaust emissions.

Traditionally, the use of biodiesel results in reduced emissions of hydrocarbons (HC), carbon monoxide (CO), and particulate matter (PM). However, nitrogen oxides (NO_x) emissions typically increase with biodiesel use [3, 4, 6, 8, 10, 11, 13-17]. Of the hazardous emissions leaving a compression ignition engine, NO_x is a large factor mitigated by the Environmental Protection Agency (EPA) due to its negative environmental and health effects. NO_x emissions, specifically NO and NO_2, are known to be a major contributor to creation of photochemical smog and acid rain [18]. In this area of research, extensive efforts by Mueller, Boehman, and Martin propose that there is no single culprit for increased NO_x from biodiesel combustion, but rather that several factors contribute [14]. Their findings illustrate that biodiesel's effect on fuel injection timing appears to increase NO_x emissions. The advanced injection, described in the previous paragraph, leads to earlier combustion and subsequent longer residence time at high temperatures for increased NO_x emissions [3, 11, 12]. Moreover, the lower PM emissions of biodiesel result in less radiative heat loss to the PM, resulting in a higher flame temperature providing an additional factor in increased NO_x emissions.

In addition, the chemistry of biodiesel may further augment its NO_x creation characteristics. Since biodiesel has a higher CN than diesel, this results in a shorter ignition delay. This attribute, combined with an earlier injection due to a higher bulk modulus, leads to an increased opportunity for NO_x to form. As a result, the start of combustion with biodiesel can be on the order of 4^0 earlier than with diesel [12]. In addition, since biodiesel is an oxygenated fuel, more heat release occurs during the premixed phase of combustion as the extra oxygen helps the hydrocarbons break down faster [3]. Biodiesel also has a higher adiabatic flame temperature due to a higher proportion of double-bonded molecules with slightly higher adiabatic flame temperatures than single-bonded molecules [17]. These factors lead to a hotter combustion process and more NO_x production [3].

While it is possible to mitigate NO_x emissions in a diesel engine using aftertreatment devices and the addition of Exhaust Gas Recirculation (EGR), these efforts are costly and require precise engine control to be successful [19, 20]. In an effort to reduce the requirement of these methods of abatement of NO_x, this paper documents an investigation into the chemical properties of the biodiesel as a method for reducing NO_x emission levels.

2. Goals of Study

This work involves an examination into the chemical structure and composition of biodiesel in order to study characteristics that directly influence emissions levels and engine performance. In particular, the authors investigate feedstocks based on the ratio of unsaturated to saturated fatty acid chains in their resultant biodiesel fuel. The composition of the fuel and the unique characteristics of each fatty acid chain such as saturation, branching, and chain length affect the fuel's cetane (CN) and iodine number (IN) [15]. The cetane number is a dimensionless number that defines the ignition delay of a particular fuel; e.g. a fuel with a high CN will have a shorter ignition delay than a fuel with a lower CN as stated before [21]. Therefore, a fuel with a high CN will result in earlier ignition, higher in-cylinder temperatures, and improved fuel economy, as long as the CN is not too high [10]. The iodine number of a fuel is determined by the number of unsaturated (double) bonds in the fuel molecules [14].

The work by McCormick et al. indicates that the CN and IN are critical properties that change engine emission levels when compared to conventional diesel through their modification to the specific amounts of premixed and diffusion burn phases. In specific, the results show that increasing biodiesel CN leads to higher NO_x emissions. In addition, research indicates that increasing IN values results in higher NO_x emissions [10, 14]. However, the degree of fuel saturation is shown to not effect fuel consumption [16]. The study by McCormick et al. also investigates the effects of CN and IN on PM emissions, but does not find any correlation between either of these properties with biodiesel PM levels [14]. In order to examine these unique biodiesel fuels, the authors compared their performance and

emissions to Ultra Low Sulfur Diesel (ULSD) in a single-cylinder engine laboratory at the University of Kansas.

3. Experimental Apparatus

In order to reduce the complexity in the comparative fuel tests, the researchers utilized a single-cylinder diesel engine. This allows operation of smaller batches of fuel providing more feedstock accessibility for analysis. Moreover, single-cylinder configurations remove the non-linearity of fluid dynamics and heat transfer in multi-cylinder engines allowing better identification of trends related directly to combustion. The specific engine is a Yanmar L100V direct-injected diesel (see **Error! Reference source not found.** for specifications). This engine uses a mechanical fuel pump-line-injector to maintain constant engine speed of 3600 rotations per minute (RPM). Injection occurs at 15.5 ± 0.5^0 before piston top-dead-center with a pressure of 19.6MPa. This mechanical system does have a physical limitation as it is not feasible to normalize the engine to expected advances in injection timing from a biodiesel fuel [3, 6, 11, 12]. Future lab upgrades will remedy this limitation as the investigators are working with an engine supplier to retrofit the engine with a common-rail system and programmable Engine Control Unit.

Table 1. Engine and Generator Specifications

Engine	Value
Manufacturer and Model	Yanmar L100V
Type	Vertical Direct-Injection Compression Ignition
Engine Intake	Naturally Aspirated
Cooling	Air-Cooled
Cycle	4-Stroke
Displacement	435 cc
Number of Cylinders	1
Number of Valves	1 Intake, 1 Exhaust
Bore	86mm
Stroke	75mm
Compression Ratio	21.2
Injection Timing	15.5 (+/- 0.5) degrees BTDC
Continuous Rated Output	8.3 hp SAE
	6.2 kW
Rated Speed	3600 RPM
Injector Pressure	19.6 MPa
Aftertreatment	None
Engine Oil Used	Shell 15W-40
Generator	
Manufacturer and Model	NorthStar 5500BDG
Maximum Output	5500 W
Continuous Output	5000 W
Voltage	120/240 V
Phase	Single-phase (4-wire)
Frequency	59.0-62.0 Hz
Power Factor	100%

Allowable Current (120V/240V)	2@20 Amp/ 1@20 Amp

To provide load on the engine, the setup employs a NorthStar electric generator coupled to the crankshaft (see **Error! Reference source not found.**). Resistance heaters supply variable electrical loading and selection of the specific power of these heaters was a function of the generator capacity to offer multiple loading events. Of interest to the reader, this setup provides a repeatable, economic alternative to an engine dynamometer. Unfortunately, original infrastructure and student availability limitations at the University of Kansas prohibited the initial installation of a more traditional setup. However, planning is underway to upgrade the system using an Alternating Current dynamometer with in-cylinder pressure measurements.

Outfitting of the engine with instrumentation included, but was not limited to ambient air temperature, pressure, and relative humidity, engine air mass flow, engine intake air temperature and pressure, fuel mass flow, fuel density, engine torque, exhaust port temperature, downstream exhaust temperature and pressure, and generator load. The researchers employed a Micro-Motion Coriolis flow (model #CMF010M) for fuel flow and density measurements. The setup includes a FUTEK rotary torque-sensor (model #TRS-705) connected between the engine and generator shafts in order to provide accurate torque values. Measurement of the engine intake airflow occurs using a Merriam laminar flow element (model #50MW20-2) and an Omega differential pressure transducer (model #PX277-30D5V). Most of the additional parameters were acquired using appropriate Omega sensors.

A Sensors, Incorporated Semtech-DS Mobile Emissions Analyzer measures carbon monoxide (CO), carbon dioxide (CO_2), diatomic oxygen (O_2), nitrogen oxide (NO), nitrogen dioxide (NO_2), and (HC) emissions from the engine during testing. A heated sample line connects to a flow straightener installed downstream of the engine muffler. The Semtech-DS passes the exhaust gas through a Fuel Ionization Detector to measure HCs, a non-dispersive infrared analyzer to measure CO, CO_2, and HC levels, and a non-dispersive ultraviolet analyzer to independently measure NO and NO_2. In addition to the gas emissions, PM collection occurs by attaching a stainless steel tube to the engine exhaust below the flow straightener complete with a 4mm diameter sampling line. Particle capture happens from the sampling line using a Dekati PM10 low-pressure cascade impactor with 25mm polycarbonate filters collecting particles in a size range of 10 to 30 micrometers. A Sogevac Leybold vacuum pump induces a flow rate of 10 Liters/minute through the collection system and by measuring the masses of the filters, before and after PM collections, the authors obtain a profile of particle size distribution and relative emission levels.

4. Test Methodology

Each fuel test consists of five loadings governed by the capacity of the NorthStar generator. These loads were approximately 0%, 25%, 50%, 75%, and 100% of the generator rated output. Of

importance, the rated continuous generator power was 80% of the engine's rated continuous power. Steady-state determination occurs by monitoring the change in the engine exhaust temperature 892mm downstream of the exhaust port. When less than a one percent change in a minute occurs, the engine is undergoing steady-state operation. Upon reaching these conditions, collection of the emissions and performance data happens as follows. The Semtech-DS analyzer collects emissions data for ten minutes at a sample rate of one sample per second. The National Instruments hardware system employed for the engine records performance data at a sample rate of ten samples per second for two minutes. Following the completion of the data collection at all generator loads, a PM collection test follows with the engine run for one hour at 25% of generator rating. Previous efforts on this engine demonstrate that this load produces the most significant PM levels. At no-load conditions, a lean fuel-to-air mixture in the engine does not permit excessive PM creation. At loads above 25% of generator rating, high in-cylinder pressures and temperatures lead to better combustion and lower PM levels. Results to date are presented in Figure 1.

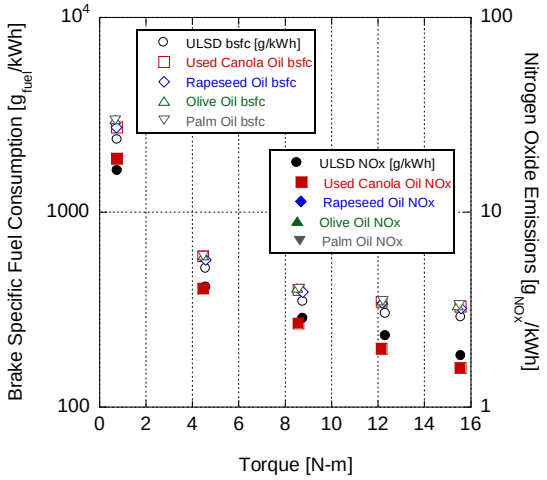

Figure 1. Yanmar Single Cylinder Test Cell Results to Date.

Acknowledgments

This research was funded by the University of Kansas, Transportation Research Institute from Grant #DT0S59-06-G-00047, provided by the US Department of Transportation - Research and Innovative Technology Administration.

Efforts

- Eric Cecrle implemented and initially tested the data acquisition system used to collect and analyze the different biodiesel and assisted in the writing of the Experimental Apparatus section.
- Dr. Chris Depcik is reviewing and analyzing the engine performance data.

- Dr. Edward Peltier is reviewing and analyzing the emissions data.
- Dr Susan Stagg-Williams is reviewing and analyzing the measured biodiesel properties from the developed biodiesel blends.
- Andrew Duncan developed and analyzed the biodiesel blends and will provide data for the paper as to its specifications.
- Jing Guo setup the Semtech-DS Mobile Emissions Analyzer and will provide the emissions results for the paper.
- Mike Mangus performed the testing of the data, wrote the review section and analyzed the combustion properties of each biodiesel blend.

References

1. Tsolakis, A., A. Megaritis, and M.L. Wyszynski, *Low Temperature Exhaust Gas Fuel Reforming of Diesel Fuel.* Fuel, 2004. **83**(13): p. 1837-1845.
2. Apostolescu, N. and R. Chiriac, *A Study of Combustion of Hydrogen-Enriched Gasoline in a Spark Ignition Engine.* SAE Paper 960603, 1996.
3. Mueller, C., A. Boehman, and G. Martin, *An Experimental Investigation of the Origin of Increased NOx Emissions When Fueling a Heavy-Duty Compression-Ignition Engine with Soy Biodiesel.* SAE International Journal of Fuels and Lubricants, 2009. **2**(1): p. 789.
4. Balat, M., *Potential alternatives to edible oils for biodiesel production-A review of current work.* Energy Conversion and Management, 2010.
5. Pinto, A., et al., *Biodiesel: an overview.* Journal of the Brazilian Chemical Society, 2005. **16**: p. 1313-1330.
6. Duncan, A., et al., *High-Pressure Viscosity of Biodiesel from Soybean, Canola, and Coconut Oils.* Energy & Fuels: p. 125-164.
7. Gui, M., K. Lee, and S. Bhatia, *Feasibility of edible oil vs. non-edible oil vs. waste edible oil as biodiesel feedstock.* Energy, 2008. **33**(11): p. 1646-1653.
8. Enweremadu, C. and H. Rutto, *Combustion, emission and engine performance characteristics of used cooking oil biodiesel--A review.* Renewable and Sustainable Energy Reviews, 2010.
9. Agarwal, A. and L. Das, *Biodiesel development and characterization for use as a fuel in compression ignition engines.* Journal of engineering for gas turbines and power, 2001. **123**: p. 440.
10. Knothe, G., et al., *The biodiesel handbook*. 2005: AOCS press Champaign, IL.
11. McCormick, R., et al., *Effects of biodiesel blends on vehicle emissions.* Milestone Report. National Renewable Energy Laboratory, NREL/MP-540-40554, 2006.
12. Boehman, A., et al., *The impact of the bulk modulus of diesel fuels on fuel injection timing.* Energy Fuels, 2004. **18**(6): p. 1877-1882.
13. Adi, G., et al., *Soy-Biodiesel Impact on NO x Emissions and Fuel Economy for Diffusion-Dominated Combustion in a Turbo- Diesel Engine Incorporating Exhaust Gas Recirculation and Common Rail Fuel Injection.* Energy & Fuels, 2009. **23**(12): p. 5821-5829.
14. McCormick, R., et al., *Impact of biodiesel source material and chemical structure on emissions of criteria pollutants from a heavy-duty engine.* Environ. Sci. Technol, 2001. **35**(9): p. 1742-1747.
15. Knothe, G., *"Designer" Biodiesel: Optimizing Fatty Ester Composition to Improve Fuel Properties†.* Energy & Fuels, 2008. **22**(2): p. 1358-1364.
16. Benjumea, P., J. Agudelo, and A. Agudelo, *Effect of the Degree of Unsaturation of Biodiesel Fuels on Engine Performance, Combustion Characteristics, and Emissions.* Energy & Fuels: p. 125-164.

17. Ban-Weiss, G., et al., *A numerical investigation into the anomalous slight NOx increase when burning biodiesel; a new (old) theory.* Fuel Processing Technology, 2007. **88**(7): p. 659-667.
18. Perry, R. and D. Siebers, *Rapid reduction of nitrogen oxides in exhaust gas streams.* 1986.
19. Girard, J., et al., *Technical advantages of vanadium SCR systems for diesel NOx control in emerging markets.* SAE International Journal of Fuels and Lubricants, 2009. **1**(1): p. 488.
20. Nam, G., et al., *The effect of an external fuel injection on the control of LNT system; the diesel NOx reduction system.* 2007.
21. Knothe, G., *Dependence of biodiesel fuel properties on the structure of fatty acid alkyl esters.* Fuel Processing Technology, 2005. **86**(10): p. 1059-1070.

Analysis of the Effects of Reformate (Hydrogen/Carbon Monoxide) as an Assistive Fuel on the Performance and Emissions of Used Canola-Oil Biodiesel
[FINAL DRAFT]

Eric Cecrle[1], Christopher Depcik[1], Jing Guo[2] and Edward Peltier[2]

[1]Department of Mechanical Engineering
[2]Department of Civil, Environmental and Architectural Engineering
University of Kansas, School of Engineering
Lawrence, Kansas, 66045, USA

Abstract

Evolving technology and a reoccurring energy crisis creates a continued investigation into the search for sustainable and clean-burning renewable fuels. One possibility is hydrogen that has many desirable qualities such as a low flammability limit promoting ultra-lean combustion, high laminar flame speed for increased thermal efficiency and low emissions. However, past research discovered certain limiting factors in its use such as pre-ignition in spark ignition engines and inability to work as a singular fuel in compression ignition engines. To offset these issues, this work documents manifold injection of a hydrogen/carbon monoxide mixture in a dual-fuel methodology with biodiesel. While carbon monoxide does degrade some of the desirable properties of hydrogen, it acts partially like a diluent to restrict pre-ignition. The result of this mixture addition allows the engine to maintain power while reducing biodiesel fuel consumption with a minimal NO_x emissions increase.

Keywords: Hydrogen; Carbon Monoxide; Dual-Fuel; Performance; Emissions; Combustion

---

1. Introduction

When developing a sustainable renewable fuel, researchers must consider the system efficiency in the production of this fuel. Many papers investigate biofuels through in-cylinder combustion efficiency metrics alone; however, a large number of these efforts ignore the by-products created during its manufacturing. For example, the conversion of 100 pounds of oil or fat with 10 pounds of alcohol can produce 100 pounds of biodiesel along with 10 pounds of crude glycerin as a by-product [1, 2]. Just as distiller grains are critical to the economics of ethanol production, the sale of glycerin is important to the economically sustainable production of biodiesel. Biodiesel production in the United States, European Union and other countries reached 5.1 billion gallons in 2009 [3, 4]. This production generated over 3 billion pounds of excess glycerin by-product. Glycerin has many uses in the food, pharmaceutical,

[1] Corresponding author, Phone: 785-(864-3181), Email Address: ececrle1@ku.edu

automotive and demolition industries [5]. However, the market for glycerin in the U.S. is 600 million pounds per year illustrating that the excess glycerin from biodiesel production has a limited market [6]. Of importance for this effort, this surplus production of crude glycerin drives down its price and with its energy content at 7000 Btu/lb (pure glycerin is 19000 Btu/lb), this makes it an economically competitive fuel as an alternative to Compressed or Liquefied Natural Gas [7].

Glycerin as a singular fuel in a combustion engine is extremely difficult as it needs a combustion enhancer or special treatment [8]. This is due to a high amount of energy required for combustion, as glycerin cannot normally be used in an engine without requiring the chamber to first reach a temperature around 3000°F [9]. Another tactic is to use glycerin or treated glycerin as a direct fuel additive [10-12]. For example, Spooner-Wyman et al. tested the influence of di-butoxy glycerol (DBG) on diesel combustion and found a reduction in Particulate Matter (PM), but an increase in all other measured emissions [12]. Moreover, their results show a decrease in cylinder pressures resulting in a lower heat release rate and increased fuel consumption. Kinoshita et al. investigated emulsified biodiesel, consisting of Rapeseed oil methyl ether biodiesel, water and crude glycerin, and found increased levels of carbon monoxide (CO), hydrocarbons (HC), lower levels of nitrogen oxides (NO_x) and negligible change in brake thermal efficiency [11].

In deference to using liquid glycerin as fuel additive, one biodiesel system perspective under investigation at the University of Kansas (KU) is the reformation of glycerin into a hydrogen-rich fuel source in order to power a biodiesel production plant. By using the glycerin by-product as a fuel, it reduces the requirement of outside sources to power the plant; most commonly coal in the state of Kansas. Through partial oxidation processes alone, glycerin can produce a fuel source (reformate) that is 57% hydrogen and 43% carbon monoxide by volume. Combining this process with a catalyst (Ni, Pt, Pd) and adding water to the mixture promotes steam reforming and the water gas shift reaction allowing for potential hydrogen purity upwards of 97% [13, 14]. Currently, KU is investigating laboratory scale reformation of glycerin to promote hydrogen selectivity along with a full-scale reforming device connected to a Chevy V-8 350 in^3 spark-ignition (SI) engine and generator for power production. While the engine can run repeatedly on reformate produced from the conversion of glycerin, it requires novel hardware, a relatively complex control structure and the use of a catalytic material. In order to improve the economics of this process, the researchers postulated that adding reformate to the intake of a diesel generator could reduce the fuel consumption of biodiesel used in this manner. Therefore, instead of installing a complete hardware setup including reformer, engine and generator, a plant could employ an off-the-shelf diesel generator with a small reformer added to supplement the intake with glycerin reformate. While hydrogen selectivity is preferred, using a non-catalyzed process would further enhance the economics of the process.

Many researchers have attempted reforming methods in order to create a hydrogen-rich mixture using different fuel sources, like methanol and methane. The goal of these efforts is to replace petroleum fuels completely with Jamal and Wyszynski providing a semi-current historical review of these attempts [15]. They found that on-board reforming is feasible using the waste heat, and possibly the constituents from the exhaust. In particular, thermal decomposition demonstrated improved fuel economy at low loads and reduced NO_X emissions. Using steam reforming, a more efficient conversion process requiring temperatures between 800°C to 1000°C, can result in lower NO_X emissions and improved fuel economy over thermal decomposition. Partial oxidation works as well and can reduce the energy requirement in comparison to steam reforming. However, all options demonstrate considerable losses in power capacity through the conversion of an energy dense fuel to a less dense version. Moreover, the requirement of adding system energy needed to produce the hydrogen-rich fuel increases the cost of the process. Finally, there exists increased fuel consumption depending on the efficiency of the reforming process and the subsequent lower heating value of the reformed mixture. Of importance, the addition of hydrogen does alter combustion properties and illustrates its feasibility as a dual fuel in order to reduce NO_X emissions.

With respect to hydrogen as a fuel, many consider it the energy source of the future. Its combustion has many desirable traits, such as high power output and emission reductions; however, it has some limiting factors that reduce its practicality such as pre-ignition and knocking along with difficulties in storage. This research effort finds that the use of carbon monoxide in conjunction with hydrogen can provide a positive outcome through reduced fuel consumption of biodiesel. Furthermore, while hydrogen can create a faster combustion with higher temperatures, this work documents only a small increase in NO_x emissions through reformate assisted biodiesel combustion.

2. Hydrogen Combustion

In order to understand how a hydrogen-rich reformate created from glycerin can influence the combustion process of biodiesel, the authors first performed a review of hydrogen combustion. The use of this fuel dates back over one-hundred years with the first documented hydrogen-powered engine operated in 1820 by Cecil [16, 17]. With respect to a historical summary of efforts, Das provides a review in 1990 [17] that White and Lutz later expand in 2006 [16]. In 2009, Verhelst and Wallner present a further comprehensive historical summary of hydrogen-fuelled internal combustion engines [18]. This paper summarizes and expands on these reviews in the following sections.

2.1. Hydrogen Properties

Hydrogen has many desirable traits and properties that other fuels cannot match [16, 18, 19]. The next few sections delineate this information as follows: general properties, flammability limit, auto-

ignition temperature, minimum ignition energy, laminar flame speed, adiabatic flame temperature, quenching distance, and heating value. Table 1 presents a summary of fuels of interest for this paper.

2.1.1. General Properties

Hydrogen has a molar weight of 2.016 kg/kmol making it lightest and smallest molecule on the planet. Its gas constant is 4124 J/kg-K, which results in a density of 0.0824 kg/m^3 at standard atmospheric temperature and pressure (STP) (where, the pressure is 101325 Pa and temperature is 298 K). Hydrogen has a short bond length of 74 pm and bond energy of 457 kJ/kmol.

2.1.2. Flammability Limit

Flammability limit is defined as the range for which a fuel can be flammable or combustible [16]. The significance of this limit is in regards to how rich (excess fuel) or how lean (excess air) a mixture can be for combustion. A rich mixture is more likely to produce power but result in partial products of combustion lowering fuel economy along with creating more greenhouse gas emissions. A leaner mixture will promote complete combustion because of the excess oxygen present, increase fuel economy by taking advantage of the ratio of specific heats during the expansion process, and reduce greenhouse emissions. Since hydrogen has a flammability range of 4% to 75% by volume, or 0.1 to 7.1 by equivalence ratio (ϕ), it is more attractive as a fuel because of its ability to combust in an ultra-lean environment [20, 21]. Moreover, this large range allows hydrogen to burn in an oxygen deficient system when high amounts of diluents are utilized; as in the case of Exhaust Gas Recirculation (EGR) [16]. It helps balance oxygen displacement resulting from the use of EGR by replacing the hydrocarbon fuel with a fuel that burns more effectively in a reduced oxygen environment. As a result, the use of hydrogen allows for higher amounts of EGR to reduce NO_x while still providing a high combustion efficiency negating PM production [22].

2.1.3. Auto-Ignition Temperature

The auto-ignition temperature is the highest value a fuel can reach before spontaneously igniting. It is proportional to the pressure of the system and as the pressure increases, the auto-ignition temperature decreases. Hydrogen's auto-ignition temperature is 858K at standard conditions, compared to gasoline and diesel at 550K and 493K respectively [21, 23-25]. As a result, hydrogen manufacturers can use an engine with a high compression ratio improving fuel economy through a longer expansion stroke. Of importance, SI engines are more effective in promoting hydrogen combustion than compression ignition (CI) engines because of the ignition source (described further in the next section) [16, 26]. In fact, some researchers believe that hydrogen's higher auto-ignition temperature makes it impossible to ignite through compression alone [17, 27-29]. For example, researchers at Cornell University attempted to run hydrogen in a CI engine with a compression ratio of 29 and failed [27].

An important finding from Das is that the explosion limit for a hydrogen and oxygen system can vary as a function of pressure and temperature [19, 30]. This limit can relate changes in mixture composition to the auto-ignition temperature. Das concludes that hydrogen has three different limits with the first limit beginning at 1 mm_{Hg} of pressure and a temperature of 575°C that then decreases to a temperature of 400°C at 4 mm_{Hg} of pressure. Das states that the second limit involves the typical occurrence of pre-ignition and goes up to 575°C as the pressure increases to 400 mm_{Hg}. For the third limit, the temperature decreases to 440°C as the pressure increases to 10,000 mm_{Hg}. As a result, as hydrogen is being compressed in the cylinder increasing the pressure, this decreases the auto-ignition temperature that helps foster pre-ignition due to hot-spots and wall temperatures as discussed in a later section.

2.1.4. Minimum Ignition Energy

The minimum ignition energy is the lowest amount of energy required to ignite a fuel by separate means. Research has shown that it is largely a function of equivalence ratio with a minor dependency on pressure and temperature [16]. The lowest value for hydrogen is 0.02 mJ at stoichiometry, which is an order of magnitude less than gasoline at 0.24 mJ [17, 21, 26, 31]. Away from stoichiometry, the energy needed increases by almost two orders of magnitudes [16]. This further illustrates the preference of hydrogen for lean mixtures in comparison to other gases and liquid fuels. In particular, lean mixtures are harder to ignite and maintain flame propagation. Hydrogen is advantageous because even ultra lean, combustion can start easier and its lower flammability limit maintains the combustion process. This, in combination with auto-ignition properties, is why spark ignition is preferred over compression ignition for hydrogen combustion.

2.1.5. Laminar Flame Speed and Adiabatic Flame Temperature

The laminar flame speed (or velocity) is the rate at which a flame front expands through the combustion chamber. This property determines the ability of a fuel to maintain steady combustion and is also an indicator of the speed of combustion [17, 20]. In addition, it provides a relationship of the reactivity, diffusion, and exothermic properties of a fuel [32]. The adiabatic flame temperature is the highest temperature a combustion process can reach without any work or heat transfer and depends on the fuel's heat of combustion, heat of dissociation, and carbon/hydrogen ratio [33]. Both the laminar flame speed and adiabatic flame temperature are a function of the equivalence ratio of the mixture [30, 32]. At stoichiometry, hydrogen and gasoline have a laminar flame speed of 1.85 m/s [16, 21, 24] and 0.37-0.43 m/s [16] respectively. While hydrogen has a much larger flame speed, its adiabatic flame temperature is slightly lower than gasoline with the adiabatic flame temperatures provided in Table 1 solved using thermodynamic principles [33, 34].

The flame speed and adiabatic flame temperature are important parameters that help determine thermal efficiency and emissions from an engine [35]. The theoretical maximum efficiency a four-stroke internal combustion engine can obtain is calculated from the ideal constant volume cycle [36, 37]. In this cycle, combustion happens instantaneously at top dead center promoting the highest pressure theoretically possible. In real engines, combustion takes time; hence, fuels that minimize this time while providing a large energy release act closer to the ideal maximum. From hydrogen's relatively short ignition delay and its high laminar flame speed, it will follow more closely to this theoretical maximum of output than any other fuel because it minimizes the time for combustion [38].

2.1.6. Quenching Distance

The quenching distance is the distance from the cylinder wall to the flame front that extinguishes the flame due to heat losses [26]. Hydrogen's quenching distance (0.64 mm) is approximately three times smaller than other fuels (methane is 2.1 mm), making it harder to extinguish the flame front [19, 21]. As a result, hydrogen can backfire into the intake stream if there are any imperfections or improper sealing of the intake valve. Moreover, quenching distance has a strong correlation with the thermal efficiency of an engine [35]. By being able to combust closer to the wall, hydrogen can promote complete combustion that results in an increase in cylinder pressures and subsequent work output per given fuel charge.

2.1.7. Heating Value

The heating value is the amount of energy released during the combustion process and is measured on a gravimetric (per kg) or volumetric (per m^3) basis. The larger the gravimetric value of a fuel, the more power that is available during combustion in order to move passengers or haul cargo. The higher the volumetric value, the farther the vehicles are able to drive on a single tank of fuel. Hydrogen's heating value on a per mass basis is 119,700 kJ/kg, with the majority of other fuels in the range of 30,000 to 47,000 kJ/kg. This indicates that the consumption of hydrogen on a per mass basis is three times less while supplying equivalent engine power. However, using standard gas properties on a volumetric basis, hydrogen can only impart 9,970 kJ/m^3 of energy, whereas gasoline is 31,260 MJ/m^3. As a result, hydrogen does not offer the compactness of other fuels and extra effort is required in order to enhance storage techniques improving the volumetric heating value [39, 40].

Table 1. Fuel and Mixture Properties.

Property	Reformate (57% H_2 / 43% CO)	Hydrogen	Carbon Monoxide	Methane or CNG	Gasoline	No. 2 Diesel
Density[1] (kg/m^3)	0.5396	0.0824	1.1455	0.6560	719.7 (liquid) 4.212 (vapor)	832.0 (liquid) 8.179 (vapor)
Molar Weight (kg/kmol)	13.91	2.016	28.01	16.04	103	200
Stoichiometric Ratio (-)	5.3 [2]	34.2 [16]	2.5	17.2	14.7	14.7
Equivalence Ratio (ϕ)	0.1914 [2]	0.029 [16]	0.4062	0.069 [16]	0.069 [16]	0.0680 [23]
Flammability Limit (% per volume)	5.6 – 75.1 [2]	4.0 – 76.0 [16]	12.5 – 74.0 [2]	4.3 – 15.0 [16]	1.4 – 7.6 [16]	1.0 – 6.0 [23]
Flammability Limit (φ)	0.2 – 7.2 [2]	0.1 – 7.5 [16]	0.3 – 6.8 [2]	0.4 – 1.6 [16]	0.7 – 4.3 [16]	1.0 – 6.5 [23]
Octane Number (-)	-	130+ [23]	-	120 [39]	88 – 98 [23]	-
Cetane Number (-)	-		-	-10 [41]	-	40 - 55 [23]
Auto-ignition Temperature (K)	≈ 980 [30]	858 [16]	882 [42]	723 [16]	550 [16]	589 [23]
Minimum Ignition Energy (mJ)	-	0.02 [16]	-	0.28 [16]	0.24 [16]	-
Flame Speed (m/s)	≈1.0 [30]	1.85 [16]	0.19 [43]	0.38 [16]	0.37 – 0.43 [16]	-
Adiabatic Flame Temperature (K) [3]	2584 [2]	2480 [16]	2690 [34]	2214 [16]	2580 [16]	-
Quenching Distance (mm)	-	0.64 [16]	1.6 [44]	2.1 [16]	2.0 [16]	-
Gravimetric Heating Value (kJ/kg)	19,554 [2]	119,700 [16]	10,000	45,800 [16]	43,440 [23]	42,780 [23]
Volumetric Heating Value (kJ/m^3)	10,658 [2]	9,970	11,571 [2]	30,040 [2]	31.2×10^6 (liquid) 182,990 (vapor) [2]	35.6×10^6 (liquid) 349,950 (vapor) [2]
Heating Value (kJ/kmol)	257,992 [2]	241,315	280,100 [2]	734,632 [2]	4.5×10^6 [2] (liquid & vapor)	8.5×10^6 (liquid & vapor) [2]
1 – At a pressure of 101325 Pa and Temperature of 298K **2 – Solved values** **3 – At stoichiometry**						

2.2. Hydrogen Combustion Issues

Two main combustion issues limit the use of hydrogen in an engine. The first issue regards its tendency to pre-ignite, causing the fuel to combust before the designated ignition timing. Because of the small ignition energy required [16], hydrogen can easily pre-ignite from in-cylinder engine hot spots, the

heat from the spark plug in a SI engine, the exhaust valve, engine deposits [16, 17, 19, 26, 31, 45], and from relatively hot EGR (either internal residual gases left over from the previous cycle or external added to the intake) [19, 45]. This is because the retained temperature in these areas (or mixtures) and hydrogen's higher rate of diffusion (or its ability to mixture well) allows it to reach its auto-ignition temperature sooner before the desired heat release time [17, 19]. In addition, increasing pressure during the compression stroke lowers the flammability limit allowing the mixture to pre-ignite with a bare minimum level of hydrogen [19].

The second issue is knocking, which occurs from the auto-ignition of a secondary flame-front during the combustion process of a SI engine [17, 19]. Again, this is due to the low ignition energy of hydrogen and a further increase in pressure because of the second compression due to the propagation of the flame-front. In addition to the ignition energy factor, any hot spots on the surface can also cause the knocking phenomenon. Of importance, pre-ignition and knock are nearly impossible to tell apart through audio and visual signatures; however, knock is controllable through spark timing [16, 36]. Moreover, pre-ignition can happen in both SI and CI engines, whereas knock is only a SI engine issue due to the primary flame front. However, use of hydrogen in a CI engine does create the potential for an early heat release or large pre-mixed spike that could be inferred as pre-ignition. Researchers have attempted to control these issues by testing different fuel induction technologies and through dilution of the mixture.

2.3. Limited Equivalence Ratio Band

Previous researchers have investigated the maximum equivalence ratio (ϕ) allowed before pre-ignition. White's review states that Stockhausen found the maximum ϕ limit to be 0.6 [16]. Oehmichen did not encounter any issues during his testing since he never went higher than 0.67 [17]. Other researchers have found different ranges, such as 0.4 to 0.8 [27] and 0.3 to 0.5 [46]. These tests showed consistently that an increase in engine compression ratio and mixture temperature decreased the ϕ limit. The consequence of limiting reduces the peak engine power by 50% in comparison to gasoline.

2.3.1. Hydrogen Fuel Induction Techniques

There has been four different fuel induction technologies explored with respect to pre-ignition in SI engines: carburetion, continuous manifold injection (CMI), timed manifold injection (TMI), and direct-injection (DI) [25]. Carburetion is the original method of fuel induction for vehicular applications and has been phased out for gasoline fuels because of its inability to maintain a constant air to fuel ratio for aftertreatment requirements. Modifying carburetors had a minimal effect in controlling pre-ignition and this system was prone to backfire into the intake manifold [26]. For example, Bindon et al. use a carbureted hydrogen engine mainly to investigate its influence on combustion but state that pre-ignition was the cause of ignition in the manifold during their experiments [17]. Khajuria and Mathur find that

using an equivalence ratio between 0.3 and 0.8 does reduce the instances of backfire [17, 27, 46]. However, Das summarizes that carburetion is not an appropriate method for fuel induction because of this issue [27, 31] and states that deposits or a hot spark plug are the leading causes for this phenomenon [17].

Problems with CMI are similar in comparison to carburetion and depend mainly on the placement of the injector. For a carbureted system, fuel and air are mixed before the throttle valve, while in CMI injection of the fuel often occurs right before or after the throttle valve. By placing the injector in the intake ports farther away from the throttle valve, backfire into the intake manifold can be reduced. For example, Lee et al. used CMI on a four-cylinder SI engine with a compression ratio of 8.5:1 and found that pre-ignition only occurred at higher loads [47]. However, Das states that CMI demonstrates similar issues as carbureted engines reducing its feasibility [27]. The benefit of using CMI is that it does not require a large injection pressure in order to provide the necessary amount of hydrogen that can achieve comparable power results to gasoline or diesel fuels [48].

Timed manifold injection uses a timed delay in order to allow the intake air to cool EGR and any hot spots in the cylinder before injecting hydrogen [17, 24, 26, 27, 31, 49]. This methodology is an effective way to fuel a hydrogen engine [50-52]. As compared to CMI, TMI can operate over a wider range of speeds and equivalence ratios with a reduction in the instances of pre-ignition [27]. Researchers have been able to use encoders and feedback systems with electronic fuel injection in order make this concept feasible. However, the downside is an increased dependency on logic and timing adjustments in order to ensure reduced pre-ignition characteristics and proper engine fueling. Of importance, power output for any engine is dependent on its volumetric efficiency, fuel energy density, and its ability to combat pre-ignition. Each of the pre-mixed methods (carburetion, CMI, and TMI) inherently suffer because of the displacement of air in the intake stream, therefore reducing the volumetric efficiency of the engine [16, 39].

Direct injection of hydrogen into the cylinder has both positive and negative attributes. The chief benefit of using this method is that it eliminates pre-ignition that might be caused by internal EGR through residual gases in the cylinder when the intake value opens [20, 27, 31]. In addition, by controlling the injection timing, it can prevent the pre-ignition due to hot spots, external EGR added to the intake and the spark-plug [16, 26]. Another benefit is the increased volumetric efficiency DI offers, raising the fuel economy of the engine as only air enters the engine [39]. The downside of DI is that the duration of injection is short, which restricts the amount of fuel delivered to the engine; hence, a DI engine will always operate ultra-lean with reduced power output as compared to CMI and TMI techniques. This is because of the density of hydrogen at any feasible injection pressure [27]. Moreover, this system requires a higher-pressure injection system that increases the cost of the engine.

With respect to DI testing, in 1995 Naber and Siebers simulated Top Dead Center conditions and found that the ignition delay for hydrogen increased with fuel temperature [38]. In 2007, Mohammadi et al. tested the DI approach for a four-cylinder SI engine with a compression ratio of 11.5:1 via injection during the intake stroke or the compression stroke [20, 31]. Adding fuel during the intake stroke reduced the amount of air into the cylinder, similar to the TMI methodology, but reduced pre-ignition likelihood. Injection during the compression stroke increased thermal efficiencies while decreasing NO_x emissions because of the lean condition the DI timing creates.

2.3.2. Hydrogen Dilution

Hydrogen dilution is the use of a secondary gas in order to reduce pre-ignition and knocking in the engine by changing the properties of the mixture. Most researchers in this area utilize inert gases based on their heat absorption (capacity) capabilities. Adding a dilute increases the overall specific heats of the mixture and allows the mixture to adsorb more energy before an associated temperature rise. This results in a reduced potential ignition energy that can auto-ignite the mixture. In addition, this dilute can decrease the temperatures of any hot spots in the cylinder by acting as a thermal sink.

It has been found that there are four effective dilutes: External Exhaust Gas Recirculation (EGR), nitrogen (N_2), helium (He), and water vapor (H_2O). As explained earlier, some researchers have found that pre-ignition of hydrogen can be caused by EGR. To clarify this discrepancy, it is important to describe the four types of EGR: residual, internal, external, and external cooled EGR. Residual EGR involves the mixture that remains in the cylinder after the combustion and exhaust processes and retains a significant amount of energy. Internal EGR comes about through a built-in passageway in the cylinder head that uses a pressure differential, between the higher-pressure exhaust and lower pressure intake, in order to propagate un-cooled EGR. External EGR uses a mechanical system in order to regulate the addition of un-cooled EGR into the intake. Cooled external EGR uses a heat exchanger in order to reduce the temperature of external EGR for reduced cylinder charge temperatures, helping further decrease engine NO_x emissions. All EGR is comprised of engine exhaust that consists mainly of carbon dioxide (CO_2), water vapor (H_2O) and nitrogen (N_2). In terms of relative amounts of temperature, residual is the hottest followed by internal, external and cooled external respectively.

Using these species changes the specific heat characteristics of the mixture and replaces oxygen with non-combustible species. For EGR as a diluent, Das and Mathur used a cooled external EGR system [53]. Their system injected EGR at ambient conditions, which removed the potential for pre-ignition while taking full advantage of the specific heat characteristics of EGR. As a result, flame velocity decreases [17, 53] along with flame temperature, resulting in lower in-cylinder temperatures and pressures. This causes a slower and reduced energy combustion process resulting in decreased nitrogen oxide (NO_x) emissions independent of fuel composition [25, 27, 31, 53-57]. However, diluents reduce the

performance of an engine by lowering temperatures and worsening the ratio of specific heats during the expansion process [36]. This causes a reduced power output and most researchers choose to limit its amount in the overall mixture.

With respect to EGR, since hydrogen as a fuel does not contain any carbon, this increases the amount of water vapor in EGR and could increase the likelihood of water condensation in the engine [16]. In CMI or TMI operation, hydrogen injected into the intake replaces some of the air, reducing the amount of N_2 available to act as a diluent. Hence, using N_2 addition recovers this lost amount and provides extra in order to create the necessary heat absorption properties needed to reduce pre-ignition, knocking, or early heat release. Mathur and Das found that they could inject up to 30% by volume of N_2 without engine losses (knock-limited power and percent of hydrogen energy substitution; or the point of peak engine performance) and maintain smooth engine operation [27, 58, 59]. Greater than 30% displaced too much air leading to reduced combustion effectiveness. Helium demonstrates the same qualities as N_2 and Mathur and Das were able to inject up to 30% by volume of He without any knocking or engine performance degradation (engine losses) illustrated by a constant brake mean effective pressure [27, 58, 59]. Water vapor, also known as water induction, cools down in-cylinder temperatures, hot spots, and increases the density of air coming into the engine. Consequently, similar to the other species, the addition of water will assist with the reduction of pre-ignition, knocking and NO_x emissions [17, 27, 58, 59]. Mathur and Das found that the use of only 2,460 ppm of H_2O would allow up to 66% of hydrogen energy substitution without any combustion issues or engine losses. However, similar to hydrogen EGR, an increase in water condensation within the engine is possible.

Table 2. Specific Heat Capacity Table for different dilute species [60].

Temperature	Carbon Monoxide	Helium	Nitrogen	Water Vapor	Carbon Dioxide
K	kJ/kg-K	kJ/kg-K	kJ/kg-K	kJ/kg-K	kJ/kg-K
300	1.041	5.194	1.040	-	0.846
700	1.113	5.194	1.098	2.081	1.126
1100	1.204	5.194	1.187	2.360	1.259
1500	1.257	5.194	1.244	2.614	1.327
1900	1.287	5.194	1.278	2.803	1.364
2300	1.307	5.194	1.299	2.938	1.388

Investigating the properties of these different mixtures in Table 2 illustrates that EGR, which is comprised of mainly CO_2, H_2O, and N_2, will have an approximate heat capacity between 1.0 and 2.4 kJ/kg-K depending on the temperature. For helium, since it is a monatomic element, its heat capacity remains constant throughout the entire temperature range. Moreover, it is five times higher than other

species; hence, Das and Mathur conclude that a significant amount is not needed in order act as a heat sink. For N_2, based on a similar specific heat capacity as compared to EGR, it follows with the EGR dilute practices at a maximum value of 30%. Water induction is unique based on its additional heat absorption potential due to the phase change it undergoes. This method injects liquid water into the air intake stream or in-cylinder. As a result, the water absorbs significant energy as it undergoes conversion to a gas; hence, reducing temperatures without increasing the temperature of the water. This is why Das and Mathur state in their efforts that they only require a small amount of water (2,460 ppm) in comparison to nitrogen. Of significant importance for this paper, the inclusion of CO in the table demonstrates it actually contains a larger specific heat capacity than nitrogen, giving credence to the results discussed later in this paper.

2.4. Hydrogen Combustion Emissions

One of the main benefits of hydrogen as a fuel is that its only emissions will be H_2O and NO_x as compared to carbon-based fuels that promote the additional generation of CO_2, carbon monoxide (CO) and hydrocarbons (HC). However, a hydrogen-fuelled engine has a greater chance to have increased NO_x emissions because of its larger laminar flame speed and smaller quenching distance that can create a shorter combustion leading to higher in-cylinder pressures and temperatures [20, 47]. This is all a function of the equivalence ratio of the mixture and the geometric compression ratio of the engine [27, 61]. For NO_x to form, high temperatures must be reached in an oxygen rich environment in order to promote the dissociation of N_2 into NO and NO_2 [36]. As a result, adding enough fuel to promote a large energy release while still remaining lean and/or using a high compression ratio engine to start combustion at a higher temperature after compression of the mixture can cause the temperatures required.

Under ultra-lean conditions ($\phi \leq 0.5$), the combustion temperature is low enough that significant dissociation does not happen and NO_x emissions meets regulatory standards [16, 19, 28, 62, 63]. However, NO_x emissions start to rapidly increase after an ϕ of 0.5 [16, 62] with research demonstrating that hydrogen engine running a ϕ of 0.6 to 0.7 had higher NO_x emissions when compared to a gasoline engine [17]. Similar to traditional engine operation, it is possible to adjust injection and spark timing to counteract NO_x emissions at higher equivalence ratios by promoting a later burn in the expansion stroke [20]. Of interest, since a DI engine has a restricted amount of time to inject hydrogen, it has a difficult time reaching the equivalence ratios needed for NO_x production [20].

2.5. Dual-Fuel Hydrogen Combustion

In the 1980's, researchers began investigating the concept of using hydrogen as a fuel additive in order to reduce fuel consumption of other fuels while combating the pre-ignition and knock issues of hydrogen as a main fuel. This work began when Mathur investigated hydrogen with gasoline and found

that the engine's flame speed increased when carefully monitoring the carburetor system within a narrow equivalence ratio [27]. In 1982, Lucas and Richards also investigated the addition of hydrogen to gasoline and saw up to a 30% reduction in fuel consumption rate [17, 62]. This was due to an increase in part-load efficiency by throttling the engine less creating a leaner mixture and using hydrogen to promote lean-burn gasoline combustion. Their work also demonstrates a reduced heat loss to the coolant, lower CO and NO_x emissions but higher HC emissions with the addition of hydrogen. In 1987, Petkov and Barzev investigated this method and found an increase in NO_x emissions because of more constant volume combustion [17, 64, 65]. In 2007, Wang et al. discovered better brake specific thermal efficiency, an increase in heat release rate, lower HC and CO_2 emissions, but higher NO_x emissions [39]. Other researchers using this tactic indicate contradicting results:

- Thermal efficiency increases or decreases [17, 27, 62]
- HC emissions increase [17, 62]or decrease [27, 64]
- NO_x emissions increase or decrease [17, 27, 62, 64, 65]

In addition, researchers have investigated reforming other fuels to create a hydrogen-rich reformate mixture for this dual-fuel approach [15].

With respect to hydrogen-assisted diesel combustion, early work by Kudryash et al. used two different engine designs and found that the amount of hydrogen had to be limited in order to prevent pre-ignition and early heat release [17]. Of interest, they were able to reduce NO_x emissions by modifying a swirl chamber that led to a higher heat release rate that an undivided combustion chamber. In 1982, Gopal et al. determined that as hydrogen is added, in-cylinder pressures increased with an increase in thermal efficiency as a function of the heat released by hydrogen [66]. In 1983, Rao at el. demonstrated that the addition of hydrogen increases flame speed and in-cylinder pressures; however, their results did find that pre-ignition or excessive pre-mixed heat release occurred [67].

Two decades later, Kumar and Nagalingam tested hydrogen and biodiesel dual-fuel combustion [68]. They used Jatropha oil biodiesel and observed an enhancement of thermal efficiency, reduction in HC and CO emissions, and an increase in NO_x emissions. In 2008 and 2009, Saravanan and Nagarajan tested hydrogen enriched diesel combustion [28, 29, 49]. They investigated how the concentration of hydrogen changes thermal efficiency and emissions under different power output situations. They were able to achieve lower NO_x emissions at high loads using a high hydrogen concentration that resulted in reduced in-cylinder temperatures; however, they encountered severe pre-ignition at high loads and at more than 30% hydrogen mixture by volume. It is commonly assumed that adding hydrogen should increase cylinder temperatures and NO_x emissions through more constant-volume like combustion. Hence, the authors postulate that they added excess hydrogen, which acted as a diulent (constant pressure specific heat is 14.5 kJ/kg-K) in order to reduce the in-cylinder temperature. They determined that a 30%

hydrogen replacement of diesel could achieve the best results under high load conditions. In 2005, a unique methodology proposed by Tsolakis et al. reformed diesel fuel using external EGR in order to create a hydrogen-rich stream which was then directed back into the intake manifold [15, 54]. Of significant importance for this work, they created CO in conjunction with hydrogen in the reforming process. Their efforts demonstrate that the flame speed and rate of combustion increased, but NO_x emissions decreased. They postulated that the use of EGR's heat absorption capabilities along with the added hydrogen resulted in this enhanced combustion but reduced NO_x characteristics.

In the 2000's, many researchers tried compressed natural gas (CNG) and hydrogen in a dual-fuel manner. Similar to hydrogen, CNG has excellent fuel properties; however, it easier to transport, store, and is currently cheaper than diesel and gasoline [50, 69]. In addition, CNG is not limited to SI applications and is feasible for use in CI engines as its auto-ignition temperature is low enough to promote compression ignition. The addition of hydrogen to CNG has proven to reduce carbon-based emissions (CO, CO_2 and HC) because of its direct replacement of fuel carbon [69]. However, adding too much hydrogen does increase NO_x emissions as it facilitates a faster and hotter burn [39, 40]. Of importance, using hydrogen-assisted CNG in a CI engine does not appear to encounter the same pre-mixed heat release phenomenon because of CNG's low cetane number; e.g. it has a longer ignition delay [39, 40, 69]. On a similar but different tactic, Ílbas el al. finds that methane-assisted hydrogen combustion decreases NO_x emissions through decreasing in-cylinder temperatures [61]. Hence, it can be inferred that hydrogen-assisted methane combustion (CNG is approximately 96% methane [39, 40]) will increase NO_x emissions. Finally, in 2007, Han et al. reformed methane and used the subsequent reformate in order to increase the flame velocity of the resulting mixture [70]. They found a decrease in NO emissions because of increased allowable EGR in the mixture due to hydrogen addition.

From this review, research dictates that singular use of hydrogen as a fuel is limited to spark ignition engines and requires dilution in order to prevent pre-ignition and knock. Moreover, DI and TMI strategies are preferred, but DI is limited by the speed of hydrogen addition along with the cost of the system. TMI uses new multi-port fuel injection technology and engine timing in order to obtain higher hydrogen flow rates and can eliminate pre-ignition with proper timing. Use of hydrogen will result in no carbon-based emissions and high thermal efficiencies, but necessitates an ultra-lean equivalence ratio in order to prevent excessive NO_x. For compression ignition engines, use of hydrogen is only possible in a dual-fuel manner and can increase fuel economy. Similar to SI engine usage, hydrogen addition must be closely monitored otherwise an increase in NO_x will result along with the potential for pre-ignition or a large pre-mixed heat release spike.

Current interdisciplinary efforts at KU involve biodiesel combustion, exhaust aftertreatment and glycerin reformation. It was a congruence of this work and the review from above, that led to the

postulation of glycerin reformation as a combustion additive. In particular, the reformation efforts of Tsolakis et al. were modeled in an exhaust aftertreatment paper of the second author [71] and the investigators realized they had a similar mixture in their glycerin reforming work. While many researchers endeavor to eliminate carbon monoxide production in the reformation of glycerin for high hydrogen selectivity [72-79], the researchers discovered that including it in a dual-fuel manner with biodiesel is advantageous. Carbon monoxide is largely considered a hazardous species as it can inhibit the intake of oxygen in the blood causing carbon monoxide poisoning. However, it does contain energy for combustion and is relatively easy to create through partial oxidation, gasification or reforming of fuels. Moreover, the fact that it has low energy content while retaining a high flammability limit allows it to act similar to a diluent, unknown at the initiation of the work.

3. Experimental Apparatus

The engine used for testing was a Yanmar L100V single-cylinder directed-injected diesel with specifications presented in Table 3. This engine has a compression ratio of 21.2, significantly higher than previous research for hydrogen or hydrogen-assisted combustion. In particular, SI engines ranged from 8.0 to 12.0 [20, 39, 40, 47, 62] while the CI engines were within values of 15.0 to 16.5 [28, 29, 48, 49, 66-68]. Of interest, not all papers indicate the compression ratio of the engine they are using; hence, it is feasible that others have used an engine with a compression ratio as large as this effort. This engine uses a mechanical fuel pump-line-injector to maintain constant engine speed of 3600 rotations per minute (RPM). Injection occurs at 15.5±0.5° before piston top-dead-center with a pressure of 19.6MPa. This mechanical system does have a physical limitation, as it is not feasible to adjust injection timing. Future lab upgrades will remedy this limitation as the investigators are working with an engine supplier to retrofit the engine with a common-rail system and programmable Engine Control Unit.

Table 3. Engine Specifications

Engine	Value
Manufacturer and Model	Yanmar L100V
Type	Vertical Direct-Injection Compression Ignition
Engine Intake	Naturally Aspirated
Cooling	Air-Cooled
Cycle	4-Stroke
Displacement	435 cc
Number of Cylinders	1
Number of Valves	1 Intake, 1 Exhaust
Bore	86mm
Stroke	75mm
Compression Ratio	21.2
Injection Timing	15.5 (+/- 0.5) degrees BTDC
Continuous Rated Output	8.3 hp SAE (6.2 kW)

Rated Speed	3600 RPM
Injector Pressure	19.6 MPa
Aftertreatment	None
Engine Oil Used	Shell 15W-40
Generator	
Manufacturer and Model	NorthStar 5500BDG
Maximum Output Rated	5500 W
Continuous Output Rated	5000 W
Voltage	120/240 V
Phase	Single-phase (4-wire)
Frequency	59.0-62.0 Hz
Power Factor	100%
Allowable Current (120V/240V)	2@20 Amp/ 1@20 Amp

To provide load on the engine, the setup employs a NorthStar electric generator coupled to the crankshaft with specifications presented in Table 3. Resistance heaters supply variable electrical loading and selection of the specific power of these heaters was a function of the generator capacity to offer multiple loading events. Of interest to the reader, this setup provides a repeatable, economic alternative to an engine dynamometer. Unfortunately, original infrastructure and student availability limitations at the University of Kansas prohibited the initial installation of a more traditional setup. However, planning is underway to upgrade the system using an Alternating Current dynamometer with in-cylinder pressure measurements.

The engine and test stand are outfitted with variable sensors to measure the ambient air temperature, pressure, and relative humidity, engine air mass flow, engine intake air temperature and pressure, fuel mass flow, fuel density, engine torque, exhaust port temperature, downstream exhaust temperature and pressure, and generator load. This test stand uses a Micro-Motion Coriolis flow (model #CMF010M) for fuel flow and density measurements. The torque is measured using a FUTEK rotary torque-sensor (model # TRS-705) connected between the engine and load cell in order to provide accurate torque values. Moreover, to measure the engine intake airflow rate, a Meriam laminar flow element (model # 50MW20-2) and an Omega differential pressure transducer (model #PX277-30D5V) were used. Most of the additional parameters were monitored using appropriate Omega sensors.

A Sensors, Inc., Semtech-DS Mobile Emissions Analyzer measured carbon monoxide (CO), carbon dioxide (CO_2), diatomic oxygen (O_2), nitrogen oxide (NO), nitrogen dioxide (NO_2), and hydrocarbons (HC) emissions from the engine during testing. A heated sample line connects to a flow straightener installed downstream of the engine muffler. The Semtech-DS passed the exhaust gas through a Fuel Ionization Detector to measure HCs, a non-dispersive infrared analyzer to measure CO, CO_2, and HC levels, and a non-dispersive ultraviolet analyzer to independently measure NO and NO_2.

Connected to the intake of this engine acting in a CMI manner is the reformate assistive test stand comprised of a LinWeld Series 3210 Two-Stage Stainless Steel High-Purity regulator coupled to a Brooks Instrument SLA5850 thermal mass flow controller. The Brooks mass flow controller is calibrated for a 50% H_2 and 50% CO mixture with a volumetric flow range from 0 to 20 splm (standard liters per minute) at an inlet pressure of 75 psig with a pressure drop of 50 psig. The benefit of using the thermal mass flow controller is that this setup can test any fuel additive mixture needed by simply adjusting respective constants in an associated LabView program. The complete system complies with the necessary safety standards for hydrogen testing. All the plumbing is double reinforced stainless steel hoses and all fitting and sensors are stainless steel. In addition to the thermal mass flow controller, three Omega PX-319 pressure transducers and three Omega K-type thermocouples measure respective fluid properties. They are paired before and after the thermal mass flow controller with a third pair installed in a mixing chamber in the air intake stream. The LabView system monitors and controls all parameters and using this system requires a hydrogen compliant tank with a 350CGA (Compressed Gas Association standards) fitting.

4. Reformate Assisted Experiments

The objective of the Reformate Assisted experiments involve investigating the performance and emissions resulting from a 57% H_2 and 43% CO mixture added to biodiesel combustion. This mixture was chosen as it represents the full partial oxidation of glycerin, $C_3H_5(OH)_3$, without any formation of complete products of combustion. Hence, it represents the best-case scenario for a non-catalyzed system in regards to assisted mixture energy. This reformate was injected continuously into the intake air stream (CMI) of a compression ignition engine at a variety of flow rates under pre-set load percents. Each fuel test consists of five loadings governed by the capacity of the NorthStar generator. These loads were approximately 0% - 0,000 watts, 25% - 1,250 watts, 50% - 2,500 watts, 75% - 3,450 watts, and 100% - 4,200 watts. Under 0% load, the measured voltage output is about 120 VAC and at full load (100%) the measured voltage is 110 VAC; hence, de-rating the continuous generator power to 80% of the engine's rated continuous power. Steady-state determination occurs by monitoring the change in the engine exhaust temperature 892 mm downstream of the exhaust port. When less than a one percent change in a minute occurs, the engine is undergoing steady-state operation. Upon reaching these conditions, collection of the emissions and performance data happens as follows. The Semtech-DS analyzer collects emissions data for ten minutes at a sample rate of one sample per second. The National Instruments hardware system employed for the engine records performance data at a sample rate of ten samples per second for two minutes.

The fuel used in this experiment comes from the KU Biodiesel Initiative [80] that recovers the waste-cooking (canola) oil produced on campus. Biodiesel production transpires through conventional

batch processing technology with methanol as the alcohol and sodium methoxide or potassium hydroxide as the base. The reformate mixture properties are described in Table 1. With respect to a few of the properties, the density of the reformate is 6.5 times greater than hydrogen alone and its flammability limit was calculated using Le Chatelier's mixing rule for combustion; 5.61% to 75.13% by volume or ϕ from 0.2 to 7.2. The adiabatic flame temperature computed at stoichiometry ($\phi = 1.0$) was 2584K and the gravimetric and volumetric lower heating values are 19,554 kJ/kg and 10,658 kJ/m^3 respectively. In the figures that follow, the error bars associated with actual data measurements indicate the average standard deviation in measurement of the respective parameter. The error bars associated with the values associated with calculations come from the root-sum-squared computation for uncertainty.

5. Results

During the experiments, the investigators monitored seven facets commonly studied in hydrogen research: pre-ignition/excessive or early heat release, power output, fuel economy, volumetric efficiency, emissions, combustion efficiency, and thermal efficiency. Of particular importance, audible monitoring occurred in order to monitor the early stages of hydrogen-assisted combustion. Using the continuous manifold injection method was a risk in that it provided a higher likelihood of this phenomenon. While running the experiments no noticeable change in auditory level occurred; therefore, the authors infer that minimal or no early heat release occurred. Future work will instrument the engine with auditory and vibration sensors, along with performing an in-cylinder heat release calculation in order to determine if the reformate mixture changes the pre-mixed heat release characteristics.

This result can be explained by the high-level of CO in the reformate mixture. As elucidated before, past researchers utilized diluents, such as He, N_2, and H_2O, in order to prevent hydrogen from igniting too early. This research shows that these diluents did reduce and even removed pre-ignition using any type of fuel induction method. While CO may be technically considered a fuel source with a lower heating value of 10 MJ/kg, in this manner it acts in a dual capacity as a fuel and a diluent. This is evident by an increase of CO emissions during testing, as a portion of the CO injected goes unburned as explained later in Section 5.4, and its specific heat characteristics given in Table 2.

5.1. Power Output and Fuel Economy

Since the engine self-modulates the biodiesel fuel level through the mechanical injection system in order to maintain 3600 rpm and the energy required by the resistance heaters, any level of reformate added to the engine does not influence the power output. This is illustrated in Table 4 from the low standard of deviation at all measured loads as a function of reformate flow rate. It is important to note that the 0% load condition does produce a small amount of torque due to the linkages and load cell attached.

Table 4. Torque output and standard deviation under different reformate flow rates between 0 and 15 liters per minute.

Load	Average Torque [N-m]	Standard Deviation from Average [N-m]
0%	0.714	0.014 (1.98%)
25%	4.431	0.060 (1.36%)
50%	8.609	0.042 (0.49%)
75%	12.138	0.061 (0.50%)
100%	15.582	0.064 (0.41%)

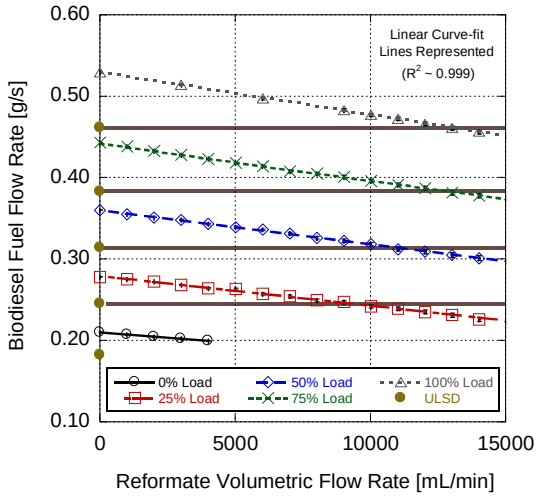

Figure 1. Biodiesel fuel flow rate for all loads and different reformate flow rates.

When adding reformate to the intake of the engine, the biodiesel fuel flow rate drops significantly as indicated in Figure 1. Moreover, this figure illustrates that the reformate mixture increases the fuel economy of biodiesel under all loading conditions with a direct linear trend found as a function of reformate flow rate added. In fact, the results demonstrate that using reformate in this manner can match the fuel consumption rate of Ultra Low Sulfur Diesel (ULSD) making the energy content of reformate-assisted biodiesel equivalent. In addition, at some of the test points, the reformate biodiesel fuel economy actually surpasses that of the diesel fuel with the total percentage fuel economy benefit over the entire range of reformate flow rates equal to 5.24%, 19.78%, 15.14%, 15.80% and 14.93% for the different loading conditions respectively. This augmentation with respect to fuel economy is more advantageous at lower loads as the reformate mixture is in relatively larger proportions to the biodiesel fuel flow rate.

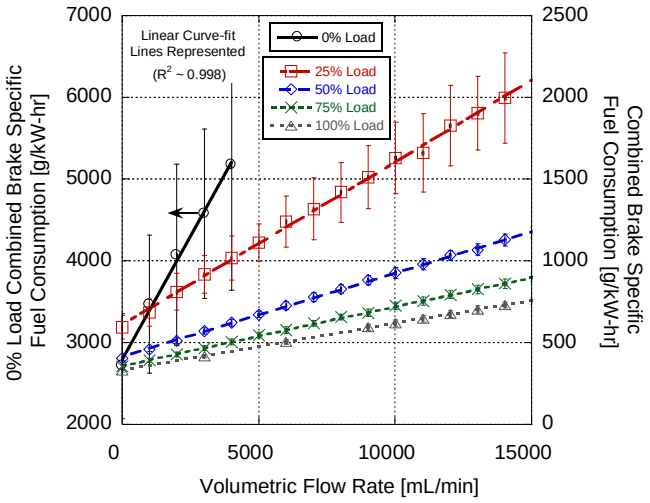

Figure 2. Brake Specific Fuel Consumption for all loads and different reformate flow rates.

However, it is important to mention that including the reformate flow rate into a combined Brake Specific Fuel Consumption (BSFC) value increases fuel consumption as illustrated in Figure 2. BSFC is used to relate the fuel consumed by any engine size in order to standardize fuel economy with a lower value indicating that the engine is producing more power from less fuel [36]:

$$BSFC_i = \frac{\dot{m}_{f,i}}{P} \quad (1)$$

where, *i* represents the individual fuel or combined fuel type, $\dot{m}_{f,i}$ is the measured mass flow rate of the specific fuel, and *P* is the power produced by the engine [36]:

$$P = 2\pi\tau N \quad (2)$$

where τ is the measured torque and *N* is the engine speed. The large BSFC standard deviation bars at 0% and 25% load in Figure 2 relate to the relatively low load conditions where torque fluctuates because of less than ideal combustion conditions and fuel flow is low but accurately measured as demonstrated via Figure 1. Since the torque sensor-sampling rate is relatively high, the torque sensor measures different points during the engine cycle (intake, compression, combustion, expansion) leading to a repeatable measurement after averaging, but a relatively large standard deviation. This effect will also be evident in the brake specific emission plots indicated later. Efforts are underway to filter the power data coming from the engine in order to reduce this time shifting phenomenon.

It is important to include all fuels added in a system perspective in order to describe the actual fuel economy of the engine. Past research illustrates that the addition of only hydrogen does decreases BSFC because of its large lower heating value [28, 69]. While biodiesel fuel-only BSFC would decrease

as indicated in Figure 1, the combined BSFC increases because of the heating value of the reformate mixture. This relates to the lower heating value of this mixture that can be calculated using [34]:

$$Q_{LHV,mixture} = \sum_{i=1}^{n} X_i Q_{LHV,i} \quad (3)$$

where X_i is the mass fraction of each fuel and $Q_{LHV,i}$ is the lower heating value of each individual fuel. Recalling from Table 1, hydrogen as a gravimetric lower heating value of 119,700 kJ/kg; however, carbon monoxide only has a value equal to 10,000 kJ/kg. Therefore, the combined value of the reformate mixture is 19,555 kJ/kg, making it less powerful as a fuel. As a result, in order to match the same energy potential of 1 g/s of diesel fuel, approximately 2.2 g/s of reformate is needed. This results in an increase in the overall BSFC; however, it is important to mention that reformate is being created from a by-product of the biodiesel production process. Moreover, the biodiesel utilized in this testing is itself a waste product of general consumption. Therefore, while the BSFC of the combined fuel increases, the researchers are using a waste product of a waste product to improve fuel economy of the main constituent beyond ULSD.

5.2. Volumetric Efficiency

As anticipated, Figure 3 demonstrates that the addition of the reformate mixture into the air intake reduces volumetric efficiency calculated as [36]:

$$\eta_v = \frac{\dot{m}_a}{2 \cdot \rho_a \cdot N \cdot V_d} \quad (4)$$

where $\dot{m}_a$ is the measured air mass flow rate, ρ_a is the air density of the environment and V_d is engine displacement volume. In order to solve for the air density, the ideal gas law is utilized [34, 36]:

$$\rho_a = \frac{p_{env}}{R_{air} \cdot T_{env}} \quad (5)$$

where p_{env} is the barometric pressure of the test cell and T_{env} is the test cell temperature. The displacement volume is calculated based on the b is the bore of the cylinder and s is the stroke of the piston [36]:

$$V_d = \frac{\pi b^2}{4} s \quad (6)$$

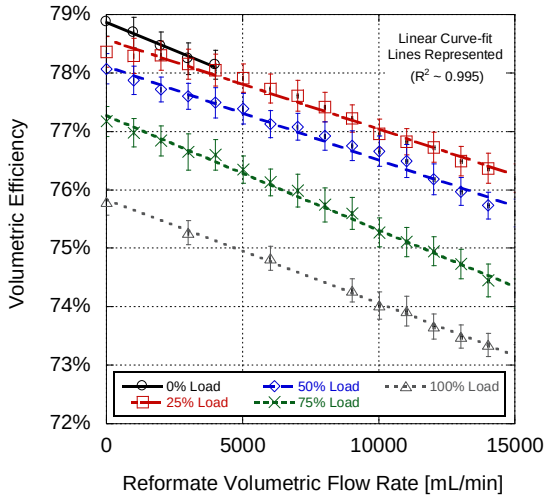

Figure 3. Volumetric efficiency for all loads and different reformate flow rates.

The reduction is similar to previous findings of hydrogen injection through CMI/TMI techniques and lessens the amount of oxidizer available for combustion of biodiesel, hydrogen, and carbon monoxide. This can potentially lead to higher emissions from the engine and a later section will discuss these results. The degradation in volumetric efficiency is less than anticipated with the average change in volumetric efficiency for full sweeps (reformate flow rate from 0 to 15 L/min) only 2.56%. The smallest change was 2.16% for 25% load, while the largest change was 2.94% for 75% load.

5.3. Exhaust Temperatures

Past research has largely concluded that the addition of hydrogen as a secondary fuel with other primary fuels, such as gasoline, diesel, and methane, resulted in higher in-cylinder pressures and temperatures. This is because it replaces a slower burning hydrocarbon based fuel with a faster component reducing the time for combustion and making the process more like constant-volume. Moreover, they find that the hydrogen quenching distance leads to a more complete combustion as the flame is able to get closer to the wall before extinguishing. If combustion timing and EGR levels are not changed, this should result in a hotter and more complete burn leading to larger in-cylinder temperatures and exhaust temperatures. As Figure 4 elucidates, this is what the authors found in their tests with the average increase of exhaust temperature for a full sweep equal to 21.9K (39.42°F). Moreover, exhaust temperature increases with load as anticipated through the combustion of more fuel.

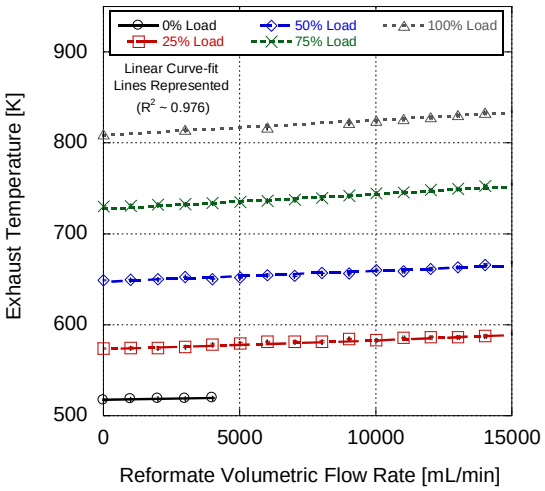

Figure 4. Exhaust temperature for all loads and different reformate flow rates.

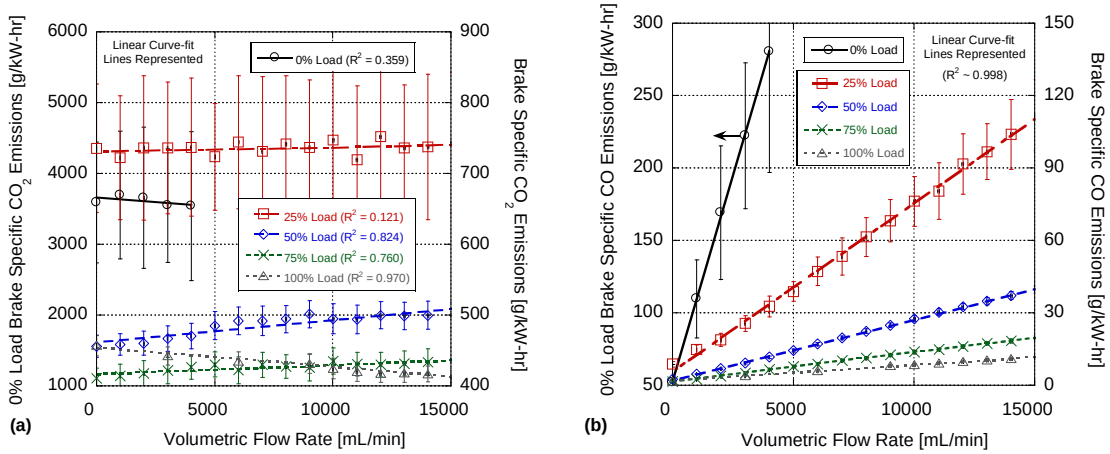

Figure 5. Brake Specific Emissions for (a) carbon dioxide and (b) carbon monoxide at all loads and different reformate flow rates.

5.4. Emissions

A Brake Specific Emission (BSE) value allows for a normalization of the production of gaseous emissions from any size engine. A lower BSE value describes less production of the corresponding emission species and illustrates a cleaner engine [36]:

$$BSE_i = \frac{\dot{m}_{i,e}}{P} \quad (7)$$

where i represents the individual emission species and $\dot{m}_{i,e}$ is the mass flow rate of the specific emission calculated as:

$\dot{m}_{i,e} = \dot{m}_t \cdot X_{i,e}$	(8)

where $\dot{m}_t$ is the total mass flow rate of the combined air, fuel, and reformate and $X_{i,e}$ is the measured emission species mass fraction.

Investigation into CO_2 emissions, as illustrated in Figure 5a, does not demonstrate any definite trend of BSE values. A reduction in biodiesel usage (Figure 1) would act to lower CO_2 emissions as the reformate mixture is replacing a large x in the higher hydrocarbon compound (C_xH_y) with hydrogen (no carbon) and carbon monoxide (singular carbon). However, we find that CO_2 increases at middle loads; whereas at full load it decreases. Therefore, no definite trend can be stated.

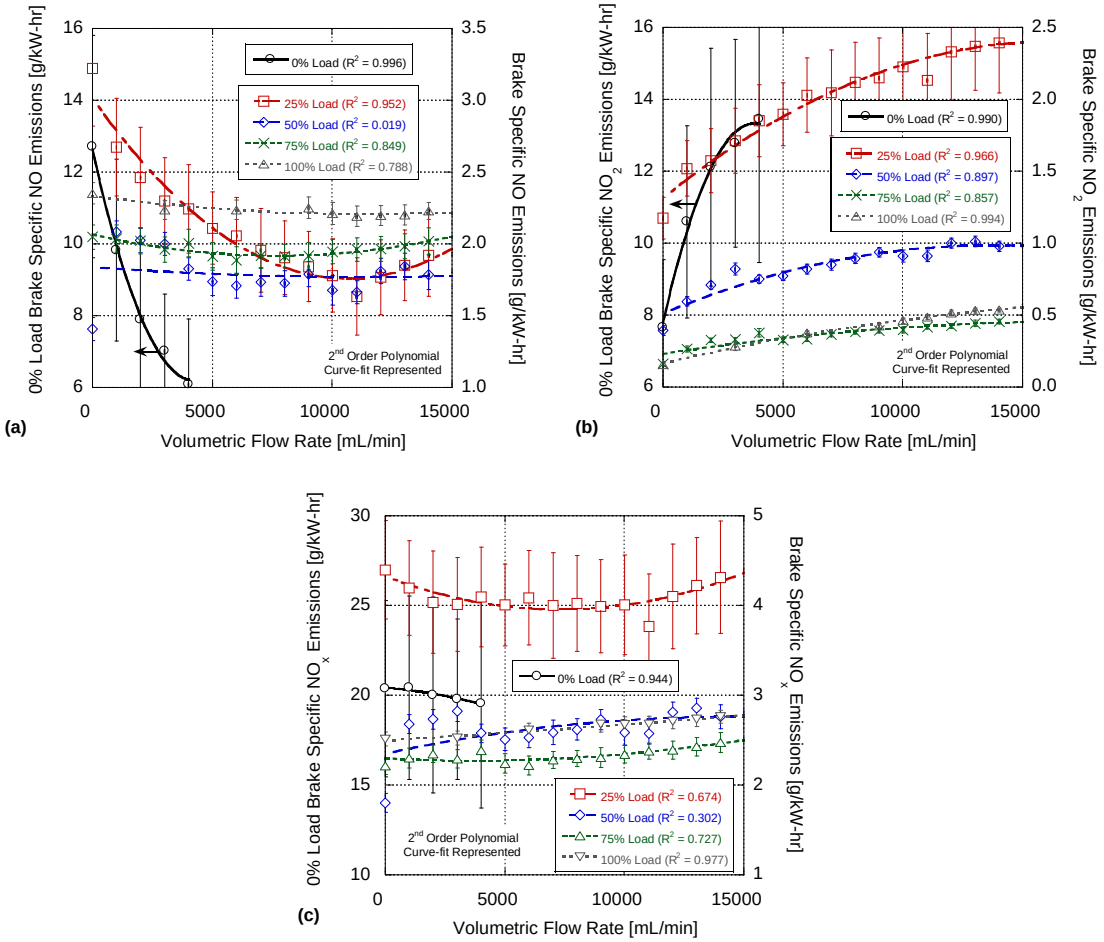

Figure 6. Brake Specific Emissions for (a) nitric oxide, (b) nitrogen dioxide, and (c) NO_x at all loads and different reformate flow rates.

What is more illuminating is the trend of CO in Figure 5b. It increases with reformate fuel flow under all situations. This indicates that some CO added is combusting leading to the non-trend in CO_2 and some CO passes right through the engine. If the CO acted purely as a diluent, CO_2 emissions should decrease through the reduction in biodiesel usage. If CO acted purely as a combustion enhancer, CO BSE

levels would remain the same within experimental data accuracy. Hence, just as EGR, He and N_2 acted to reduce pre-ignition, CO appears to act similarly while also adding a small amount of energy release. Overall, results demonstrated that CO emission levels increase by a factor of 35.1, 12.9, 16.5, 14.0 and 5.2 for each of the respective loadings (zero to full). This indicates that the higher the load, the more CO that is converted due to the hotter temperature during combustion. This result does lead to some concern with respect to exhaust aftertreatment as excess CO can inhibit a catalyst surface leading to a reduction in device efficiency.

Investigation into NO levels through Figure 6 demonstrates a general trend of decreasing amounts as a function of reformate level. However, NO_2 shows an increase in Figure 6b that offsets this trend resulting in an overall increase in NO_x levels as revealed in Figure 6c. As described in the Exhaust Temperature section, a hotter burn is anticipated which would lead to an increase in NO_x emissions. However, the mechanism for NO_x production is highly non-linear and involves a complex pathway through the Super Extended Zeldovich Mechanism [81]. In this reaction mechanism, H, OH and H_2 species all play a role; however, no function of CO is indicated.

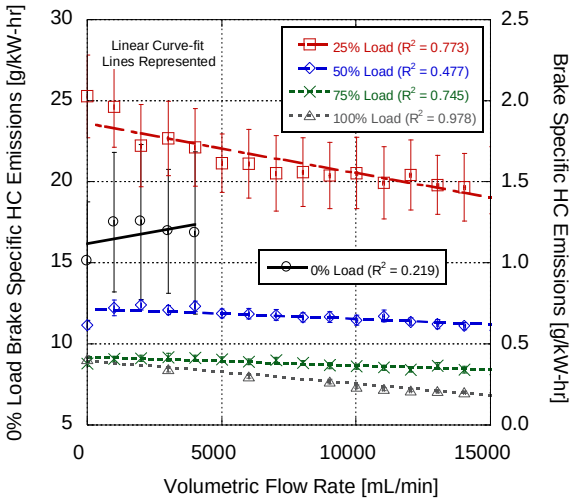

Figure 7. Brake Specific Emissions for total Hydrocarbons at all loads and different reformate flow rates.

With respect to NO_2, its formation from NO happens quickly at high temperatures in the flame front areas; however, if the temperature remains high, it can be easily destructed back to NO [36]. It remains in the form of NO_2 when the periphery of these flame fronts is quickly cooled through quenching from the surrounding air. This demonstrates why the lower loads (relatively cooler burning mixtures) have a higher amount of NO_2. Moreover, volumetric efficiency is decreasing replacing nitrogen with other species that would act to reduce NO_x levels. Finally, CO acts partially like a combustion enhancer and partially like a dilute that decreases combustion temperatures. Hence, it is impossible to distinguish the overriding factor in the increase of NO_x emissions. Overall, the largest change between each of the

loads (excluding idle) was at 25% load with a change of 1.00 g/kW-hr. Comparing these values to the Tier 4 non-road Environmental Protection Agency emission regulations makes this engine non-compliant [82]. As a result, biodiesel fuel injection timing will need to be adjusted (retarded) in order to reduce NO_x levels. This will decrease some of the gain in biodiesel fuel economy through addition of reformate.

The addition of reformate does act to reduce total HC emissions as depicted in Figure 7. Since biodiesel (C_xH_y) fuel flow rate is decreasing by replacing its energy with reformate, this would act to reduce HC emissions. Moreover, a hotter burn would also act to diminish levels by promoting complete combustion. The trend with zero load can be explained by investigation into the fuel system. This engine uses a self-contained and self-adjusting fuel pump that is based on the engine load resulting in a change in fuel timing at the same time as hydrogen and carbon monoxide is acting to augment combustion. Hence, there is some non-linearity during a time of lower combustion efficiency (described later), but as more reformate is added, this appears to act similarly as the other loads.

5.5. Combustion, Thermal and Fuel Conversion Efficiency

There are three fundamental efficiencies when it comes to analysis of in-cylinder combustion; fuel conversion, combustion and thermal. Fuel conversion efficiency is a measure of how mechanically efficient the fuel is in producing work. Larger fuel conversion efficiencies indicate that more input energy, contained in the form of chemical potential, transfers to the crankshaft in order to create useful power. Its value comes from power divided by the total energy input to the engine:

$$\eta_f = \frac{P}{Q_{in}} \tag{9}$$

where Q_{in} is total amount of energy inputted by all fuels added:

$$Q_{in}(W) = \sum_{i=1}^{n} \dot{m}_{f,i} Q_{lhv,i} \tag{10}$$

with *i* representing the individual fuels, $\dot{m}_{f,i}$ the individual fuel flow rates and $Q_{lhv,i}$ the lower heating value of each fuel.

Combustion efficiency describes the liberation of fuel chemical energy during the combustion process. Hence, it denotes how much initial added energy is actually available to move the piston and perform work. Its computation uses the exhaust species constituents that have energy, like CO and HC, and compares this amount to the input fuel energy:

$$\eta_c = 1 - \frac{\sum_{j=1}^{n} X_j \cdot Q_{lhv,j}}{\sum_{i=1}^{n} \dot{m}_{f,i} Q_{lhv,i} \Big/ \left(\sum_{i=1}^{n} \dot{m}_{f,i} + \dot{m}_a \right)} \tag{11}$$

where *i* represents the different input fuels, *j* represents the emissions species, X_j is the measured emissions fraction, and Q_{lhv} is the lower heating value of emissions and fuels. Note, for this calculation the lower heating value used for HC emissions was estimated at 44,700 kJ/kg-K. Dividing the fuel conversion efficiency by the combustion efficiency results in the thermal efficiency:

$$\eta_t = \frac{\eta_f}{\eta_c} \tag{12}$$

This parameter relates the actual work produced to the amount of fuel chemical energy released in the combustion process.

The main items of interest are the combustion efficiency and the thermal efficiency. Combustion efficiency will indicate how much of the fuel is actually available to perform work. Unfortunately, H_2 and H_2O levels leaving the engine are difficult to measure and were not available during the testing process. Since H_2 has a large lower heating value, its calculation in combustion efficiency is important. As a result, using a generalized lean combustion reaction, the authors estimated H_2 levels. This happens by writing the reaction as follows while assuming complete combustion:

$$\begin{aligned} &C_xH_yO_z + aCO + bH_2 + c\left(O_2 + 3.76N_2\right) \\ &\quad \rightarrow \left(x+a\right)CO_2 + \left(b+\tfrac{y}{2}\right)H_2O + \left(c+\tfrac{a+z}{2}\right)O_2 + 3.76cN_2 \end{aligned} \tag{13}$$

Where the biodiesel carbon constituent is given in a previous paper of the second author [83] , and the C:H and O:H levels were analyzed to equal 1.87 and 0.102. By converting mass flow rates of the reformate into molar values (*a*, *b*) normalized to 1 mole biodiesel and using the measured air-to-biodiesel ratio in order to calculate *c*, this allows an estimate of H_2O emissions based on load. From this, the authors assumed a similar molar ratio of H_2:CO as H_2O:CO_2 with subsequent conversion to mass-basis. Hence, all efficiencies are available from measurable parameters with the results provided in Figure 8.

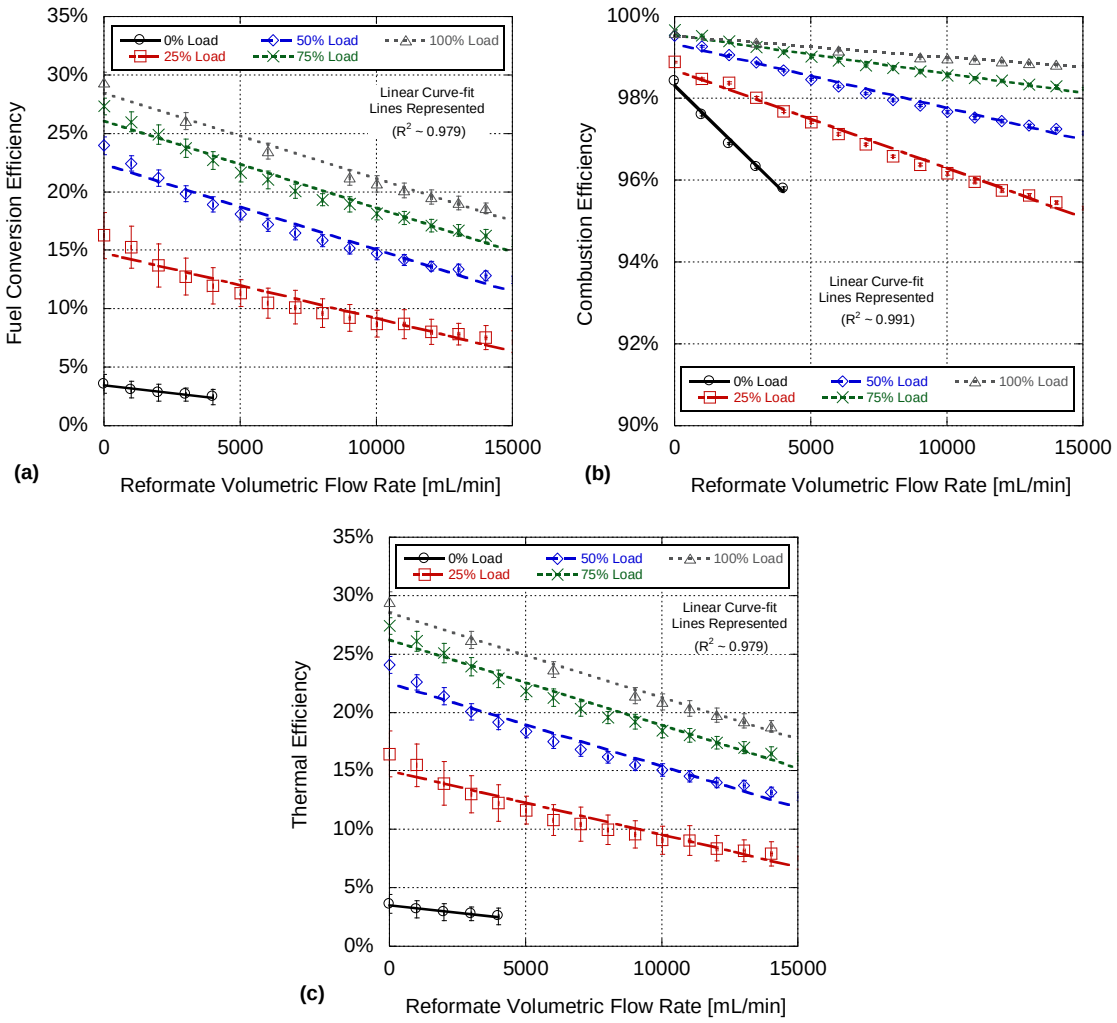

Figure 8. (a) Fuel conversion, (b) combustion and (c) thermal efficiency for all loads and different reformate flow rates

Figure 8b demonstrates that as more reformate is added, combustion efficiency decreases albeit slightly. Since diesel engines operate lean with excess air, combustion efficiency is typically near 100% and increases with load because of hotter combustion. However, as CO emissions in Figure 5b dictate, some CO acts as a diluent and will act to reduce combustion efficiency because input energy is leaving through the exhaust. Overall, the fuel conversion efficiency of the engine depicted in Figure 8a decreases as a lower energy fuel (reformate) is replacing a higher energy fuel in order to provide the same power (seen previously as BSFC in Figure 2). It was initially postulated that calculating the thermal efficiency would demonstrate a rise with reformate added. However, Figure 8c illustrates that this does not happen. The previous exhaust temperature section assumes that more constant volume combustion is happening resulting in a hotter burn. This may indeed be the case (also justified by increased NO_x emissions); however, this slight increase in speed of combustion may be offset by the significant amount of reformate

added. Moreover, since the engine self-regulates biodiesel injecting timing and EGR levels through an internal EGR passageway, a myriad of different operations are happening within the engine. Hence, it is possible that the engine retards fuel injection timing and/or EGR levels increase acting to reduce thermal efficiency. It is important to mention that increasing exhaust temperatures can result if the fuel is burning closer to exhaust valve opening (reduced time for heat transfer losses). As a result, it is not possible to conclude without further analysis and investigation of in-cylinder pressure traces. This engine upgrade is currently underway and follow-up efforts are planned.

6. Conclusion

The combustion augmentation of diesel or biodiesel with hydrogen is not a new topic. What is novel is the use of a reformate mixture consisting of hydrogen and carbon monoxide in this process. Moreover, the system methodology proposed of reforming glycerin, the by-product of biodiesel production, into a combustion enhancer of biodiesel is new to the literature. This tactic has potential for industrial applications in achieving an enhanced economic profile of biodiesel production methods. Results in this paper find the following:

1. A denser gas mixture compared to hydrogen; the addition of CO increases the density by approximately 6.5 times.
2. Wide flammability limits of the reformate from 5.61% to 75.13%, similar to hydrogen's flammability limit of 4.00% to 76.00%. This allows use of an ultra lean environment for combustion to promote fuel economy and reduce emissions.
3. Maintaining power output while improving fuel economy of biodiesel.
4. Decreasing volumetric efficiency using continuous manifold injection (CMI).
5. Decreasing fuel conversion, combustion and thermal efficiency with the addition of reformate to the engine.
6. Slight increased CO emissions from this component acting in dual capacity as a combustion enhancer and diluent.
7. No pre-ignition or large pre-mixed heat release due to the diluent effect of CO.
8. Relatively small increase in NO_x as a function of increasing reformate mixture.

This initial work demonstrates the synergy between glycerin reformation and biodiesel combustion; however, further research is needed in order to find complete answers across all engine speeds and loads. This involves the installation of an in-cylinder pressure transducer and crankshaft encoder in order to measure pressure traces while calculating ignition delay. This, along with the install of auditory and vibration sensors, will provide a quantification of any levels of pre-ignition and the pre-mixed heat release rate. Through a subsequent heat release analysis [84], in-cylinder temperatures can be

calculated. Combining this with the placing of surface-mounted thermocouples on the exterior walls of the engine will help validate an increase in combustion temperature.

Additional testing will revisit the emissions data in order to validate the original results and to investigate H_2 and CO influence on NO_x production. Moreover, an engine upgrade will occur in order to allow the researchers complete biodiesel fuel control in order to better normalize all results to a minimum fuel consumption per reformate level. Finally, since catalytic research demonstrates that CO is as equally effective as H_2 for regeneration of NO_x on the surface [85, 86], efforts will involve the addition of reformate to the exhaust stream to demonstrate its influence on converter efficiency.

Acknowledgments

This research was partially funded by the University of Kansas, Transportation Research Institute from Grant # DT0S59-06-G-00047, provided by the US Department of Transportation – Research and Innovative Technology Administration. Additional funding was supplied by R^3 Technology of Lenexa, Kansas, and by Kansas soybean farmers through the Kansas Soybean Commission, the Soybean Checkoff.

Efforts

- Eric Cecrle setup the experiment, completed the historical review, performed the tests, analyzed the data and wrote up the results.
- Dr. Chris Depcik reviewed the paper and performed some of the analysis and graph generation.
- Jing Guo assisted in the setup of the emissions equipment.
- Dr. Edward Peltier reviewed the paper.

Nomenclature/Variables

Variable	Description:	Units:
BSE	Brake Specific Emission	g/kW-hr
BSFC	Brake Specific Fuel Consumption	g/kW-hr
BSPM	Brake Specific Particulate Matter	g/kW-hr
CI	Compression Ignition	-
CMI	Continuous Manifold Injection	-
CNG	Compressed Natural Gas	-
CO	Carbon Monoxide	-
CO_2	Carbon Dioxide	-
CR	Compression Ratio	-
DBG	Di-Butoxy Glycerol	-

DI	Direct Injection	-
EGR	Exhaust Gas Recirculation	-
H_2	Hydrogen	-
H_2O	Water	-
He	Helium	-
N_2	Nitrogen	-
NO	Nitric Oxide	-
NO_2	Nitrogen Dioxide	-
NO_X	Nitrogen Oxide	-
ϕ	Equivalence Ratio	-
SI	Spark Ignition	-
STP	Standard Temperature and Pressure	-
TMI	Timed Manifold Injection	-
a	Carbon Dioxide Moles	mol
b	Water Moles	mol
B	Cylinder Bore	m
c	Nitrogen Moles	mol
$\dot{m}_a$	Air Mass Flow Rate	g/s
$\dot{m}_{f,i}$	Specific Fuel Mass Flow Rate	g/s
$\dot{m}_{i,e}$	Specific Emission Mass Flow Rate	g/s
i	Specific Term for Fuel, Emissions, etc	-
n	Number of terms	-
N	Engine Speed	1/s
η_c	Combustion Efficiency	%
η_f	Fuel Conversion Efficiency	%
η_t	Thermal Efficiency	%
η_{th}	Volumetric Efficiency	%
p_{env}	Environmental Barometric Pressure	N/m^2
P	Power Produced	W
$Q_{LHV,i}$	Lower Heating Value for Specific Fuels	kJ/kg

$Q_{LHV,mixture}$	Lower Heating Value for Reformate Mixture	kJ/kg
Q_{in}	Total Amount of Energy Inputted	W
ρ_a	Air Density	kg/m^3
R_{air}	Gas Constant for Air	J/kg-K
S	Cylinder Stroke	m
T_{env}	Environmental Temperature	K
V_d	Engine Displacement Volume	m^3
x	Carbon Moles for a Specific Fuel	-
X_i	Mass Fraction	%
y	Hydrogen Moles for a Specific Fuel	-
z	Oxygen Moles for a Specific Fuel	-

References

1. (2007) *National Biodiesel Board - Biodiesel Production and Quality*.
2. Boyd, J. *Biotech breakthrough could end biodiesel's glycerin glut*. 2007; Available from: http://www.eurekalert.org/pub_releases/2007-06/ru-bbc062607.php.
3. Carriquiry, M., et al. *World Market Impacts of High Biofuel Use in the European Union*. 2010; Available from: http://ageconsearch.umn.edu/bitstream/91923/2/10-WP_508.pdf.
4. marketsandmarkets.com, *Global Biodiesel Market* 2010: Dallas, TX.
5. Pagliaro, M. and M. Rossi, *Future of Glycerol: New Usages for a Versatile Raw Material* 2008, London, UK: Royal Society of Chemistry.
6. Zeman, N. *The Preventative Chemist*. Biodiesel Magazine 2007; Available from: http://www.biodieselmagazine.com/articles/1435/the-preventative-chemist/.
7. Lemke, D., *Syrupy Sweet Fuel? Biodiesel Processing Is Yielding Surpluses of Glycerin That May Be Burned for Energy.* Oil Mill Gazetteer, 2007. **112**: p. 2.
8. Bohon, M.D., et al., *Glycerol combustion and emissions.* Proceedings of the Combustion Institute, 2011. **33**(2): p. 2717-2724.
9. *MK Glycerin Burner Technology*. 2011; Available from: http://www.glycerinburners.com/glycerin_burning.php.
10. Jaecker-Voirol, A., et al., *Glycerol derivatives for diesel fuel reformulation.* SAE Paper 2005-01-2203, 2005.
11. Kinoshita, E., et al., *Combustion Characteristics for Diesel Engines with Emulsified Biodiesel without Adding Emulsifier.* SAE Paper 2004-01-1860, 2004.
12. Spooner-Wyman, J.K., D.B. Appleby, and D.M. Yost, *Evaluation of Di-Butoxy Glycerol (DBG) for Use As a Diesel Fuel Blend Component.* SAE Paper 2003-01-2281, 2003.
13. Dou, B.L., et al., *Hydrogen production by sorption-enhanced steam reforming of glycerol.* Bioresource Technology, 2009. **100**(14): p. 3540-3547.
14. Adhikari, S., S. Fernando, and A. Haryanto, *Production of hydrogen by steam reforming of glycerin over alumina-supported metal catalysts.* Catalysis Today, 2007. **129**(3-4): p. 355-364.
15. Jamal, Y., *On-Board Generation of Hydrogen-Rich Gaseous Fuels - A Review.* International Journal of Hydrogen Energy, 1993. **19**(7): p. 557-572.

16. C.M. White, R.R.S., A.E. Lutz, *The hydrogen-fuel internal combustion engine: a technical review.* International Journal of Hydrogen Energy, 2006. **31**: p. 1292-1305.
17. Das, L.M., *Hydrogen engines: A view of the past and a look into the future.* International Journal of Hydrogen Energy, 1990. **15**(6): p. 425-443.
18. Verhelst, S. and T. Wallner, *Hydrogen-fueled internal combustion engines.* Progress in Energy and Combustion Science, 2009. **35**(6): p. 490-527.
19. Das, L.M., *Hydrogen-Oxygen reaction mechanism and its implication to hydrogen engine combustion.* 1995: p. 707-715.
20. Mohammadi, A., *Performance and combustion characteristics of direct injection SI hydrogen engine.* International Journal of Hydrogen Energy, 2007. **32**(8): p. 296-304.
21. Gupta, R.B., ed. *Hydrogen Fuel: Production, Transport, and Storage*. 1st ed. 2008, CRC Press. 624.
22. Apostolescu, N. and R. Chiriac, *A Study of Combustion of Hydrogen-Enriched Gasoline in a Spark Ignition Engine.* SAE Paper 960603, 1996.
23. Energy, D.o. *Fuel Data Sheet*. www.afdc.energy.gov/afdc/pdfs/fueltable.pdf 2010.
24. Das, L.M., *Safety aspects of hydrogen-fuelled engine system development.* International Journal of Hydrogen Energy, 1991. **16**(9): p. 619-624.
25. Das, L.M., *Near-term introduction of hydrogen engines for automotive and agricultural application.* International Journal of Hydrogen Energy, 2002. **27**(5): p. 479-487.
26. McCormick, R., et al., *Impact of biodiesel source material and chemical structure on emissions of criteria pollutants from a heavy-duty engine.* Environ. Sci. Technol, 2001. **35**(9): p. 1742-1747.
27. Das, L.M., *Hydrogen Engine: research and development (R&D) programmes in Indian Institute of Technology (IIT), Delhi.* International Journal of Hydrogen Energy, 2002. **27**(9): p. 953-965.
28. Saravanan, N., *An experimental investigation of hydrogen-enriched air induction in a diesel engine system.* International Journal of Hydrogen Energy, 2008. **33**: p. 1769-1775.
29. Saravanan, N., *Combustion analysis on a DI engine with hydrogen in dual fuel mode.* Fuel, 2008. **87**: p. 3591-3599.
30. Sun, H., *High-pressure laminar flame speed speeds and kinetic modeling modeling of carbon monoxide/hydrogen combustion.* Proceedings of the Combustion Institute, 2007. **31**: p. 439-446.
31. Das, L.M., *Fuel Induction technques for a hydrogen operated engine.* International Journal of Hydrogen Energy, 1990. **15**(11): p. 833-842.
32. Natarajan, J., *Laminar flame speeds of H2/CO mixtures: Effect of CO2 dilution, preheat temperature, and pressure.* Combustion and Flame, 2007. **151**: p. 104-119.
33. Mishra, S.K., *Adiabatic Flame Temperature of Hydrogen in Combination with Gaseous Fuels.* International Journal of Hydrogen Energy, 1989. **14**(11): p. 839-844.
34. M.J. Moran, H.N.S., *Fundamentals of Engineering Thermodynamics*. 5th ed. 2004, Danvers: Wiley & Sons, Inc.
35. Shudo, T., *Thermal efficiency analysis in a hydrogen premixed combustion engine.* Journal of Society of Automotive Engineering Review, 2000. **21**(2): p. 177-182.
36. Heywood, J.B., *Internal Combustion Engine Fundamentals.* . 1988, New York: McGraw-Hill, Inc.
37. Sonntag, R., C. Borgnakke, and G.J. van Wylen, *Fundamentals of Thermodynamics*. 6th ed. 2002, New York: Wiley.
38. Naber, J.D., *Hydrogen combustion under diesel engine conditions.* International Journal of Hydrogen Energy, 1998. **23**(5): p. 363-371.
39. Wang, J., *Combustion behaviors of a direction-injection engine operating on various fractions of natural gas-hydrogen blends.* International Journal of Hydrogen Energy, 2007. **32**(4): p. 3555-3564.
40. Huang, Z., *Combustion Characteristics of a Direct-Injection Engine Fueled with Natural Gas-Hydrogen Mixtures.* Energy & Fuel, 2006. **20**: p. 540-546.

41. Board, T.R., *Guidebook for Evaluating, Selecting, and Implementing Fuel Choices for Transit Bus Operations*. 1998, Washington DC.
42. *Fuel and Chemicals - Auto Ignition Temperatures*. 2011; Available from: http://www.engineeringtoolbox.com/fuels-ignition-temperatures-d_171.html.
43. Dong, C., et al., *Experimental study on the laminar flame speed of hydrogen/carbon monoxide/air mixtures.* Fuel, 2009. **88**(10): p. 1858-1863.
44. Norden, P.A., *Determination of quenching distance for carbon monoxide-air flames.* Journal of Engineering Physics and Thermophysics, 1965. **9**(1): p. 77-78.
45. Watson, M., *Some Problems and Benefits from the Hydrogen-Fuelled Spark Ignition Engine.* SAE technical paper series, 1978(789212).
46. H.B. Mathur, P.R.K., *Performance and emission characteristics of a hydrogen-fuelled spark ignition engine.* International Journal of Hydrogen Energy, 1984. **21**(8): p. 729-736.
47. Lee, S., *Combustion characteristics of intake port injection type hydrogen fueled engine.* International Journal of Hydrogen Energy, 1995. **20**(4): p. 317-322.
48. Masood, M., M.M. Ishrat, and A.S. Reddy, *Computational combustion and emission analysis of hydrogen-diesel blends with experimental verification.* International Journal of Hydrogen Energy, 2007. **32**(13): p. 2539-2547.
49. Saravanan, N., *Experimental Investigation in Optimizing the Hydrogen Fuel on a Hydrogen Diesel Dual-Fuel Engine.* Energy & Fuel, 2009. **23**: p. 2646-2657.
50. Das, L.M., *A comparative evaluation of the performance characteristics of a spark ignition engine using hydrogen and compressed natural gas as alternative fuels.* International Journal of Hydrogen Energy, 2000. **25**: p. 783-793.
51. Mathur, H.B., *Performance characteristics of a hydrogen fuelled S.I. engine using timed manifold injection.* International Journal of Hydrogen Energy, 1991. **16**(2): p. 115-127.
52. Das, L.M., *Performance evaluation of a hydrogen-fuelled spark ignition engine using electronically controlled solenoid-actuated injection system.* International Journal of Hydrogen Energy, 2000. **25**(6): p. 569-579.
53. Das, L.M., *Exhaust gas recirculation for NOx control in a multicylinder hydrogen-supplemented S.I. engine.* International Journal of Hydrogen Energy, 1993. **18**(12): p. 1013-1018.
54. Tsolakis, A., *Partially premixed charge compression ignition engine with on-board H2 production by exhaust gas fue reforming of diesel and biodiesel.* International Journal of Hydrogen Energy, 2005. **30**: p. 731-745.
55. Maiboom, A., *Experimental study of various of exhaust gas recirculation (EGR) on combustion and emissions of an automotive direct injection diesel engine.* Energy, 2008. **33**(1): p. 22-34.
56. Cairns, A., *The Effects of Combined Internal and External Exhaust Gas Recirculation on Gasoline Controlled Auto-Ignition.* SAE technical paper series, 2005. **2005-01-0133**.
57. Chen, R., *The Thermal Effect of Internal Exhaust Gas Recirculation on Controlled Auto Ignition.* SAE technical paper series, 2003. **2003-01-0751**.
58. Mathur, H.B., *Hydrogen fuel utilization in CI engine powered end utility systems.* International Journal of Hydrogen Energy, 1992. **17**(5): p. 369-374.
59. Mathur, H.B., *Hydrogen-fuelled diesel engine: Performance improvement through charge dilution techniques.* International Journal of Hydrogen Energy, 1993. **18**(5): p. 421-431.
60. *NIST Chemistry WebBook*. 2011; Available from: http://webbook.nist.gov/chemistry/.
61. Ilbas, M., *Investigations of hydrogen and hydrogen-hydrocarbon composite fuel combustion and NOx emission characteristics in a model combustor.* International Journal of Hydrogen Energy, 2005. **30**: p. 1139-1147.
62. Andrea, T.D., *The addition of hydrogen to a gasoline-fuelled SI engine.* International Journal of Hydrogen Energy, 2004. **29**(14): p. 1541-1552.
63. Das, L.M., *Exhaust emission characterization of hydrogen-operated engine system: Nature of pollutants and their control techinques.* International Journal of Hydrogen Energy, 1991. **16**(11): p. 765-775.

64. Petkov, T. and K. Barzev, *Possibilities of improving the performance of a spark ignition engine working with hydrogen as supplementary fuel.* International Journal of Hydrogen Energy, 1987. **12**(10): p. 701-704.
65. Petkov, T.I. and K.N. Barzev, *Some aspects of hydrogen application as a supplementary fuel to the fuel-air mixture for internal combustion engines.* International Journal of Hydrogen Energy, 1987. **12**(9): p. 633-638.
66. Gopal, G., *Use of hydrogen in dual-fuel engines.* International Journal of Hydrogen Energy, 1982. **7**(3): p. 267-272.
67. Rao, B.H., *Hydrogen for dual fuel engine operation.* International Journal of Hydrogen Energy, 1983. **8**(5): p. 381-384.
68. Kumar, S., *Use of hydrogen to enhance the performace of a vegetable oil fuelled compression ignition engine.* International Journal of Hydrogen Energy, 2003. **28**(10): p. 1143-1154.
69. Akansu, S.O., *Internal combustion engines fuel by natural gas -- hydrogen mixtures.* International Journal of Hydrogen Energy, 2004. **29**(14): p. 1527-1539.
70. Han, P., *Hydrogen from reformer gas a novel fuel and bridging technology: A combustion perspective.* International Journal of Hydrogen Energy, 2007. **32**: p. 1416-1420.
71. Depcik, C., A. Kobiera, and D. Assanis, *Influence of Density Variation on One-Dimensional Modeling of Exhaust Assisted Catalytic Fuel Reforming.* Heat Transfer Engineering, 2010. **31**(13): p. 1098-1113.
72. Adhikari, S., S. Fernando, and A. Haryanto, *A Comparative Thermodynamic and Experimental Analysis on Hydrogen Production by Steam Reforming of Glycerin.* Energy & Fuels, 2007. **21**: p. 2306-2310.
73. Adhikari, S., S. Fernando, and A. Haryanto, *Glycerin steam reforming for hydrogen production.* Transactions of ASABE, 2007. **50**(2): p. 591-595.
74. Adhikari, S., S.D. Fernando, and A. Haryanto, *Hydrogen production from glycerin by steam reforming over nickel catalysts.* Renewable Energy, 2008. **33**(5): p. 1097-1100.
75. Buffoni, I.N., et al., *Nickel Catalysts Applied in Steam Reforming of Glycerol for Hydrogen Production.* Catalysis Communications, 2009. **10**: p. 1656-1660.
76. Czernik, S., et al., *Hydrogen by Catalytic Steam Reforming of Liquid Byproducts from Biomass Thermoconversion Processes.* Ind. Eng. Chem. Res., 2002. **41**: p. 4209-4215.
77. Douette, A.M.D., et al., *Experimental Investigation of Hydrogen Production from Glycerin Reforming.* Energy & Fuels, 2007. **21**(6): p. 3499-3504.
78. Hirai, T., et al., *Production of Hydrogen by Steam Reforming of Glycerin on Ruthenium Catalyst.* Energy & Fuels, 2005. **19**: p. 1761-1762.
79. Wang, X., et al., *Thermodynamic Analysis of Glycerin Steam Reforming.* Energy & Fuels, 2008. **22**: p. 4285-4291.
80. University of Kansas Biodiesel Initiative. *KU Biodiesel Initiative*. 2009; Available from: http://biodiesel.ku.edu/index.php.
81. Miller, R.H., et al., *A Super-Extended Zeldovich Mechanism of NO_x Modeling and Engine Calibration.* SAE Paper 980781, 1998.
82. *EPA Emission Regulations*. 2011; Available from: http://www.epa.gov/nonroaddiesel/2004fr/420r04007a.pdf.
83. Duncan, A., et al., *High-Pressure Viscosity of Bio-diesel from Soybean, Canola, and Coconut Oil.* Energy and Fuels, 2010. **24**(10): p. 5708-5716
84. Depcik, C., et al., *Instructional Use of a Single-Zone, Pre-mixed Spark-ignition Heat Release Simulation.* International Journal of Mechanical Engineering Education, 2007. **35**(1): p. 1-31.
85. Li, Y., et al., *Study of Factors Influencing the Performance of a NOx Trap in a Light-Duty Diesel Vehicle.* SAE Paper 2000-01-2911, 2000.
86. Abdulhamid, H., E. Fridell, and M. Skoglundh, *Influence of the type of reducing agent (H_2, CO, C_3H_6 and C_3H_8) on the reduction of stored NO_x in a Pt/BaO/Al_2O_3 model catalyst.* Topics in Catalysis, 2004. **30/31**: p. 161-168.